Investigating Tau pathology in an *in vitro* model for Alzheimer's disease

by

Yigael Samuel Louis Powrie

Thesis presented in fulfilment of the requirements for the degree of Master of Science in the Faculty of Science at Stellenbosch University

Supervisor: Dr Benjamin Loos

December 2016

Declaration

By submitting this thesis electronically, I declare that the entirety of the work contained therein is my own, original work, that I am the sole author thereof (save to the extent explicitly otherwise stated), that reproduction and publication thereof by Stellenbosch University will not infringe any third party rights and that I have not previously in its entirety or in part submitted it for obtaining any qualification.

December 2016

Abstract

Introduction

Alzheimer's disease is a neurodegenerative disease of the brain and the leading cause of dementia globally. Severe cognitive and short term memory deficits are commonly associated with this disease. The pathology is characterised by two molecular hallmarks that manifest in brain tissue, which are intercellular plaques composed of β-amyloid, and intracellular protein aggregates known as neurofibrillary tangles (NFTs) composed of phosphorylated Tau, a microtubule (MT) associated protein (MAP). Under homeostatic conditions Tau facilitates the dynamic polymerisation of the microtubule network, which acts as part of the cytoskeleton and platform for vesicular transport. Tau is generally phosphorylated to modulate its binding affinity to the network. However, under pathological conditions it becomes hyperphosphorylated, leading to dissociation from the MT. Dissociated Tau is thought to form NFT aggregates, which causes the MT to become susceptible to cleavage by the severing proteins, Katanin p60 and Spastin. However, it has not been determined when this process occurs in disease progression and whether it is indeed a confounding factor leading to the onset of neuronal cell death. Moreover, although dysfunction of the autophagic lysosomal pathway, an inherent proteolytic process for long-lived proteins and organelles, has been shown to be implicated in the onset of protein aggregation, its role in the context of MT dysfunction remains unclear.

Aims and Methods

The aims of this study were to assess microtubulin and Tau dynamics in an in vitro model of autophagic dysfunction that is similar to the Alzheimer's disease pathology. It was hypothesized that a disruption in the autophagy process would lead to maladaptive changes in the microtubulin and Tau dynamics prior to the onset of cell death.

GT1-7 neuronal cells were cultured under standard conditions and treated with Chloroquine diphosphate (CQ), a lysosome deacidifying agent, to induce an autophagic dysfunctional state. Two time points of exposure to CQ were established using a WST-1 assay to assess the molecular changes occurring prior to and during the onset of cell death. Western blot analysis was utilised to quantify protein levels of acetylated α-tubulin, Tau, pTau, Katanin p60 and Spastin in response to CQ-induced autophagy dysfunction. Furthermore, cells were transfected with a GFP-Tau DNA construct, using the Neon® transfection system. Additionally, cells were fixed and stained post-transfection with fluorescent Alexa® Fluor secondary antibodies against primary antibodies recognising acetylated α-tubulin, pTau, Katanin p60 and Spastin. Fluorescent microscopy analysis was performed using Super Resolution Structured Illumination Microscopy (SR-SIM), Stochastic Optical Reconstruction Microscopy (STORM),

Correlative Light and Electron Microscopy (CLEM) and confocal microscopy techniques on the LSM-780 Elyra PS.1 system to assess protein localisation in response to CQ treatment. Moreover, co-localisation was assessed between acetylated α-tubulin and Tau, pTau, Spastin and Katanin p60 respectively.

Results

Fluorescent microscopy analysis revealed that CQ-induced autophagy dysfunction caused acetylated α-tubulin protein structure to become progressively impacted, which manifested as breakages in the network. Tau protein levels decreased non-significantly, but fluorescent microscopy revealed the formation intracellular Tau aggregates. In addition, Tau co-localised with acetylated α-tubulin under control conditions and remained co-localised in response to CQ treatment. Phosphorylated Tau protein levels did increase non-significantly, but fluorescent microscopy revealed no aggregate formation. Katanin p60 protein levels significantly increased, however, the protein did not co-localise with acetylated α-tubulin under control conditions or in response to CQ-induced autophagy dysfunction. Spastin protein levels increased non-significantly, however, Spastin co-localised with acetylated α-tubulin under control conditions, which significantly increased in response to autophagy dysfunction.

Discussion and Conclusion

Our results indicate that CQ-induced autophagy dysfunction causes Tau aggregation, but no dissociation from the microtubule network. Furthermore, the microtubulin network becomes unstable, despite its continuous association with Tau, which may be caused by increased Spastin-mediated severing.

To conclude, the data clearly demonstrate that these pathological perturbations occur prior to the onset of cell death, which not only highlights novel therapeutic targets, but also the lack of optimal timing in the therapeutic interventions utilised in Alzheimer's disease treatment.

Opsomming

Inleiding

Alzheimer's siekte is 'n neurodegeneratiewe siekte van die brein en die hoofoorsaak van demensie ter wêreld. Hewige kognitiewe en korttermyngeheue gebreke word algemeen geassosiëer met hierdie siekte. Die patologie word gekenmerk deur twee molekulêre kenmerke wat manifesteer in die breinweefsel. Dit sluit in intersellulêre plaakvorming wat bestaan uit amiloïed-β, en intrasellulêre aggregate, ook bekend as neurofibrillêre knope (NFK), wat uit Tau, 'n mikrotubulêre (MT) geassosiëerde proteïn (MAP) bestaan. Onder homeostatiese toestande fasiliteer Tau die dinamiese polimerisasie van die mikrotubulêre netwerk, wat dien as deel van die sitoskelet, en ook as 'n platform vir vesikulêre vervoer funksioneer. Tau is normaalweg gefosforileer om die bindingsaffiniteit vir die mikrotubulêre netwerk te moduleer. Nieteenstande, onder patologiese toestande word Tau gehiperfosforileer wat veroorsaak dat dit van die mikrotubulêre netwerk dissosiëer. Gedissosieerde Tau vorm vermoedelik neurofibrillêre knope, wat veroorsaak dat die mikrotubulêre netwerk vatbaar is vir degradasie deur die proteïne, katanin p60 en spastin. Nieteenstaande, is dit nog nie vasgestel waneer hierdie proses in die siekte progressie plaas vind nie, en of dit 'n bepalende faktor is wat lei tot die aanslag van neuronale seldood. Hoewel disfunksionering van die autofagiese lisosoomsisteem, 'n proteolitiese proses vir verouderde en beskadigde proteïne en organelle, geimpliseerd is in die aanslag van die vervorming van proteïn aggregate, is dit in die konteks van mikrotubulêre netwerk destabilisasie steeds onduidelik.

Doel en Metodes

Die doel van hierdie studie was dus om die dinamika van Tau en die mikrotubulêre netwerk in 'n in vitro model van autofagiese dusfunksionering, wat soortgelyk is aan die Alzheimer's siekte patologie, te ondersoek. Die hipotese wat gestel is, is dat 'n ontwrigting in die outofagiese proses tot wanaangepaste veranderinge in die dinamika van Tau en die mikrotubulêre netwerk voor die aanslag van seldood sal aanleiding gee.

GT1-7 neuronale selle was deur middel van selkultuur geweek onder standaardtoestande met 'n lisosomiese onversuringsmiddel, chlorokiendifosfaat (CQ) behandel, om 'n outofagiese disfunksionele toestand te veroorsaak. Twee CQ blootstellingsperiodes was vasgestel met 'n WST-1 toets om molekulêre veranderinge, voor en gedurende die aanvang van seldood, te ondersoek. Western blot analiese is gebruik om die proteïnvlakke van geasetileerde α-tubulien, Tau, pTau, katanin p60 en spastin in reaksie op CQ-geïnduseerde autofagiese disfunksie, te kwantifiseer. Selle was getransfekteer met 'n GFP-Tau DNS plasmied met die

Neon® transfekteringsstelsel. Verder, was selle chemies gepreseveer na transfektering en met fluoresserende Alexa® Fluor sekondêre teenliggaampies teen die primêre teenliggaampies wat geasetileerde α-tubulien, pTau, katanin p60 en spastin erken, gekleur. Fluoressensie mikroskopie is gebruik met behulp van Super Resolusie Gestruktureerde Verligtings Mikroskopie (SR-SIM), Stogastiese Optiese Rekonstruksie Mikroskopie (STORM), Korrelatiewe Lig en Elektron Mikroskopie (CLEM), en konfokale mikroskopiese tegnieke op die LSM-780 Elyra PS.1 stelsel, om proteïenlokalisering te evalueer in reaksie op CQ behandeling. Verder, was ko-lokalisering tussen geasetileerde α-tubulien en pTau, katanin p60 en spastin onderskeidelik geëvalueer.

Resultate

Fluoressensie mikroskopie analiese het gewys dat CQ-geïnduseerde outofagiese disfunksie ’n progressiewe impak op die geasetileerde α-tubulien struktuur gehad het, wat gemanifesteer as gebreke in die netwerk. Tau proteïenvlakke het nie betekenisvol afgeneem nie. Fluoressensie mikroskopie analiese het ook gewys dat Tau aggregate in reaksie op CQ behandling gevorm het. Benewens, het Tau geko-lokaliseer met geasetileerde α-tubulien onder onbehandelde toestande, en só gebly tydens outofagiese disfunksie. Gefosforileerde Tau proteïenvlakke het nie betekenisvol toegeneem nie, en geen proteïenaggregate het gevorm nie. Katanin p60 proteïenvlakke het beduidenlik toegneem, maar het nie met die geasetileerde α-tubulien die in onbehandelde toestande òf gedurende outofagiese disfunksie geko-lokaliseer nie. Spastienproteïenvlakke het nie betekensvol toegneem nie. Spastien het geko-lokaliseer met die geasetileerde α-tubulien onder onbehandelde toestande, en het progressief en beduidenlik geko-lokaliseer tydens outofagiese disfunksie.

Bespreking en gevolgtrekking

Ons resultate toon dat CQ-geïnduseerde outofagiese disfunksie veroorsaak dat Tau aggregate vorm, maar nie van die mikrotubulêre netwerk dissosiëer nie. Verder, word die mikrotubulêre netwerk onstabiel ten spyte van die gedurende assosiëering met Tau, wat mag aandui dat daar ’n toename in spastien bemiddelde degradasie van die netwerk is.

Opsommend demonstreer hierdie data dat die patologiese versteurings voor die aanslag van seldood plaasvind. Dit beklemtoon nie net moontlike nuwe terapeutiese teikens nie, maar ook die gebrek aan optimale tydsberekening in terapeutiese intervensies wat gebruik word in Alzheimer’s siekte behandeling.

Acknowledgements

I would like to thank the following people and organisations:

The National Research Foundation for their financial support of the study, Dr Peter Davies from the Albert Einstein Institute (New York) for the kind gift of the CP27 Tau antibody. The CAF Fluorescent Microscopy Unit of Stellenbosch University for the numerous hours spent assisting with the acquisition, processing and interpretation of fluorescent microscopy data. Specifically, to Mrs Lize Engelbrecht and Ms Dumisile Lumkwana, who were instrumental in the success of this project and without whom it would not have been possible.

Dr Lucy Collinson and Dr Marie-Charlotte Domart from the Crick Institute (UK) for providing me with the basic knowledge of Correlative Light and Electron Microscopy as well as enlightening me to the exciting field of microscopy in the first world.

Dr Craig Kinnear for the clonal expansion and purification of the plasmid DNA constructs utilised in the fluorescent microscopy analysis.

I would personally like to thank the following people:

My supervisor and mentor Dr Ben Loos, who provided constant support and encouragement, who pushed me to do more than my best and who provided me with the freedom and platform to grow as a scientist.

Dr Tanja Davis, who was always there to help with the experimental woes and to offer encouragement where it was necessary.

My mother Madaleinne, my sister Jade and my father Owen for the emotional support and unending encouragement during the duration of this degree

My labmates Jurgen Kriel, Claudia Ntsapi, Dumisile Lumkwana and Danielle Millar who always provided me with lab and emotional support during times of difficulty.

And finally the Department of Physiological Sciences at Stellenbosch University for allowing me to undertake my Masters studies in their facilities.

List of Conferences

- Microscience Microscopy Conference (July 2015). Manchester Convention Complex, Manchester, UK. Oral Presentation: “Investigating Tau pathology in an *in vitro* model for Alzheimer’s disease”.
- Physiological Society of Southern Africa Conference (September 2016). River Club, Cape Town, South Africa. Oral Presentation: “Investigating Tau pathology in an *in vitro* model for Alzheimer’s disease”.
- Microscopy Society of Southern Africa (December 2016). Boardwalk Convention Center, Port Elizabeth, South Africa. Oral Presentation: “Investigating Tau pathology and the associated microtubulin instability in an *in vitro* model for Alzheimer’s disease”.

Articles

- YSL Powrie, B Loos. Investigating Tau pathology and the associated microtubulin instability in an *in vitro* model for Alzheimer’s disease: In process of submission

Index

List of Figures

List of Tables

List of Abbreviations

+TIPs	Microtubule plus-end tracking protein
AAA	ATPases Associated with diverse cellular Activities
ACD	Autophagic Cell Death
ACh	Acetylcholine
AD	Alzheimer's disease
ADAM10	Distintegrin or metalloproteinase 10
AD-HSP	Autosomal Dominant – Hereditary Spastic Paraplegia
ALP	Autophagy Lysosome Pathway
AMBRA	Activating Molecule in Beclin 1-Regulated Autophagy
AMP	Adenosine monophosphate
AMPK	Adenosine monophosphate kinase
APOE-ε4	Apoliprotein-ε4
APP	Amyloid Precursor Protein
Atg	Autophagy related protein
ATP	Adenosine Triphosphate
Aβ	Amyloid-β
BACE1	β-site APP cleaving Enzyme 1
BSA	Bovine Serum Albumin
CDK	Cyclin-Dependent Kinase
Cdk5	Cyclin-dependent kinase 5
CHIP	C terminus of Hsp70-interacting protein
ChIP	Chromatin Immunoprecipitation
CLEM	Correlative Light and Electron Microscopy
CO2	Carbon Dioxide
CoQ	Co-enzyme Q
CQ	Chloroquine
CytC	Cytochrome C

dH2O	Distilled Water
DMEM	Dulbecco's Modified Eagle's Medium
DMSO	Dimethyl Sulfoxide
DNA	Deoxyribonucleic acid
Drp	Dynamin related protein
DUB	De-ubiquitinating enzymes
ECD	Excitotoxic Cell Death
ECL	Enhanced Chemiluminescence
EDTA	Ethylene-diamine-tetra-acetic Acid
EE	Early Endosome
ELP	Endosome Lysosome Pathway
ER	Endoplasmic Reticulum
ESCRT	Endosomal Sorting Required for Transport
ETC	Electron Transport Chain
FAD	Early-onset Familial Alzheimer's disease
FADD	Fas Death Domain
Fas	Fatty acid synthase
FasL	Fas Ligand
FasR	Fas Receptor
FBS	Foetal Bovine Serum
FTDP-17	Frontotemporal Dementia linked to chromosome 17
GLP	Glucagon-Like Peptide
GSK3-β	Glycogen Synthase kinase 3 - beta
GTP	Guanine triphosphate
HDAC6	Histone Deacetylase 6
HRP	Horse Radish Peroxidase
HSP70	Heat shock protein 70
ILVs	Intraluminal Vesicles

JNK	c-Jun N-terminal kinases
LAMP-2A	Lysosome associated membrane protein type 2A
LC3-I/II	Microtubule-associated protein 1A/1B-light chain 3 I/II
LE	Late Endosome
LOAD	Late Onset Alzheimer's disease
LTP	Long Term Potentiation
MAP	Microtubule associated protein
MAPT	Microtubule associated protein Tau gene
MARK	Microtubule Affinity Regulating Kinase
MEFs	Mouse Embryonic Fibroblasts
Mfn1/2	Mitofusin1/2
MOA	Monoamine Oxidase α
MOC	Mander's Overlap Co-efficient
mRNA	messenger ribonucleic acid
MSEs	Microtubule Severing Enzymes
mtDNA	mitochondrial deoxyribonucleic acid
MTOC	Microtubule organising centre
mTORC1	mammalian Target Of Rapamycin Complex 1
NFTs	Neurofibrillary Tangles
NMDA	N-methyl-D-aspartate
NMDAR	N-methyl-D-aspartate Receptor
OPA1	Optic Atrophy 1
PAGE	Polyacrylamide Gel Electrophoresis
PARP	Poly (ADP-ribose) Polymerase
PE	Phosphatidylethanolamine
PI3K CIII	Phosphatidylinositol 3-kinase complex 3
PI3K	Phosphatidylinositol 3-Kinase
PI3P	Phosphatidyl-Inositol-3-Phosphate

PINK1	PTEN-induced putative kinase 1
PSEN-1/-2	Presenilin-1 and -2
PTEN	Phosphate Tensin Homologue
PVDF	Polyvinylidine fluoride
RE	Recycling Endosome
RIPA	Radio-immunoprecipitation
ROS	Reactive Oxygen Species
Rpn	Regulatory particle non-ATPase
SDS	Sodium Dodecyl Sulphate
SDS-PAGE	Sodium Dodecyl Sulphate Polyacrylamide Gel Electrophoresis
SEM	Scanning Electron Microscopy
SFs	Straight filaments
SNX	Sorting Nexin
SQSTM1	Sequestosome 1 (p62)
SR-SIM	Super-Resolution Structured Illumination Microscopy
STORM	Stochastic Optical Reconstruction Microscopy
TCA	Tricarboxylic acid cycle
TGN	Trans-Golgi-Network
TNFR1	Tumour Necrosis Factor-α Receptor 1
TNF-α	Tumour Necrosis Factor – α
TRADD	Tumour Necrosis Factor-α Death Domain
TTLL6	Tubulin Tyrosine-Like Ligase 6
Ub	Ubiquitin
ULK	unc-51 like autophagy activating kinase 1
UPS	Ubiquitin Proteasome System
UV	Ultra Violet
v-ATPase	Vacuole- ATPase
WHO	World Health Organization

Units of measurements

%	Percentage
˚C	Degrees Celsius
A	Ampere
G	Gram
kDa	Kilodalton
L	Litre
M	Molar
MDa	Megadaltons
Mg	Milligram
mL	Millilitre
mM	Milimolar
nm	Nanometer
nM	Nanomolar
µg	Microgram
µL	Microliter
µm	Micrometer
µM	Micromolar

Chapter 1: Literature Review

1.1 Introduction

Alzheimer's disease is a progressive neurodegenerative disease of the brain and the leading cause of dementia globally. It is characterised by progressive synaptic dysfunction and neuronal loss that manifests symptomatically as behavioural changes, cognitive decline and memory deficits (Nixon & Yang 2011; Musiek & Holtzman 2015). The disease is presently incurable and current treatment modalities are aimed at ameliorating symptoms and slowing down progression (Kumar *et al*. 2015; Rafii & Aisen 2015). The available treatments and available care place a large burden on the global economy with estimated cost of care to be approximately $604 billion annually (Prince *et al*. 2015).

The latest estimation of the current global prevalence is approximately 44 million, with women being affected more (Carter *et al*. 2012; Olayinka & Mbuyi 2014). A paucity exists on the exact prevalence of AD in South Africa (Lekoubou *et al*. 2014). In the South African context, it was found that up to 79% of patients were being cared for by family members, many of which had given up employment to do so (Kalula *et al*. 2010). In addition, more than 40% of the South African population live within remote rural areas, which has a negative impact on the treatment and diagnosis of dementia (de Jager *et al*. 2015). Additionally, the global prevalence is expected to increase to 135 million people by the year 2050 and will inexorably shift to developing states such as South Africa, which may place further strain on the growing economy (Prince *et al*. 2015).

The disease pathophysiology is multifactorial and highly complex, having both genetic and possible environmental causes (Reitz & Mayeux 2014; Musiek & Holtzman 2015). Multiple co-morbidities, such as diabetes and vascular damage, are associated with an increased risk for developing AD and dementia related disorders (Reitz & Mayeux 2014). Since the disease predominantly affects the aged population, advanced age remains the highest risk (Reitz & Mayeux 2014).

There are two subsets of the disease. The first being the least common early-onset Familial Alzheimer's disease (FAD), with strong genetic links; and the second, sporadic late-onset Alzheimer's disease (LOAD), which has no clear cause (Reitz & Mayeux 2014; Musiek & Holtzman 2015). Current estimations suggest that LOAD sufferers make up 95% of the total affected global population (Reitz & Mayeux 2014).

AD has an expansive prodromal stage which, in most cases, precedes symptom onset by at least 20 - 30 years (Caselli & Reiman 2012; Cash *et al*. 2013). In this time, pathological molecular changes occur within brain tissue. These changes present mainly as two physical

hallmarks which manifest as a result of perturbations in cellular proteostasis - the appropriate balance of protein synthesis, processing, and turnover in the cell – although the precise mechanisms often remain unclear (Ballatore *et al*. 2007; Lee *et al*. 2013). The first molecular hallmark is the manifestation of extracellular aggregates, commonly known as senile plaques, which are composed of the membrane associated protein β-amyloid (Musiek & Holtzman 2015). The second is the appearance of intracellular aggregates, known as neurofibrillary tangles (NFTs), which are mainly composed of the hyperphosphorylated microtubule associated protein (MAP) Tau (Nixon & Yang 2011). Tau stabilises the microtubule network, which is a crucial part of the cytoskeleton – serving as a track for organelle and vesicular transport (Avila *et al*. 2004). Under physiological conditions Tau is phosphorylated to modulate its binding affinity to the microtubule. However, under pathological conditions, Tau becomes hyperphosphorylated and prone to aggregation, causing dissociation from the microtubule (Lee *et al*. 2013). Consequently, the dissociation of Tau leads to microtubule instability and fragmentation – a process that still remains largely unknown. Multiple lines of evidence have shown that amyloid pathology is the driving force responsible for Tau hyperphosphorylation, but the exact mechanism is not fully understood (Jean & Baas 2013). Furthermore, AD affected neurons exhibit a progressive loss in axonal branching and size as a result of the microtubule loss. In fact, the microtubule network is capable of being cleaved by specialised microtubule severing enzymes (MSEs) (Jean & Baas 2013). Spastin and Katanin are the most commonly studied amongst the MSEs in neurons (Zhang *et al*. 2007). Current evidence suggest that the Tau protein may participate in the regulation of these enzyme activities by decreasing the availability of exposed microtubule surface area needed for optimal MSE binding (Baas & Qiang 2005).

Recently, proteolytic processes aiding in the clearance of protein aggregates have also been implicated in the disease pathophysiology. These proteolytic pathways include the ubiquitin-proteasome system (UPS), the autophagy-lysosomal pathway (ALP) and the endocytic-lysosomal pathway (ELP). Dysregulation of these systems has been well documented in AD pathophysiology and evidence suggests that this occurs prior to the appearance of Aβ and Tau pathology, suggesting a potential causality (Nixon & Yang 2011; Lee *et al*. 2013; Perez *et al*. 2015; Cataldo *et al*. 2000). Dysregulation of the ALP/ELP has received particular attention as they depend on the microtubule network for proper functioning. In addition, it is currently unknown what effect ALP/ELP dysregulation associated with AD has on MSE activity. Suggestively, the mechanism underlying the regulation of MSE turn-over also remains largely unknown. A potential interaction between ALP/ELP dysregulation and MSEs may provide a novel association between Tau dissociation and subsequent microtubule collapse as observed in AD.

Much about the AD aetiology still remains largely unknown, indicating the dire need for further investigation. Elucidating key intracellular pathways of neurons, such as the ALP, in homeostasis and in the AD pathogenesis may help in the development of effective therapies targeted at slowing down progression and ultimately curing the disease instead of treating the symptoms.

1.2 Protein degradation

1.2.1 Autophagy-Lysosomal Pathway

Autophagy is a major lysosomal-mediated catabolic process which is responsible for the degradation of long -lived proteins and damaged organelles. It serves as a stress-mediated response, i.e. during nutrient deprivation, but is also active under basal conditions to maintain functional turn-over of proteins and organelles, thus preventing their abnormal accumulation (Loos *et al*. 2013; Mizushima *et al*. 2008; Klionsky 2005). There are mainly three known types of autophagy; namely chaperone-mediated autophagy, microautophagy and macroautophagy (Fig 1.1). All share a common end in which the isolated protein is digested by lysosomal enzymes resulting in the release of nutrients, mainly amino acids, back into the cytosol (Mizushima *et al*. 2008; Klionsky 2005).

The lysosome is a single membrane organelle that contains a vast amount of soluble and membrane associated hydrolases with characteristic acidic pH optima, capable of digesting macromolecules and cell constituents (Nixon 2007). These hydrolases include nearly 24 different types of a protease called cathepsins, which act across a broad range of low pH's with varying catalytic classes and peptide specificities (Nixon 2007). The lysosomal lumen low pH environment is maintained by a vacuolar- ATPase (v-ATPase) membrane protein that pumps protons into the vesicle (Deter *et al*. 1967). Lysosomal dysfunction has been associated with the AD pathogenesis (Nixon *et al*. 2008).

In chaperone-mediated autophagy, the protein destined for degradation is recognised by a chaperone complex. HSC70, a protein in the chaperone complex recognises the proteins through a KFERQ motif located on the target protein peptide sequence. The substrate-chaperone complex is then transported to the lysosome where it binds to the lysosome associated membrane protein type 2A (LAMP-2A) receptor (Cuervo 2010). This binding allows for the translocation of the protein across the lysosomal membrane into the lumen, where it is degraded. In microautophagy, part of the lysosomal membrane invaginates and pinches off small vesicles containing trace amounts of cytosol and proteins, into the lysosomal lumen.

Macroautophagy, the overall contributing form to the autophagic rate of protein degradation in most cells, occurs through sequestration of large amounts of cytosolic proteins and organelles by a double membrane vesicle to form a structure termed an autophagosome. The autophagosome fuses with the lysosome releasing its contents into the lumen and allowing protein digestion to take place (Singh & Cuervo 2011).

Macroautophagy (hereafter referred to simply as autophagy) is essential for cell viability. Functional disruption of autophagy leads to the accumulation of undigested proteins, which may interact with normal molecular functions and elicit pathological responses, therefore regulation of autophagy is a tightly controlled and complex process (Hara *et al*. 2006; Nixon & Yang 2011).

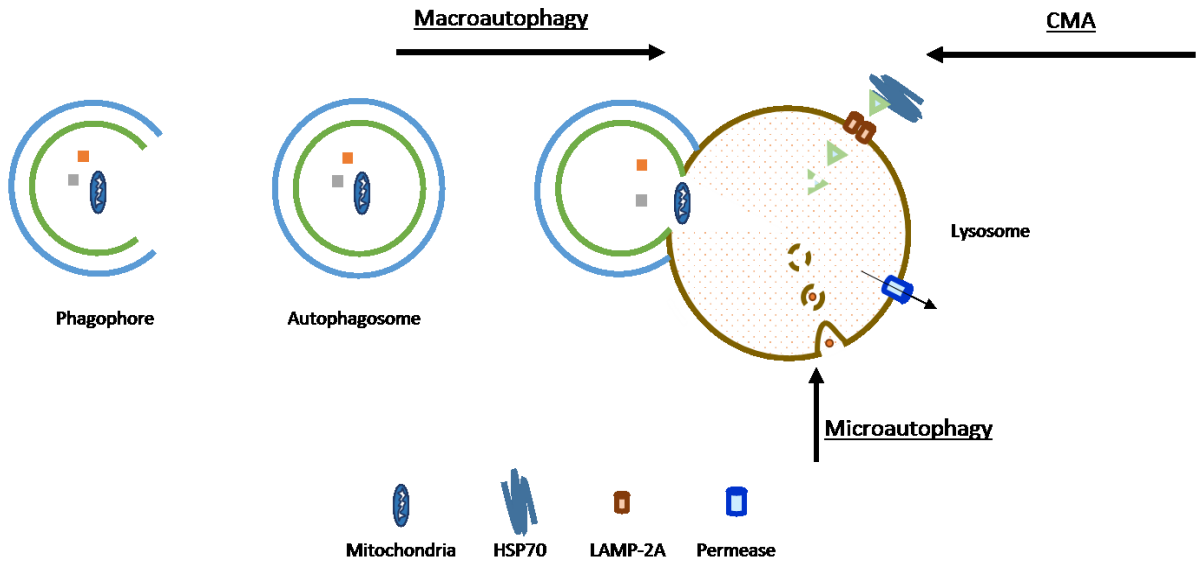

Figure 1.1: The three autophagy pathways. *Macroautophagy, Microautophagy and Chaperone-Mediated Autophagy (CMA). HSP70 – Heat Shock Protein 70; LAMP-2A – Lysosome Associated Membrane Protein type 2A.*

1.2.1.1 Autophagy regulation

Autophagy occurs at basal levels under normal homeostatic conditions, with rates higher in neural tissue (Mizushima 2003). The rate of protein degradation through autophagy is referred to as autophagic flux (Mizushima & Yoshimori 2007). Basal activation helps in the maintenance of protein quality and turn-over. The process of autophagy can be categorized into several stages, namely; induction, cargo recognition and selection, vesicle formation, autophagosome-lysosome fusion, cargo digestion, release of substrates into the cytosol and finally feedback (Loos *et al*. 2013; Loos *et al*. 2014). More than 30 genes and their variant transcripts (termed autophagy-related proteins or Atg) have been found to participate in

autophagy induction and regulation. There are several signalling mechanisms that regulate autophagy, but the most characterised is the mTOR pathway, which is activated in response to nutritional changes or periods of stress (Singh & Cuervo 2011).

The mTORC1 (mammalian target of rapamycin complex 1) protein complex and AMPK (Adenosine Monophosphate Kinase) are central to the induction of autophagy, serving as a nutrient sensor and a master regulator respectively (Loos *et al*. 2013). In a fed state mTORC1 phosphorylates and actively recruits ULK1 into a complex with Atg13 and FIP200, keeping them inactive. In a state of nutrient deprivation or stress, AMPK is activated and phosphorylates mTORC1 – relieving its inhibitory effect on ULK1. The activated ULK1-Atg13 complex shuttles Atg9 to the site of autophagosome formation. ULK1 phosphorylates AMBRA, a component of the PI3K CIII complex which triggers its recruitment to the growing isolation membrane, i.e. the phagophore (Fig 1.2) (Singh & Cuervo 2011). In addition to AMBRA, the complex consists of Beclin-1, Atg14, Vps34 and Vps15. The PI3K complex generates PI3P, which binds to its effector WD repeat domain phosphoinositide-interacting (WIPI) type 1 and 2 proteins. The binding in turn catalyses two ubiquitination-like reactions, which requires the actions of Atg9, to expand the autophagosomal membrane. In the first such reaction Atg5 forms a complex with Atg12 facilitated by Atg7 and Atg10 (Nixon, 2013) (Fig 1.2). Another complex consisting of Atg5-Atg12-Atg16 attaches to the forming membrane and, through the action of the first complex, facilitates the lipidating reaction between phosphatidylethanolamine and LC3-I. This lipidation process forms LC3-II which facilitates the closure of the membrane, forming an autophagosome (Ichimura *et al*. 2000) (Fig 1.2). Atg4 then removes LC3-II bound to the outside of the membrane and LC3-II bound to the inside of the membrane is degraded once the autophagosome binds to the lysosome to form an autophagolysosome or simply termed an autolysosome. LC3-II protein levels thus directly correlate with the number of autophagosomes in the cell (Mizushima & Yoshimori 2007)

The process reaches an end point when the cargo is degraded and amino acids and other nutrients are released back into the cytosol via permeases located on the autolysosomal membrane (Loos *et al*. 2013). Lysosomes are then reformed containing mainly hydrolases. Interestingly, it has been found that this reformation process is also regulated by mTOR (Yu *et al*. 2010).

The source of the autophagosomal membrane during autophagosome biogenesis has been the subject of contentious debate in the autophagy field. In recent years many studies have suggested that multiple organelles are the source of the membrane, including the endoplasmic reticulum (ER), plasma membrane and even recycling endosomes (Shibutani & Yoshimori 2014). However, the general consensus in mammals is that it is likely the ER which is the main

source, although the exact molecular mechanisms underlying its role in autophagosome membrane biogenesis are yet to be elucidated (Shibutani & Yoshimori 2014)

Furthermore, autophagy may also occur in a selective or non-selective manner. In selective autophagy, p62 (also known as sequestersome 1/SQSTM1) acts as an adapter protein between LC3-II residues on the forming phagophore and targeted poly-ubiquinated proteins (Klionsky 2005; Singh & Cuervo 2011). Since p62 and LC3-II are both degraded during autophagy, their lysosomal-dependent turnover has emerged as a measure of relative autophagic flux which can reliably be determined through Western blot analysis. Although p62 is an indicator of selective autophagy, deducing results based on protein selectivity becomes complicated since it is also an autophagy target (Bjorky *et al*. 2005; Mizushima & Yoshimori 2007; Rubinsztein *et al*. 2009).

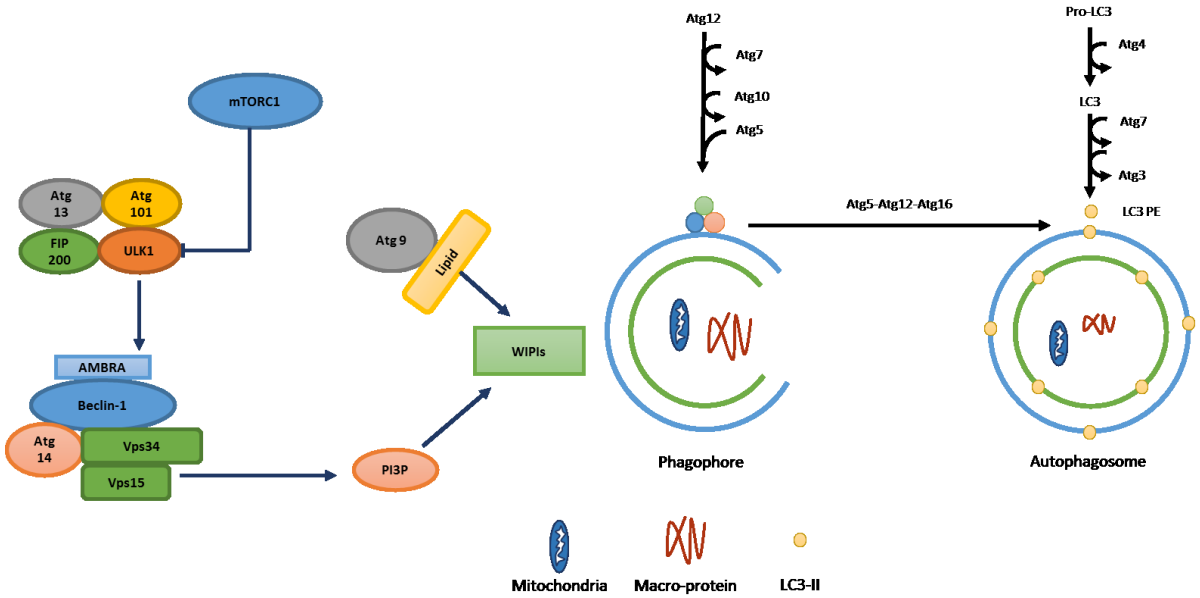

Figure 1.2: The regulation of macroautophagy (autophagy). *Induction, elongation of the autophagosomal membrane (phagophore) and vacuole formation. Atg – Autophagy Related Protein; ULK - unc-51 like autophagy activating kinase 1; FIP - focal adhesion kinase family interacting protein; mTORC1 - mammalian Target Of Rapamycin Complex 1; AMBRA - Activating Molecule in Beclin 1-Regulated Autophagy; VPS - vacuolar protein sorting; PI3P - Phosphatidyl-Inositol-3-Phosphate; WIPI - WD-repeat protein interacting with phosphoinositides. Adapted from Nixon 2013*

1.2.2 Endosome- Lysosome Pathway

Closely linked to autophagy is the endocytic pathway, in which cargo-receptor molecules from the cell surface are internalised after which they are either recycled, modulated or ultimately digested (Fig. 1.3) (Hu *et al*. 2015). It is composed of a series of vesicular structures that differ according to their localisation and function within the pathway. They are broadly organised into three categories namely early endosomes (EEs), recycling endosomes (REs) and late

endosomes/multi-vesicular bodies (LEs) (Huotari & Helenius 2011). The pathway is initiated by the internalisation of cargo and the formation of EEs, which have two potential trafficking destinies, either ending in the recycling or the digestive pathway.

1.2.2.1 Recycling Pathway

EEs usually form from clathrin coated pits on the plasma membrane, budding off internally to form vesicles. These vesicles can then fuse with one another or ultimately with pre-existing EEs, a process that is facilitated by the GTPase, Rab5 (Hu *et al*. 2015). EEs form with a low intraluminal pH to facilitate receptor ligand dissociation, thereby acting as a sorting station by allowing the newly freed receptors to be trafficked back to the plasma membrane or the Trans-Golgi-Network (TGN) via REs and Retromer complexes respectively (Hu *et al*. 2015; Hunt & Stephens 2011; Huotari & Helenius 2011). The Retromer is a protein complex that exists for exclusive retrograde transport of cargo between the TGN and endosomes. It is composed of sorting nexins (SNXs) and cargo recognition trimers, such as Vps26–Vps29–Vps35, that recognise proteins on the cytosolic membrane of endosomes (Huotari & Helenius 2011). When trafficked from EEs to REs, the process is accompanied by an association of Rab5 to that of Rab4 and Rab11. Of note, the majority of cargo internalised by the endosomes in mammalian systems is recycled back to the plasma membrane (Steinman *et al*. 1983).

1.2.2.2 Digestion Pathway

EEs destined for digestion are trafficked, while maturing into late endosomes, from the periphery to the cell centre. A number intraluminal vesicles (ILVs) develop, an important maturation step for the transition into late endosomes/multi-vesicular bodies. The lumen also becomes increasingly acidic with the help of v-ATPase pumps located at the endosomal surface. Maturation is accompanied by a change of association with Rab5 to Rab7, a process termed “Rab conversion”. LE trafficking usually ends with lysosomal fusion and the digestion of their cargoes, but may also lead to fusion with autophagosomes prior to lysosomes, to form hybrid structures termed amphisomes (Nixon 2007). Additionally, LEs may also exchange ILVs with each other or with lysosomes through a “kiss and run” action before full lysosomal fusion takes place (Huotari & Helenius 2011; Nixon 2007).

Digestion of late endosomes is tightly controlled by the ESCRT (endosomal sorting complex required for transport) systems, which sort ubiquitin tagged proteins for degradation. The ESCRT machinery has four distinct complexes; namely ESCRT-0, -I, -II and –III. It acts in a “conveyor belt model” by sequentially sorting ubiquinated proteins into LEs starting with ESCRT -0 and ending with –III, each having a distinct function in the system (Hu *et al*. 2015).

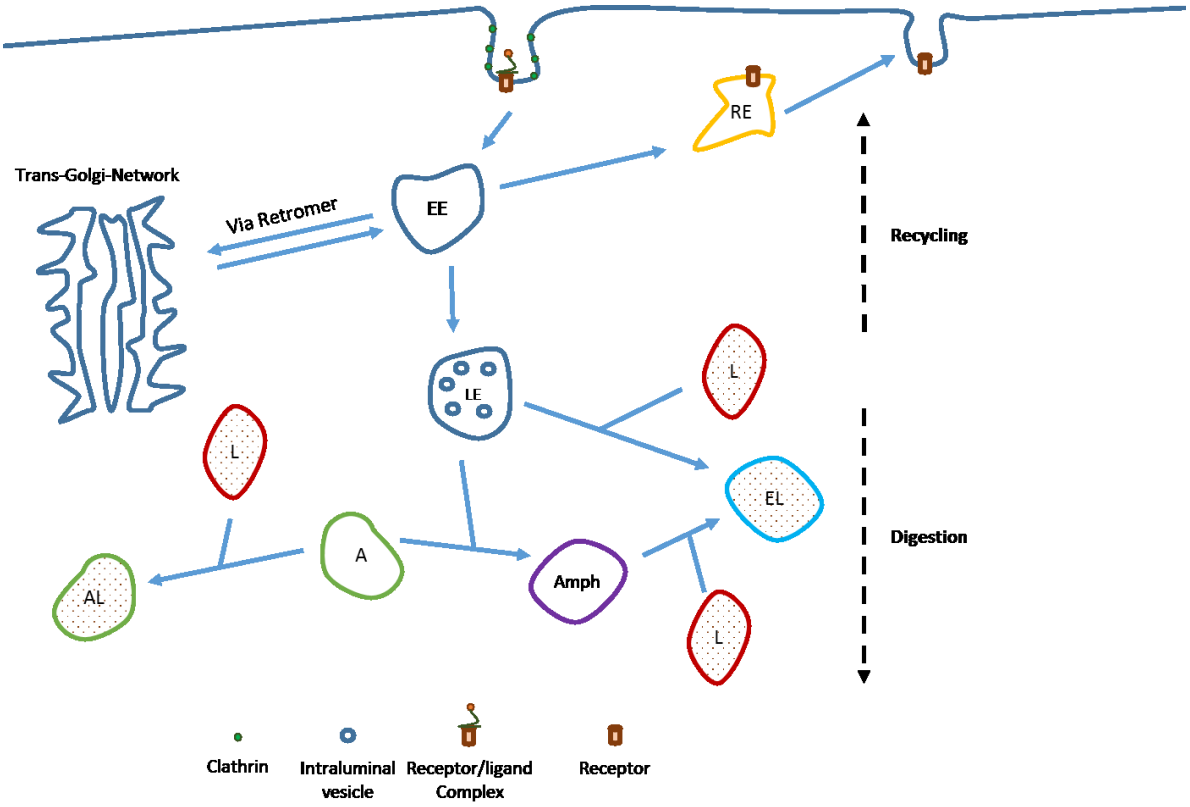

***Figure 1.3: The endosomal pathway**: The process of endocytosis (A) Autophagosome; (AL) Autophagolysosome; (Amph) Amphisome; (EE) Early Endosome; (EL) Endolysosome; (LE) Late Endosome; (L) Lysosome; (RE) Recycling Endosome. Adapted from Hu et al. 2015*

1.2.3 UPS

The third main proteolytic process is the UPS (Fig. 1.4). This highly regulated process initiates a specific form of proteolysis by targeting small proteins. Only proteins conjugated to a poly-peptide ubiquitin molecule (Ub), through a series of reactions, are degraded.

The conjugation of the substrate to Ub is regulated through three types of enzymes; namely E1, E2 and E3 ligases. Ub is first activated by E1 type enzymes, through the hydrolysis of ATP. During activation a high energy thiol-ester Ub-AMP intermediate is formed. The E1 enzymes are the least physiologically regulated, but play an important role in maintaining the threshold of UPS initiation. The two most commonly known enzymes to initiate ubiquitination are UBA1 and UBA6 (Schulman & Wade Harper 2009). Activated Ub is transferred to an E2 type enzyme which then facilitates the conjugation of Ub to the substrate through E3 ubiquitin ligases. The human genome encodes for 40 isoforms of E2 type enzymes, indicating some degree of substrate specificity. E3 type enzymes ligate the Ub-molecule to a Ɛ-amino group of a lysine residue on the substrate. A poly-Ub chain grows by conjugation of a new Ub molecule onto one of seven different lysine residues on the first Ub. E3 type enzymes are

highly diverse with an estimated 600 isoforms - a number which may indicate their determining presence in UPS-mediated substrate selectivity (Lee *et al*. 2013).

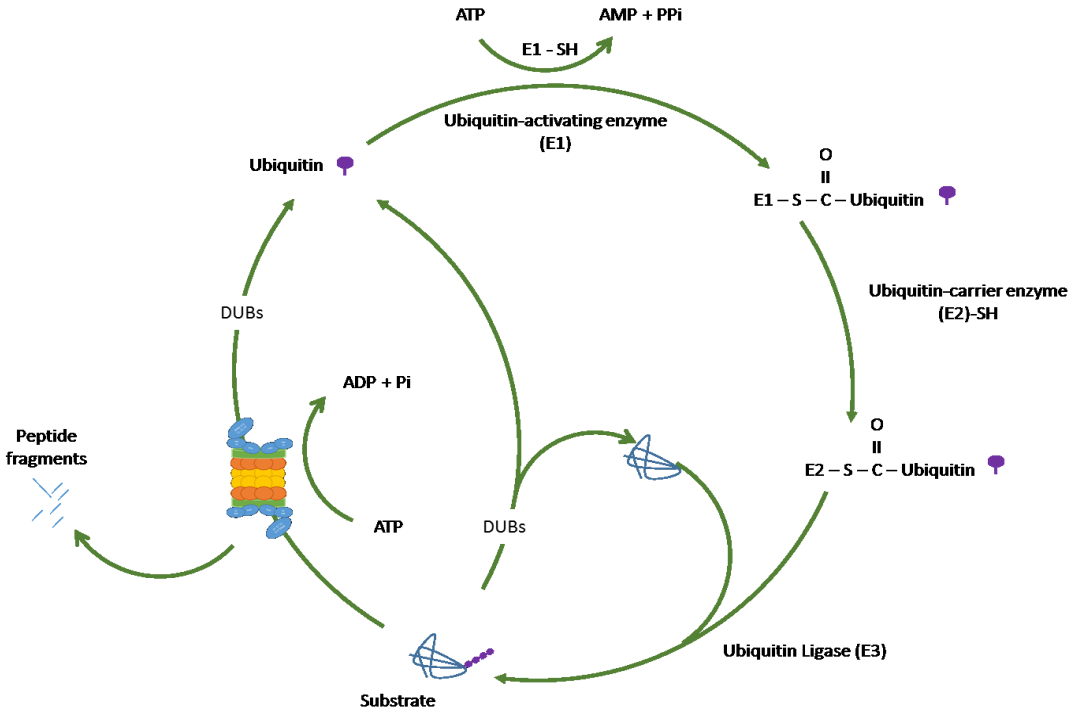

Figure 1.4: The UPS. *E1 enzymes conjugate with Ub molecules, allowing for their activation. The E1 enzyme then transfers the activated Ub molecule to the E2 enzyme which translocates the activated Ub molecule to the substrates that require proteasomal degradation. Finally the E3 enzyme targets the polyubiquitinated substrate to the 26s proteasome for substrate degradation. DUBs recycle Ub molecules as well as de-ubiquitinate erroneously tagged substrates. Adapted from Hegde 2010*

The poly-ubiquinated substrate is degraded through an ATP-dependent reaction by a proteolytic complex known as the 26S proteasome. The 26S proteasome is a ~2.5 MDa holoenzyme structure composed of multiple subunits. Ubiquitin is not degraded, but the Ub-chain is disassembled by de-ubiquitinating enzymes (DUBs) and subsequently recycled into the cytosol. In addition, DUBs can disassemble Ub-chains on erroneously tagged substrates to prevent their degradation (Hegde & Upadhya 2011; Lee *et al*. 2013).

The 26S holoenzyme (Fig 1.5) is composed of a 20S cylindrical catalytic core and two 19S regulatory subunits attached to either end of the core. The 20S subunit consists of two outer rings with seven α subunits (α1-α7) in each ring and two inner rings consisting of seven β subunits (β1-β7) (Fig. 1.5). The catalytic activity is provided by three of the seven β subunits (β1, β2 and β5) with active sites at their N-termini, which are located on the inside of the core particle catalytic chamber (Hegde & Upadhya 2011) (Fig. 1.5). The opening of the chamber has a pore size of ~13Å in diameter. Unfolding occurs through the action of ATPases located

at the base of the 19S regulatory subunit. The 19S is composed of 6 ATPase subunits; Rpt1-Rpt6 and four non-ATPase subunits; Rpn1, Rpn2, Rpn10 and Rpn13. Rpn10 and Rpn13 act as receptors that recognise the ubiquinated substrate. The 19S also has a "lid" consisting of non-ATPase subunits; Rpn3, Rpn5, Rpn6-9, Rpn11-12 and Rpn15). Rpn11 and Rpn12 provide structural integrity to the complex (Lee *et al*. 2013; Weissman *et al*. 2011) (Fig. 1.5). In addition, Rpn11 and Rpn13 can also act as DUBs that facilitate the de-ubiquitination of the substrate.

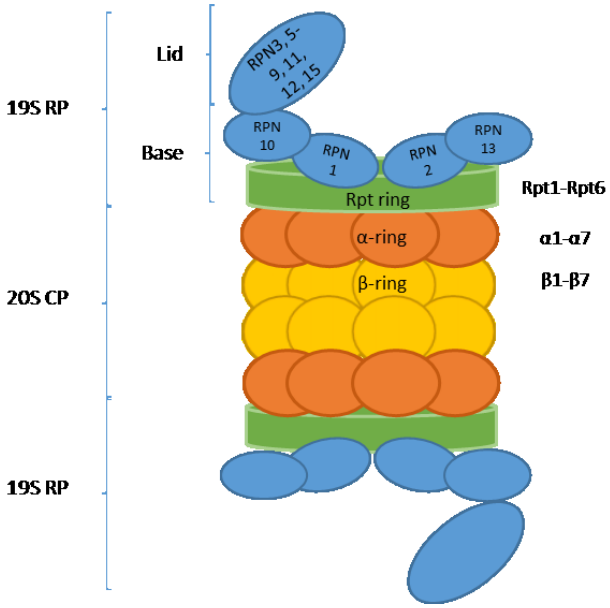

Figure 1.5: The 26S proteasome. *The 26S proteasome consists of a 20S core subunit and two 19S regulatory subunit on either end. Adapted from Weissman et al. 2011*

1.2.4 Proteostatic Perturbations in AD

In addition to the Aβ plaques and NFT aggregates observed in AD brain tissue are gross focal swellings of neuronal axons and dendrites, which are termed dystrophic neurites. When viewed with an electron microscope these neurites appear to be severely impacted, displaying electron dense lysosomal bodies containing undigested protein (Fig. 1.6). This has been attributed to dysfunction of both the ALP and ELP (Nixon & Yang 2011; Nixon *et al*. 2005; Cataldo *et al*. 2000). ALP and ELP dysfunction have in fact been linked to Aβ pathology, as endosomes and autophagosome are known sites of Amyloid Precursor Protein (APP) production and modulation (Perez *et al*. 2015; Cataldo *et al*. 2000). The ALP and UPS are both important in the turn-over of Tau and dysfunction of these systems have been shown to promote Tau aggregation (Hamano *et al*. 2008; Hamano *et al*. 2009; Wang & Mandelkow 2012; Lee *et al*. 2013) Of note, lysosome-related dysfunction occurs very early in the disease,

preceding both Aβ and Tau pathology, which may suggest a major role for lysosomal dysfunction in the manifestation of AD (Perez *et al*. 2015; Cataldo *et al*. 2000). In fact, Aβ has been found to localise in autophagosome membranes and the pathological induction of autophagosome synthesis as well as defective autophagosome clearance have both been suggested as primary sources of Aβ in AD (Nixon 2007).

Additionally, UPS dysfunction has also been linked to Tau pathology in late AD. The available evidence suggests that NFT aggregation may in fact be the cause of this dysfunction rather than a consequence. It is theorised that aggregated and hyperphosphorylated Tau blocks the pores of the proteasome, thus rendering it dysfunctional (Lee *et al*. 2013).

Moreover, the build-up of these vesicles containing undigested protein impacts normal axonal transport of other vesicles and organelles, such as autophagosomes and mitochondria, along the microtubule network (Lee *et al*. 2011; Torres *et al*. 2012). However, the exact molecular mechanisms leading to the onset of these axonal transport deficits remain elusive.

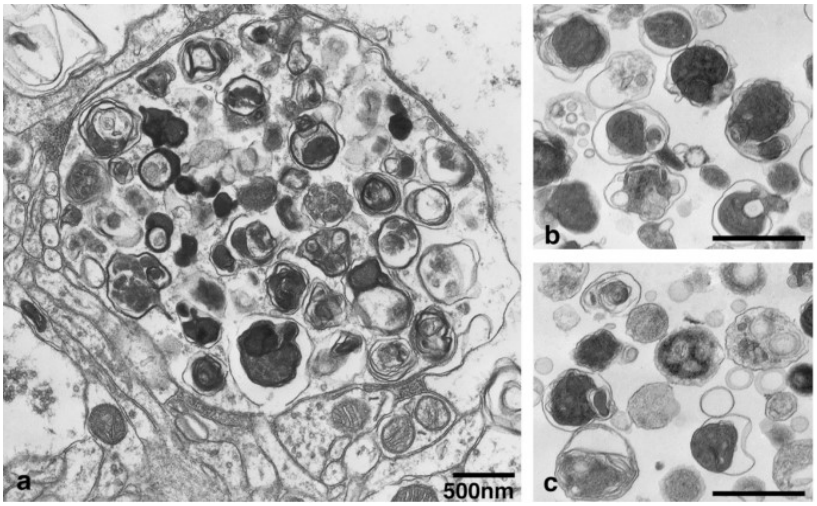

Figure 1.6: Ultrastructural appearance of autophagic vacuoles in AD brain*. (a) "Ultrastructural appearance of autophagic vacuoles in AD brain". (b, c) "Highly purified subcellular fractions from mouse liver. Dystrophic neurites contain abundant vesicles with a range of distinct morphologies similar to those of AVs highly purified from mouse liver by a well-established subcellular fractionation techniques". Source:* Nixon *et al*. 2005.

1.3 Microtubulin Network

1.3.1 Microtubulin Dynamics

The microtubule system is an essential constituent of the cytoskeleton, which plays a major role in vesicular transport, neuronal morphogenesis, cell migration, intracellular organisation and differentiation (Avila 1992). It is a hollow tubular structure, with a diameter of approximately 24 nm, composed of α- and β-tubulin heterodimers (Avila 1992). The two ends are structurally differentiated into positive and negative poles, with β-tubulin orientated towards the former and α-tubulin towards the latter (Fig.1.7). Polymerisation is faster on the positive end which allows extension into the cytoplasm whilst the negative end is anchored to a nucleated area known as the MTOC (microtubule organising centre) located near the centrosome of the cell (De Forges *et al*. 2012). Anchoring and capping of the negative pole requires another tubulin isomer known as γ-tubulin, which forms the γ –TuRC (γ -tubulin ring complex). As such, polymerisation from the negative end is rarely, if at all observed in vitro (van der Vaart *et al*. 2009). Polymerisation of the microtubule occurs in a very dynamic fashion, a process termed dynamic instability (Mitchison & Kirschner 1984). This behaviour entails phases of growth and shrinkage of the polymer separated by periods of catastrophe, i.e. the transition from growth to shrinkage, and rescue, i.e. the transition from shrinkage to growth. To facilitate polymerisation, GTP bound to β-tubulin, is hydrolysed. The short period between GTP hydrolysis and polymerisation allows for the formation of a GTP-tubulin cap which stabilises the process. A loss of the GTP-tubulin cap results in rapid depolymerisation, i.e. catastrophe.

The microtubule determines the polarity of neuronal cells in higher eukaryotes. In the axon, all microtubules have a positive-end orientation, whereas the dendrites have mixed orientations (De Forges *et al*. 2012). Specialised motor proteins known as Kinesins and Dyneins facilitate the transport of cellular machinery along the microtubule. In addition, polarised arrays of microtubules are generated through transport of microtubule polymers from the MTOC in a Dynein-dependent manner (Ahmad & Baas 1995).

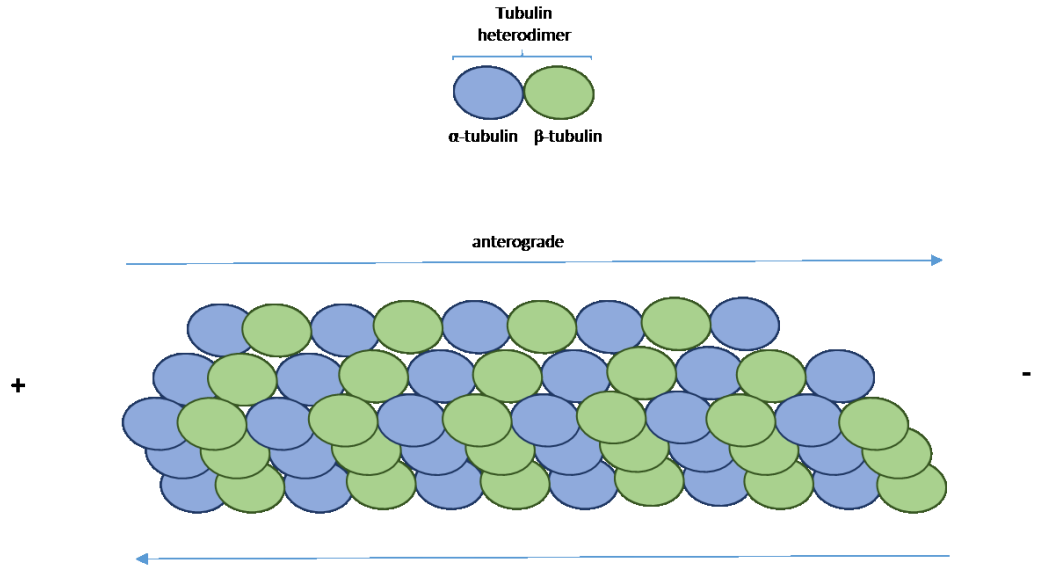

Figure 1.7: The structure of the microtubule. *The microtubule consists of αβ-heterodimer microtubulin. Indicated are the directions of transport along the network.*

1.3.1.1 Microtubule Regulation

During cell growth and branch formation, microtubules are severed at specific sites to generate shorter repeats through the actions of specialised microtubule severing enzymes (MSEs). Such repeats are subsequently transported via motor proteins to the site of branch formation and are polymerised throughout the newly grown neurite. Severing generally occurs through the action of mainly two enzymes; namely Katanin and Spastin (discussed further in 1.3.2). Generation and transport of these short microtubule repeats is critical to the growth of the microtubule network and the viability of the cell (Yu *et al*. 2008).

Microtubules are also prone to post-translational modification such as tyrosination, glutamylation and acetylation. Tyrosination of the microtubule is the result of the enzyme tubulin-tyrosine ligase, which acts by catalysing the addition of a tyrosine residue to the C-terminal of the tubulin tail (De Forges *et al*. 2012). Tyrosination of tubulin has been shown to induce a positive effect on stabilisation, by recruiting stabilising factors and affecting destabilising MAP binding affinity (Wloga & Gaertig 2010). Polyglutamylation of the microtubule has been found to increase binding affinity of not only several neuronal MAPs and motor proteins, but also the recruitment of Spastin (Bonnet *et al*. 2001; Lacroix *et al*. 2010). Acetylation occurs on the α-subunit of the microtubule heterodimer and is associated with increased binding for motor proteins to the microtubule (De Forges *et al*. 2012). Acetylated tubulin has also long been associated with stability, but recent evidence suggests that the acetylation may have a modest or no effect at all on stability (Howes *et al*. 2014; Quinones *et al*. 2011). In fact, it was shown that the microtubule binding of Histone deacetylase 6 (HDAC6), a deacetlyating enzyme, showed stabilizing effects rather than acetylation itself (Asthana *et*

al. 2013). It has also been shown that the fusion between autophagosomes and lysosomes is dependent on the association with acetylated microtubulin, which usually occurs close to the centrosome of the cell (Schulze 1987; Xie *et al*. 2010). Although the role of acetylation in tubulin stability has been a topic of debate, the consensus agrees that acetylated tubulin is a suitable marker for stable microtubulin.

Microtubules are further extrinsically regulated through MAPs, which help facilitate polymerisation of the microtubule by stabilising and destabilising the process. The most abundantly studied stabilising MAPs are the neuron-specific Tau (discussed later in 1.3.1), MAP2 and the non-neuronal MAP4 (De Forges *et al*. 2012).

Lastly, other known important classes of stabilising MAPs are plus end tracking proteins (+TIPs), that dynamically track the polymerisation of the positive end of the microtubule, and destabilising MAPs, such as stathmin and SCG10 that are important for neuronal growth (Akhmanova & Steinmetz 2010; Grenningloh *et al*. 2004). These proteins will, however, not be discussed for the purposes of this review as it is beyond the scope of the research project.

1.3.2 MAPs

1.3.2.1 Tau

Tau is a hydrophilic structural MAP that is predominantly localises in the axons of neurons. Tau supports the dynamic polymerisation of the microtubule as well as allowing post-translational modification of the microtubule network. There are six isoforms of Tau, which are all derived from the Tau gene (MAPT) located on chromosome 17q21, through alternative mRNA splicing (Fig 1.8). These isoforms differ from each other in length, domain composition and post-translational modifications. Only 4 isoforms are expressed in the adult brain (Avila *et al*. 2004).

The Tau protein structure is characterised by a projection domain containing the amino-terminal and the microtubule binding domain containing the carboxyl-terminal. The projection domain contains a region composed of acidic residues with one, two or no insertions (N) of ~29 amino acid long repeats (depending on the isoform) and a proline-rich region (Lee *et al*. 2013). The microtubule binding domain comprises of three or four semi-conserved “pseudo-repeats”(R) of ~31 amino acids in length. Different isoforms contain either repeats R1-R4 or R3-R4. In addition, the projection domain protrudes away from the microtubule surface, possibly as the result of an electrostatic repulsion (Ballatore *et al*. 2007).

Tau is also subject to post-translational modifications including glycosylation, ubiquitination, acetylation and phosphorylation, which occurs on the serine/threonine residues. There are

~79 serine/threonine phosphorylation sites on the longest isoform of Tau which has a 441 amino acid sequence. Phosphorylation of Tau occurs through the action of various enzymes including cdk5, GSK3-β, p38 and JNK (Flaherty *et al*. 2000). Phosphorylation regulates the binding affinity of the Tau protein to the microtubule – the more phosphorylated, the less binding affinity it has for microtubulin. Phosphorylation is also developmentally regulated - foetal neurons have a high degree with the overall rates decreasing with age (Stoothoff & Johnson 2005). Hyperphosphorylated Tau is implicit in the formation of NFTs (Armstrong 2014).

Figure 1.8: The 6 isoforms of the Tau protein. *The different Tau isoforms vary in length and amino acid composition. N – N-terminal; N1/N2 – Acidic residue insertion; PD – Proline rich region; R – Pseudorepeat insertion; C – C-terminal.*

1.3.3 Tau Pathology and Neurofibrillary Tangles

In AD, dissociated and abnormally hyperphosphorylated Tau termed “pretangle material”, initially accumulates in a non-fibrillar form (Braak & Del Tredici 2015). Pretangles arrange in a β-sheet conformation to form paired helical filaments (PHF) or straight filaments (SF). NFTs almost exclusively consists of PHFs, but also contain other proteins such as unphosphorylated Tau, MAP1, MAP2, as well as ubiquitin molecules (Lee *et al*. 2013; Alonso *et al*. 1994).

The intracellular levels of hyperphosphorylated Tau increase before NFT formation in AD affected brains (Bancher *et al*. 1989). It is not entirely known what initiates this hyperphosphorylation of Tau, but dysregulated activity of specific protein kinases and phosphatases have been found to facilitate this modification. The identified kinases include GSK3β, cdk5, MARK, Fyn, and phosphatases PP2A and PP2B (Plattner *et al*. 2006; Kimura

et al. 2014; Mandelkow *et al*. 2004; Wang *et al*. 2007). Whether an increase in activity of phosphorylating kinases or a decrease in dephosphorylating enzymes contributing to Tau hyperphosphorylation is not known, as evidence for both of these scenarios has been identified in AD brain tissue (Wang *et al*. 1995; Wang *et al*. 1996; Wang *et al*. 2007).

In FAD, Aβ aggregation is a characteristic initial event that leads to hyperphosphorylation of Tau downstream and it appears that the toxic effects of Aβ pathology are dependent on the missorting and hyperphosphorylation of Tau (Armstrong 2014; Zempel *et al*. 2013). Tau aggregates also correlate better with the clinical progression of AD as opposed to Aβ (Braak & Braak 1991).

Tau pathology can also occur in the absence of Aβ aggregation in diseases termed Tauopathies. Frontotemporal Dementia with Parkinsonism linked to chromosome 17 (FTDP-17) is one such Tauopathy that is thought to result from a mutation in the MAPT gene, which produces mutated Tau (P301L) that is prone to spontaneous aggregation and NFT formation (Boxer *et al*. 2013).

It is thought that NFTs elicit their toxic effect by impairing axonal transport, because of the role Tau plays in microtubulin dynamics and the cytoskeleton changes observed in early AD. Particularly the “disintegration’ of microtubulin networks – is a mechanism that is still poorly understood (Braak *et al*. 1994; Baas & Qiang 2005). It has been suggested that there is an increase in Tau protein levels and subsequent binding on the microtubule. This causes anterograde transport to be blocked by limiting binding of motor proteins (Baas & Qiang 2005). The cell then hyperphosphorylates Tau to combat this effect and allows motor protein binding, but in doing so also exposes the network to destabilising proteins such as MSEs and stathmin (Baas & Qiang 2005; Mandelkow *et al*. 2004). Furthermore, Tau appears to induce alterations in NMDA receptor phosphorylation by interfering with the action of the kinase Fyn (Ittner & Götz 2011).

What causes the initial accumulation of Tau remains to be determined, however since Tau is a substrate of both the ALP and UPS pathways, proteostatic perturbations are likely to play a key role in this process (Lee *et al*. 2013; Wang & Mandelkow 2012; Liu *et al*. 2009; Hamano *et al*. 2008).

1.3.4 Microtubule severing enzymes

Microtubule severing enzymes (MSEs) are specialised proteins capable of cleaving the microtubule (Yu *et al*. 2008). They function to generate shorter microtubule repeats, which are required and transported via motor proteins to sites of branch formation, but are also critical

to the maintenance of cellular homeostasis (Yu *et al*. 2005; Yu *et al*. 2008). Spastin and Katanin are the most studied MSEs in neurons and have received much attention in recent years, especially in their potential involvement in microtubulin instability associated with AD pathogenesis (Jean & Baas 2013).

1.3.4.1 Katanin

Katanin is a heterodimeric protein comprising of two subunits, P60 and P80, which are thought to form a hexameric ring around the microtubule. The P60 subunit cleaves the microtubule lattice by hydrolysing ATP, whilst P80 targets it to the centrosome for other processes (Yang *et al*. 2013). It was recently shown that Katanin p60 in fact severs the lattice by generating a mechanical force between the hexameric pore and the acidic tail residues of both α and β tubulin dimers (Fig 1.9) (Johjima *et al*. 2015). Severing of the lattice creates short microtubules within cellular compartments, such as in the axon or dendrites for branch formation. It was expected that both subunits were equimolar in cytosolic concentration, but current research indicates that concentrations of both proteins vary significantly relative to each other, be it the developmental state of the organism, tissue type and/or cellular localisation. Additionally, it has been found that P60 can sever microtubules in the absence of P80, but may operate more efficiently in its presence (Yu *et al*. 2005). Protein levels are higher during development, but diminish over time. Neurons are known to have a higher concentration of Katanin relative to other tissue types. In addition, cytosolic protein levels are higher during axon formation and diminish once their targets are reached, indicating a significant role in axon generation (Yang *et al*. 2013; Karabay *et al*. 2004).

The relative protein levels of Katanin within neurons at any time should theoretically sever all the microtubules within the cell – which questions how its activity is regulated. Protein levels are higher in mitotic cells compared to interphase cells, suggesting a link between Katanin regulation and phosphorylation (McNally *et al*. 2002). However, Katanin has so far not been found to be a target of phosphorylation. Thus, it is likely that phosphorylation of other proteins regulates binding activity of Katanin, particularly those interacting with the microtubule. In extracts of xenopus eggs arrested in interphase, it was revealed that XMAP4, the human analogue of MAP4, acts as an inhibitor of Katanin severing activity (Vale 1991). Of note, MAP4 is a major non-neuronal MAP and shares very similar microtubule-binding domain structure with neuronal MAP2 and Tau (Dehmelt & Halpain 2005). Importantly, in neurons Tau protects the microtubule from severing by Katanin, by only allowing severing at sites of branch formation where Tau has dissociated (Chen *et al*. 2008; Qiang *et al*. 2006). Another study

revealed that Katanin severing is enhanced when α-tubulin is acetylated and decreased upon deacetylation, suggesting another potential regulatory mechanism (Sudo & Baas 2010).

It remains unknown how the turnover of Katanin is regulated. A study conducted in cultured hippocampal neurons described a molecular relationship between Katanin, HSP70 and USP47, a ubiquinating enzyme. It is suggested that USP47 plays a role in the control of axonal growth by counteracting CHIP (C terminus of Hsp70-interacting protein)-mediated ubiquitination and destabilisation of Katanin p60. A potential complex-interaction between Katanin p60 and USP47 is yet to be elucidated (Yang *et al*. 2013).

Currently there are no known genetic mutations or specific diseases that have been linked to Katanin expression or activity.

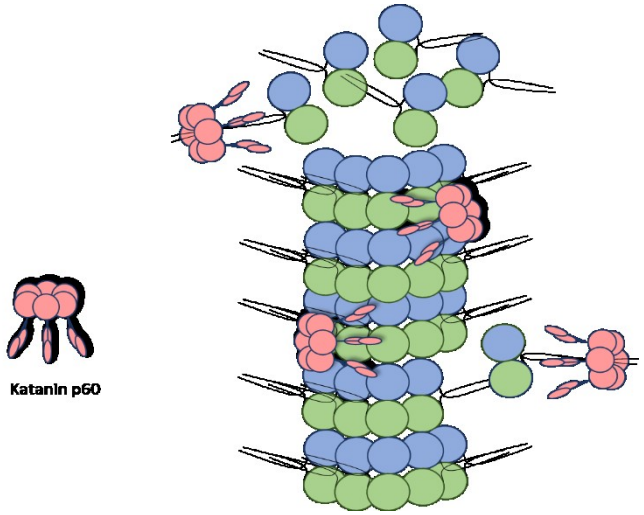

Figure 1.9: Katanin p60 mechanism of action. *Katanin p60 severs the lattice by generating a mechanical force between the hexameric pore and the acidic tail residues of both α and β tubulin dimers. Adapted from Johjima et al. 2015*

1.3.4.2 Spastin

Spastin in its active state, similarly to Katanin, is thought to form a homohexameric ring around the microtubule dimer acidic tails and to induce mechanical severing through ATP hydrolysis (Fig 1.10) (Eckert, Link, *et al*. 2012; Eckert, Le, *et al*. 2012). The protein is encoded by the SPG4 gene (Claudiani *et al*. 2005). Mutations of SPG4 are the cause of 40% of cases of Autosomal Dominant Hereditary Spastic Paraplegia (AD-HSP). HSP is a genetically heterogeneous disease characterised by retrograde axonal degeneration of corticospinal tracts as well as posterior columns, which leads to weakness and spasticity of the lower limbs (Charvin *et al*. 2003; Papadopoulos *et al*. 2015). Spastin is ubiquitously expressed, but most abundantly in neural tissue, with the exception of glial cells (Dráberová *et al*. 2011). Two

isoforms, M87 and M1, exist through the translation of alternative start codons of the SPG4 gene. M1 is the full length 616-amino form and M87 is the truncated form, lacking the N-terminal 86 amino acid residues (Claudiani *et al*. 2005). M87 is cytosolically localised, and is usually more abundant than M1, which favours ER and nuclear localisation (Claudiani *et al*. 2005). However, M1 appears to be the predominant isoform in neurons, particularly in the adult spinal cord (Solowska *et al*. 2008).

Like the other proteins in this family, Spastin has diverse cellular functions, but recently lipid metabolism and activity in membrane modelling has also been reported, specifically in endosome formation, sorting and trafficking (Lumb *et al*. 2012; Connell *et al*. 2009; Papadopoulos *et al*. 2015). Spastin interacts with ESCRT-III, which controls the formation and sorting of cargo into internal vesicles within late endosomes/multi vesicular bodies. It was suggested that Spastin cleavage of tubules of early endosome compartments is required for functional cargo sorting and trafficking. This was indeed suggested when cells knocked down for Spastin showed an increase in early endosomal tubulation and decreased sorting (Allison *et al*. 2013). This may explain the swollen axons and defective retrograde and anterograde vesicle transport, which results in cargo accumulation seen in models and patient derived tissues with SPG4 mutations (Tarrade *et al*. 2006; Kasher *et al*. 2009). Of note, this shows an insidious similarity with the gross accumulation of vesicles containing undigested protein observed in AD affected neurons (Nixon & Yang 2011).

Spastin has been shown to preferentially bind to and sever poly-glutamylated tubulin. Amyloid-β induced Tau missorting has directly been shown to increase tubulin poly-glutamylation in dendrites by recruiting TTLL6 (tubulin tyrosine like ligase 6), the enzyme that confers the polyglutamylation modification (Lacroix *et al*. 2010). The mechanism underlying Tau missorting and subsequent increase in TTLL6 recruitment remains to be elucidated (Zempel & Mandelkow 2014). Spastin, unlike Katanin, can sever the microtubule independent of the presence of Tau presence on the lattice (Sudo & Baas 2010).

Although partial knowledge exists on Spastin activity and regulation, much remains unknown, particularly how protein turn-over is controlled and if autophagy plays a role in this regard.

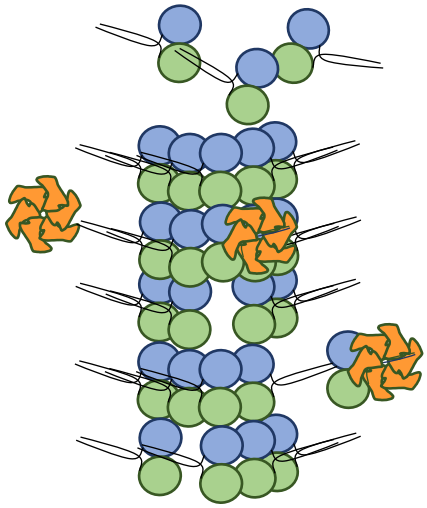

Figure 1.10: Spastin mechanism of action. *Spastin forms a homohexameric ring around the microtubule dimer acidic tails and induces mechanical severing through ATP hydrolysis. Adapted from Eckert, Link, et al. 2012.*

1.3.5 Molecular motor proteins

Transport of cytoplasmic cargo along microtubules is critical to the functioning of cells, especially in neurons. Defects in transport have clearly been identified in multiple neurodegenerative pathologies (Dixit *et al*. 2008; Kasher *et al*. 2009; Lee *et al*. 2011). Intracellular transport is mainly carried out by two types of molecular motors; namely Dynein, usually a retrograde motor protein operating from positive to negative ends of the microtubule, and Kinesin, an anterograde motor protein operating from negative to positive ends of the microtubule. They are also part of the AAA enzyme family and hydrolyse ATP to generate force for movement. Both have numerous isoforms with their own cargo specificities and adaptor proteins (Goldstein & Yang 2000).

Dynein is the larger of the two proteins and functions as the main retrograde motor. In order to function fully, Dynein requires a large multiprotein complex called dynactin that facilitates its processivity and possibly regulates its activity (Goldstein & Yang 2000; Dixit *et al*. 2008). Although mainly a retrograde motor, Dynein is also involved in the bidirectional transport of newly generated shorter microtubules, particularly to sites of new growth (i.e growth cones) (Myers *et al*. 2006; Ahmad *et al*. 2006).

Dynein is critical in the transport and fusion of autophagosomes and lysosomes along the microtubulin network (Jahreiss *et al*. 2008). Altered Dynein function leads to the accumulation of autophagosomes, highlighting the ALP reliance on Dynein based transport (Yamamoto *et al*. 2010). Furthermore, it seems that MAPs (specifically Tau) impose a spatio-temporal regulation on Dynein and Kinesin movement. Tau binding on the microtubule acts as a spatial

obstacle for the motor proteins and prevents movement of cargo (Mandelkow *et al*. 2004; Baas & Qiang 2005). When encountering this “roadblock”, Dynein appears to move in the opposite direction while Kinesin will detach from the microtubule. Kinesin also appears to be more affected by these obstacles than Dynein (Dixit *et al*. 2008; Baas & Qiang 2005).

Furthermore, both Kinesin and Dynein have been found to transport vesicles that contain amyloid precursor protein (APP). Subsequent studies have shown that this process is dependent on the actions of presenelin, a transmembrane protein involved in amyloid metabolism (Gunawardena *et al*. 2013).

1.4 Amyloid Metabolism

Although not a key focus in this study, the role of amyloid-β requires particular focus as it is thought to play critical role in the AD pathogenesis. In 1992, the scientists Hardy and Higgins were so convinced that Aβ was the cause of AD that they postulated the amyloid cascade hypothesis, which details disease progression with amyloid beta deposition as the initiator of the pathology (Hardy & Higgins 1992). Amyloid Precursor Protein (APP), as the name suggests, is the precursor to Amyloid-β (Aβ), the protein that mainly composes the senile plaques observed in AD. The APP gene is located on chromosome 21 (Musiek & Holtzman 2015).

Although the physiological function of APP is not entirely clear, it has been shown to have putative roles in signal transduction, cell migration and adhesion, as well as membrane trafficking (Nixon 2007; Mokhtar *et al*. 2013). APP is generated in the Trans-Golgi-Network (TGN), after which it is transported to the plasma membrane via the ELP. Here it is processed in either of two pathways; the so-called amyloidogenic and non-amyloidogenic pathway (Fig. 1.11) (Rajendran & Annaert 2012).

In the amyloidogenic pathway, Aβ is generated by the sequential cleavage of APP by the proteases β-secretase and γ-secretase (Nixon 2007; Rajendran & Annaert 2012). The cleavage activity of these enzymes is conferred by the β-site APP cleaving enzyme 1 (BACE1) and Presenilins (PSENs) catalytic domains, respectively. The β-cleavage of APP generates the soluble fragment sAPPβ, which is released extracellularly. The cleavage of the remaining fragment, C99 (β-CTF), by γ-secretase, generates the Aβ peptide and the APP intracellular domain known as the AICD (β-γ) (Nixon 2007; Rajendran & Annaert 2012). Aβ peptides have varying lengths, with up to 43 amino-acid sequences. Neurons mostly generate the Aβ40 and Aβ42 peptides and healthy neurons have high Aβ40/Aβ42 ratio, whereas AD neurons

generate more Aβ42 which is thought to have an extremely high propensity to aggregate and complicity facilitates plaque formation (Fig 1.11) (Nixon 2007).

In the alternative non-amyloidogenic pathway, APP is cleaved at the α-site by α-secretase, also known as distintegrin or metalloproteinase 10 (ADAM10), to generate the soluble fragment sAPPα and the still membrane bound C83 (α-CTF) respectively. C83 is then cleaved by γ-secretase to generate the AICD (α-γ) and small peptide called p3 (Fig 1.11) (Nixon 2007; Rajendran & Annaert 2012).

Amyloidogenic processing has been detected preferentially on endosomal membranes, whereas non-amyloidogenic processing occurs mainly on the plasma membrane. Intracellular Aβ is the suspected source of plaque deposits. In fact, it seems that Aβ rises substantially within endo-lysosomal compartments before deposition and remains elevated in the heavily plaque infested AD brain. Some AD model studies have even reported cognitive deficits with elevated intracellular Aβ levels in the absence of plaque deposition (Nixon 2007).

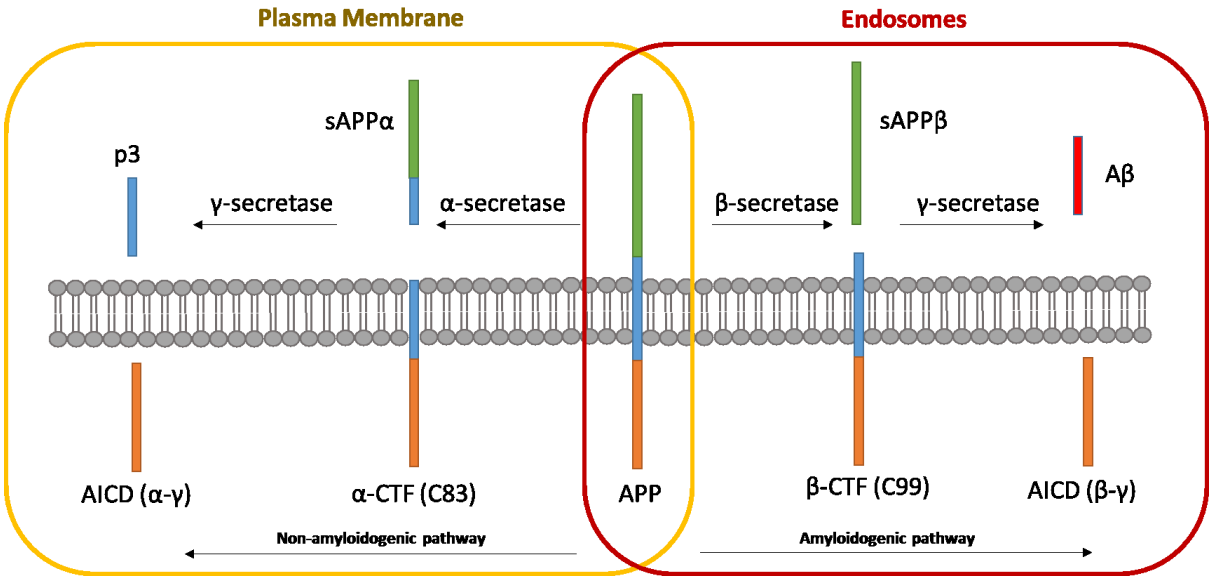

Figure 1.11: The APP processing pathway. *The amyloidogenic and non-amyloidogenic pathway as described. Adapted from Rajendran & Annaert 2012*

1.4.1 Amyloid Pathology

The aggregate prone Aβ42 accumulates in cells by arranging into soluble oligomers, insoluble fibrils and finally amyloid or “senile” plaques. However, accumulating evidence suggests that the oligomers appear to be the main source of its neurotoxicity (Shankar *et al*. 2008; Shankar & Walsh 2009; Li *et al*. 2009). The mechanisms of the toxicity is broadly linked to synaptic damage and cognitive impairment, specifically it is described as a pathological interaction

between Aβ oligomers and NMDA receptors (Musiek & Holtzman 2015; Li *et al*. 2009; Shankar & Walsh 2009).

Of note, it has been demonstrated that protein aggregation itself may not be the cause of cell death. Arrasate and colleagues have demonstrated that of cells exposed to mutant huntingtin protein, the ones containing huntingtin aggregates or protein inclusion bodies survived longer than cells containing no aggregates (Arrasate *et al*. 2004). In fact, some posit that Aβ aggregation may be a cellular protective mechanism rather than the cause of cell death (Ross & Poirier 2005).

Aβ oligomers also initiate Tau hyperphosphorylation through aberrant activation of kinases such as Fyn (Musiek & Holtzman 2015). Although a causal link between Aβ pathology and Tau hyperphosphorylation has been elucidated, the exact molecular cascade is vastly complex (Zempel *et al*. 2013; Musiek & Holtzman 2015).

Furthermore, a landmark review published by R. Nixon (2007) summarized the role that autophagy and endocytosis played in the turn-over of APP-rich organelles and subsequent generation of Aβ. It highlighted the fact that a combination of increased autophagy induction and defective clearance of Aβ-generating vacuoles play a pivotal role for Aβ accumulation in AD (Nixon 2007).

1.5 Mitochondrial dynamics

Tubulin functionality and the autophagy machinery are both intricately linked to mitochondrial function, quality control and transport. Although not a major theme of this review, the connection between microtubulin, autophagy and mitochondrial dynamics deserves attention, due to the role it plays in cell death onset.

Neurons are highly dependent on mitochondrial-derived ATP due their low anaerobic capacity and high energetic demand. ATP availability needs to be kept constant for normal cellular maintenance and growth. Mitochondria differ from each other depending on subcellular compartmental localisation (DuBoff *et al*. 2013). Neuronal mitochondria can be distinguished into two groups, synaptic and non-synaptic. These two groups differ in size, trafficking patterns and function (DuBoff *et al*. 2013). To maintain the high energy demand of synaptic transduction, synaptic mitochondria are larger and longer-lived, rendering them susceptible to accumulating damage (DuBoff *et al*. 2013).

Mitochondria are compartmentalised double membrane organelles that provide ATP to the cell through oxidative phosphorylation. Oxidative phosphorylation relies on the electron transport chain (ETC), located on the inner membrane of the mitochondria and is composed

of four biochemically linked complexes (I, II, III and IV) and two electron carriers (CoQ and CytC) (DuBoff *et al*. 2013). Mitochondria utilize cytosolic nutrient stores to produce ATP through an electrochemical gradient generated by the ETC across the membrane. Additionally, mitochondria are also the main producers of reactive oxygen species (ROS) (DuBoff *et al*. 2013). ROS have physiological functions under normal conditions, but are prone to contributing to pathological conditions when excessively produced. High levels of ROS induce lipid peroxidation, as well as DNA, mtDNA and ETC damage. To combat the damaging effects of ROS, mitochondria have an underlying quality control system for removing damaged mitochondria through fission-mediated mitochondrial autophagy (known as mitophagy) and rely on inherent anti-oxidant systems (DuBoff *et al*., 2013).

Mitochondria are maintained as short tubular structures that are highly dynamic - a property that is modulated through fission and fusion. Fission and fusion establish mitochondrial shape and size and allows for the sharing of proteins, lipids and DNA (Itoh *et al*. 2013). The sharing of contents, through fusion, acts as a compensatory mechanism; by which dysfunction is transiently buffered. Fission allows for the transport and distribution of damaged mitochondria. Fission and fusion dynamics are mediated through dynamin related proteins (DRPs). DRPs belong to the GTPase family, which are dependent on GTP hydrolysis for self-assembly and subsequent modulatory effects (Itoh *et al*., 2013; DuBoff *et al*., 2013).

During fission, Drp1 assembles into helical structures that wrap around mitochondria and scissions it into two daughter mitochondria that differ energetically, with one being hyperpolarised and the other depolarised. Depolarised mitochondria are less likely to fuse and are more susceptible to mitophagy, but depolarisation alone is insufficient to induce this particular state (Itoh *et al*. 2013). During fusion, mitofusins 1 and 2 (Mfn1 and Mfn2), located on the outer membranes of adjacent mitochondria, dimerise and facilitate outer membrane fusion. Inner membrane fusion is then facilitated by OPA1 (optic atrophy 1), located in the inter-membrane space. Functional fission and fusion is essential for cellular homeostasis (Itoh *et al*. 2013).

The fission of mitochondria also allows for mitophagy, through which damaged or depolarised mitochondria are degraded. Mitophagy is controlled through the action of the two proteins called PINK1, a serine/threonine kinase located on the mitochondrial membrane, and Parkin, a ubiquinating E3 type ligase. In healthy mitochondria, PINK1 concentrations are kept low by membrane potential-dependent recruitment and proteolytic cleavage (Yan *et al*. 2013). However, damaged or depolarised mitochondria cause PINK1 accumulation that signals recruitment of Parkin, which subsequently ubiquinates the mitochondria and targets it for mitophagy (Yan *et al*. 2013). Mutations in both PINK1 and Parkin are the cause of the neurodegenerative disease autosomal recessive juvenile parkisonism (Yan *et al*. 2013).

Other than their importance in maintaining cell viability through preserving metabolic activity, rather contrastingly, mitochondria also play a major role in the control of cell death, specifically apoptotic cell death (discussed further in 1.6), which is a major cell death modality in neurodegeneration.

1.6 Mechanisms of cell death

Apoptotic neuronal cell death is a hallmark feature of both aging and neurodegenerative disease (Gorman 2008). Although neuronal cell death is recognised as a major part of neurodegenerative pathologies, it is not always clear how this occurs. Multiple modes of cell death have been elucidated in the last few decades in addition to apoptosis, which include necrosis and a third mode, termed autophagic cell death (ACD). ACD is still considered very a highly controversial “mode” of cell death because it is rarely witnessed and so far has only been observed to occur in *Drosophila* salivary glands, therefore it shares no relevance to neurodegeneration (Baehrecke, 2003).

1.6.1 Apoptosis

Apoptosis is the tightly regulated, energy-dependent and gene-controlled process of programmed cell death. It is morphologically characterised by pyknosis (nuclear condensation) and karyorrhexis (nuclear fragmentation), membrane blebbing and the separation of internal structures into apoptotic bodies (Loos *et al*. 2013). Physiologically appropriate neuronal apoptosis is crucial in normal neurodevelopment, specifically during neurogenesis (Becker & Bonni 2004; Cavallaro 2015). The activation of a family of proteases called caspases, play a centralised role in controlling apoptotic activity and act through mainly two distinct pathways; namely the intrinsic and extrinsic pathways. These two pathways differ in the initiation of the apoptotic cascade, but converge on the same execution phase that completes the mechanisms leading to cell death (Elmore 2007). These pathways are briefly summarised as follows:

1.6.1.1 Intrinsic/Mitochondrial Pathway

The intrinsic or mitochondrial pathway is, as suggested by the name, mitochondria-dependent. It is activated by non-receptor mediated stimuli that can be divided into positive and negative signals. Negative signals include, but are not limited to, the withdrawal of certain hormones or

growth factors. Positive signals can be external stressors such as hypoxia or extreme temperatures (Elmore 2007).

These stimuli cause a change in the mitochondrial inner membrane, which leads to the opening of the mitochondrial permeability pore (MTP). MTP opening leads to a loss in membrane potential and the release of two main groups of pro-apoptotic proteins. The first group of proteins include cytochrome-c, which causes the recruitment of Apaf-1 and procaspase-9 into a structure called an apoptosome. The apoptosome allows auto-activation of the initiator caspase-9 that subsequently cleaves procaspase-3 and activates the execution phase. Along with cytochrome c, AIF release takes place and causes DNA damage in a caspase-independent manner. The second group of proteins released are the Smac/DIABLO complexes that are thought to initiate apoptosis by removing the inhibitory effect of IAPs (inhibitory apoptotic proteins) (Elmore 2007; Gorman 2008).

The regulation of these mitochondrial events occurs through the actions of the Bcl-2 family of proteins, which include anti-apoptotic proteins such as Bcl-2 and Bcl-x, and pro-apoptotic proteins such as Bid, Bax and Bad (Elmore 2007). The executioner phase is initiated by the cleavage of procaspase 3 into caspase-3, also known as an “executioner caspase”. Caspase-3 cleaves cytoskeletal proteins and translocates to the nucleus, where it cleaves the nuclear material, eventually causing DNA damage and chromatin condensation. At the same time, caspase-3 also cleaves Poly (ADP-ribose) Polymerase (PARP), a DNA repair enzyme, to prevent DNA recovery – ultimately committing the cell to death (Elmore 2007).

1.6.1.2 Extrinsic/Death Receptor Pathway

The extrinsic pathway is activated by transmembrane receptor-mediated interactions of specific ligand binding. These ligands include amongst others, FasL and TNF-α, and their respective receptors, FasR and TNFR1. Ligand binding causes trimerisation of the receptor complexes and recruitment of cytoplasmic adaptor proteins with corresponding so called “death domains”, i.e FADD and TRADD. The adaptor proteins dimerize with pro-caspase 8, and subsequently leads to auto-activation which generates caspase-8 that cleaves procaspase 3 into caspase-3 and initiates the execution phase (Elmore 2007).

Ccaspase-8 has been shown to cleave the pro-apoptotic protein Bid into a tBid fragment, which subsequently leads to MTP opening and the initiation of the intrinsic pathway. This is a prime example of cross talk between pathways and clearly indicates that they do not necessarily operate in a mutually exclusive fashion (Kermer *et al*. 2004; Gorman 2008).

1.6.2 Necrosis

Necrosis is a non-programmed, energy-independent and acute form of cell death. It is morphologically characterised by a rapid loss of membrane integrity with consequent lysis and release of cell constituents into neighbouring tissue. This leads to the release of pro-inflammatory cytokines and the subsequent destruction of neighbouring cells. Necrosis is usually the result of severe stress, i.e direct trauma or toxin exposure. It does not have a clear biochemical pathway of induction and thus remains a difficult mode of cell death to fully characterise, let alone modulate (Gorman 2008; Loos *et al*. 2013).

1.6.3 Excitotoxic Cell Death

Although it is debated whether Excitotoxic Cell Death (ECD) is a true "mode of cell death" it has a significant role to play in the neuron loss witnessed in late AD. Briefly, excitotoxicity is defined as "a toxic process characterized by a sustained stimulation of excitatory amino acid receptors mainly involving N-methyl-D- aspartate Receptors (NMDARs)" (Kamat *et al*. 2016). ECD generally occurs as a result of ATP-depletion during a periods of ischemia (Kamat *et al*. 2016). The ATP loss causes depolarisation of neurons, which stimulates neurotransmitter release and failure of ATP-dependent neurotransmitter re-uptake transporters. Glutamate is the most abundant excitatory neurotransmitter in the brain and its aberrant release causes overstimulation of ion-gated NMDARs. This results in an influx of Ca^{2+} ions that can cause both ER and mitochondrial stress – ultimately leading to the onset of cell death (Gorman 2008; Kamat *et al*. 2016). Whether it exclusively causes either necrotic or apoptotic cell death remains unclear, but this seems to be dependent on general mitochondrial health (Ankarcrona *et al*. 1995)

In AD, exictotoxicity is hypothesized to occur in a "slow" tonic rather than phasic manner. Functional MRI studies in patients with prodromal AD revealed an increase in neural network activity relative to baseline, rather than a loss of activity (Putcha *et al*. 2011). Ong and colleagues suggest that this may be a compensatory mechanism by the brain to cope with early neuronal loss (Ong *et al*. 2013). The abundance of cell death witnessed in late disease correlates with symptom onset, which warrants earlier therapeutic interventions.

1.7 Summary of pathophysiology

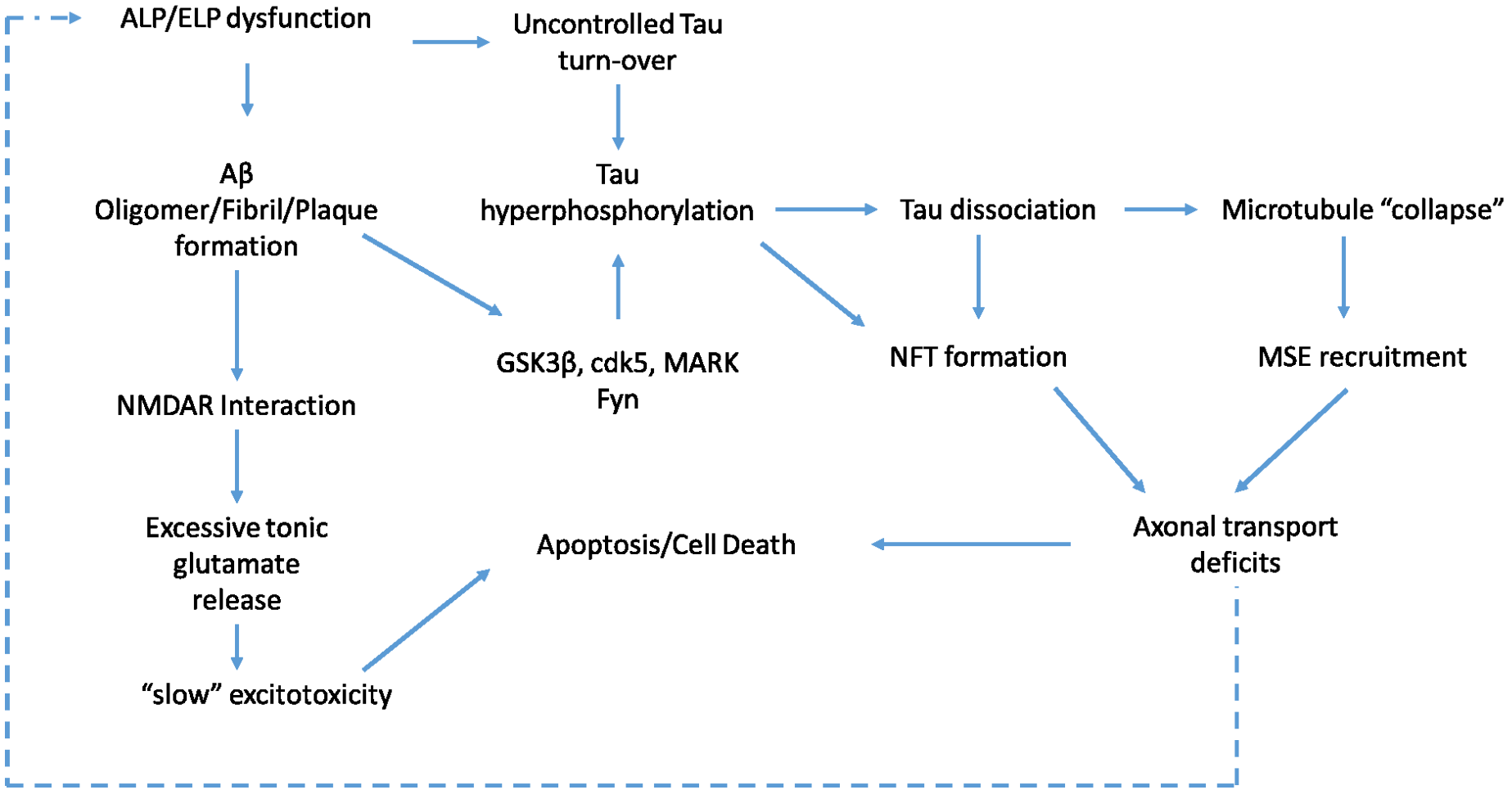

Figure 1.12: Schematic summary of AD pathophysiology in context. *Schematic summary summarising the complex pathological changes that manifest in the aetiology of Alzheimer's disease*

1.8 Current and potential treatment modalities

Multiple treatments have been developed over the years, ranging from anti-Aβ vaccines to diet modulation. However, there has been limited or no success. AD progresses in a somewhat coordinated manner in terms of spatiotemporal brain degeneration. The disease usually affects the hippocampus first and this occurs in the prodromal stage. Eventually this pathology manifests in the cortex during late disease. Braak and Braak were the first to elucidate these macroscopic changes into stages (see original review (Braak *et al*. 1994)), which demonstrates that particular neuron populations are lost in specific brain regions and can be attributed to phenotypic characteristics of the pathophysiology. Acetylcholine (ACh) secreting neurons are one such group of neurons that are lost early in the AD pathophysiology (Tiernan *et al*. 2016). The "cholinergic deficit hypothesis" postulates that many symptoms of dementia, such as behavioural and LTP (Long Term Potentiation) deficits, can be attributed to the substantial loss of cholinergic neurons and ACh (Auld *et al*. 2002). As such, many drugs were developed to treat this part of the pathology with the aim to improve ACh concentrations by inhibiting cholinesterase activity (Godyn *et al*. 2016).

Multiple clinical trials and drug development trials targeting AD and dementia-related disorders are initiated every year. There are currently more than 200 clinical trials in various stages of progress within this research area. Listed in the tables below are select past and present potential candidate drugs that highlight the complexity of the disease and the many molecular targets, of special focus are those targeting Tau pathology.

Table 1.1: ***Available Pharmacological Interventions***

Drug	Target	Disease Stage Target
Tacrine	Acetylcholinesterase inhibitor	Mild to Moderate
Rivastigmine	Acetylcholinesterase & butyrylcholinesterase inhibitor	Mild to Moderate
Galantamine	Acetylcholinesterase inhibitor	Mild to Moderate
Donepezil	Acetylcholinesterase inhibitor	Mild to Moderate
Memenatine	NMDA agonist	Mild to Moderate

Table 1.2: ***Select pharmacological Interventions currently in Clinical Trials*** *– highliited in grey are drugs targeting Tau pathology and autophagy. Partially adapted from Godyn et al. 2016.*

Drug	**Target**	**Disease Stage**	**Trial Stage**	**Country/Region**	**Clinical Trial Reference**
AADvac1	Anti-Tau vaccine	Moderate-Late	Phase I	Europe	NCT02579252
ABT-957	Adjuvant to Anti-cholinesterase drugs	Early-Moderate	Phase I	US	NCT02220738 NCT02573740
AC-1204	Ketogenic Agent	Early-Moderate	Phase II	US	NCT01741194
ACI-35	Anti-Tau vaccine	Moderate-Late	Phase I	Finland/UK	ISRCTN13033912
Albumin and Immunoglobulin	N/A	Early-Late	Phase II/III	US	NCT01561053
Allopregnanolone	Steroid	Early-Late	Phase I	US	NCT02221622
AZD 3293	β-Secretase inhibitor	Early-Late	Phase II/III	World Wide	NCT02245737
Azeliragon	RAGE inhibitor	Early-Late	Phase III	US/Canada	NCT02080364
BAN2401	Humanised monoclonal anti-Aβ antibody	Early	Phase II	World Wide	NCT01767311
Bisnorcymserine	Inhibitor of Butyrylcholinesterase	Early-Late	Phase I	US	NCT01747213
Carvedilol	non-selective α/β-adrenergic receptor antagonist and vasodilator	N/A	Phase IV	US	NCT01354444

Crenezumab	Humanised monoclonal anti-Aβ antibody	Moderate-Late	Phase II	World Wide	NCT01723826
E2609	β-Secretase inhibitor	Early-Late	Phase II	US	NCT02322021
Exendin-4	GLP-1 receptor agonist	Early	Phase II	US	NCT01255163
Gantenerumab	Humanised monoclonal anti-Aβ antibody	Early	Phase III	World Wide	NCT01224106
Gemfibrozil	Lipid modulator	Early	Phase 0	US	NCT02045056
Idalopirdine with Donepezil	$5\text{-}HT_6$ receptor antagonist	Moderate	Phase III	World Wide	NCT02079246
Intranasal Insulin	GSK-3β inhibitor	Early	Phase II	US	NCT02503501
MEDI1814	anti-Aβ antibody	Early Mild	Phase I	US	NCT02036645
Rasagiline	MOA inhibitor	Mild-Moderate	Phase II	US	NCT02359552
Riluzole	Glutamate neurotransmission modulator	Mild	Phase II	US	NCT01703117
Solanezumab	Humanised monoclonal anti-Aβ antibody	Mild-Moderate	Phase III	World Wide	NCT01900665
Verubecestat	β-Secretase inhibitor	Early-Moderate	Phase II/III	US	NCT01739348 NCT01953601

Although many of the available and potential drugs seem very promising in targeting what are considered “hallmark” pathologies of AD, none have had any reasonable success thus far. Also, none target proteostatic dysfunction, which has been shown to occur prior to these perturbations.

Lastly, no mechanisms have been elucidated to explain a potential link between proteostatic failure and downstream pathologies such as Tau dissociation and the associated microtubulin instability. Investigating a potential and novel relationship between these pathologies may reveal a novel therapeutic intervention in prodromal Alzheimer’s disease, which may delay or even halt the disease onset. This topic shall be the focus of this study.

1.9 Problem statement

The underlying mechanisms that govern Tau aggregation and subsequent microtubulin instability are neither fully understood nor characterized in current literature. In addition, it is not known to what extent autophagy dysfunction influences the pathological changes associated with microtubule destabilisation, Tau aggregation and proteotoxicity.

1.10 Hypothesis

Due to the dynamic nature of the MT, and the rapid turnover of the tubulin pools, a constituent basal level of Tau degradation is required. We thus hypothesize that autophagy disruption causes Tau to accumulate intracellularly, and in particular along the microtubulin network. Accumulated Tau associated with the microtubule becomes hyperphosphorylated, reducing its binding affinity and ultimately causing its dissociation. This in turn will increase microtubule susceptibility to severing enzymes such as Spastin and Katanin, causing its fragmentation and dysfunction. It is further hypothesized that these events occur prior to the onset of cell death.

1.11 Aims

The aims of this study were therefore to investigate the effects of autophagy perturbation on Tau and microtubulin dynamics in an in vitro model by:

I. Establishing two time points of autophagy inhibition. The first being an early time point at which the perturbation does not negatively impact cell viability, and a second time point at which the perturbation induces cell death in order to assess any changes in parameters of microtubule network functionality prior to the onset of cell death.
II. Assessing Tau protein dynamics in relation to its phosphorylation state and localisation with the microtubule network.
III. Assessing microtubulin stability and ultrastructure under autophagy inhibition by utilising Super Resolution microscopy techniques.
IV. Assessing the effect of chloroquine treatment on the relative autophagic flux of the system

Chapter 2: Materials and Methods

2.1 Reagents and Consumables

2.1.1 Cell Lines and General Cell Culture Reagents

Murine hypothalamus-derived GT1-7 neuronal cells were a kind gift from Prof Pamela Mellon (University of California, San Diego, USA) (Mellon *et al*. 1990). Dulbecco's Modified Eagles Medium (DMEM) (41965-039), Penicillin-Streptomycin (PenStrep) (151140-122), 0.25% Trypsin-EDTA (25200-072) and NUNC™ Lab-Tek™ II Chamber Slide™ 8-chamber dishes (154534) were purchased from ThermoFisher Scientific (TFS). Foetal Bovine Serum (FBS) (FBS-GI-12A) was purchased from CAPRICORN® Scientific. T25 (25 cm^2) (Nest®, 707001), T75 (75 cm^2) (Nest®, 708001), T175 (175 cm^2) (Nest®, 709001), 6- (Nest®, 703001), 48- (SPL®) culture flasks and plates were purchased from BiocomBiotech (South Africa).

2.1.2 Treatment and Experimental Reagents

Chloroquine diphosphate salt (C6628), WST-1 Cell Proliferative Reagent (11644807001) and 2-Cysteamine (M9768) were purchased from Sigma-Aldrich. Bafilomycin A1 (B0025) was purchased from Lkt® Labs.

2.1.3 Antibodies and Plasmid Constructs

2.1.3.1 Primary Antibodies

Primary antibodies that were used, in some cases for both immuno-fluorescent labelling and Western blots, include anti- acetylated α-tubulin, anti-CP27 (Tau) (a kind gift from Prof Peter Davies (Albert Einstein College of Medicine, Bronx, New York)), anti-Katanin p60, anti-LC3B, anti-p62, Anti-pTau, anti-Spastin and anti-β-actin.

Table 2.1: The respective information of primary antibodies utilised*. IF – Immunofluorescence Microscopy; WB – Western blot*

Antibody	Company/ Cat#	Animal Source/Target	Expected Mol. Weight	WB Dilution	IF Dilution
Anti- acetylated α-tubulin	Santa Cruz (23950)	Mouse Anti-Mouse	55 kDa	1 µL:1000 µL	1 µL:200 µL
Anti-CP27 (Tau)	N/A	Mouse Anti-Mouse	50 kDa	1 µL:1000 µL	N/A
Anti-Katanin P60	Santa Cruz (109299)	Goat Anti-Mouse	60 kDa	1 µL:1000 µL	1 µL:200 µL
Anti-LC3B	CST (2775)	Rabbit Anti-Mouse	14-16 kDa	1 µL:5000 µL	N/A

Anti-p62	Abcam (56416)	Rabbit Anti-Mouse	62 kDa	1 µL:5000 µL	N/A
Anti-pTau (S400/T403/S404)	CST (11837)	Rabbit Anti-Mouse	50-80 kDa	1 µL:5000 µL	1 µL:100 µL
Anti-Spastin	Abcam (10197)	Rabbit Anti-Mouse	64-68 kDa	1 µL:5000 µL	1 µL:100 µL

2.1.3.2 Fluorescent probes and HRP-linked Secondary Antibodies

The following fluorescent probes and Horse Radish Peroxidase (HRP) - linked secondary antibodies were used for microscopy and Western blot analysis, respectively.

Table 2.2: The respective information of secondary antibodies utilised*. IF – Immunofluorescence Microscopy; WB – Western blot*

Probe	**Company/ Cat#**	**Animal Source/Target**	**WB Dilution**	**IF Dilution**
Alexa Fluor 488	ThermoFisher (A-21202)	Donkey Anti-Mouse	N/A	1 µL:200 µL
Alexa Fluor 568	ThermoFisher (A-10042)	Donkey Anti-Rabbit	N/A	1 µL:200 µL
Alexa Fluor 568	ThermoFisher (A-11057)	Donkey Anti-Goat	N/A	1 µL:200 µL
HRP	Abcam (97110)	Donkey Anti-Goat	1 µL:20 000 µL	N/A
HRP	CST (7074)	Goat Anti-Rabbit	1 µL:10 000 µL	N/A
HRP	CST (7076)	Anti-Mouse	1 µL:10 000 µL	N/A

2.1.3.3 Transfection Reagents and DNA constructs

GT1-7 cells were transfected with the Tau plasmid construct using the NEON® Electroporation Transfection System and NEON® Transfection Kit, according to the manufacturer's protocol. The pRK5-EGFP-Tau P301L (Human Tau) (#46908) construct was purchased from AddGene®.

2.1.4 Protein determination and Western Blot Reagents

Bradford Reagent (B6916) and Bovine Serum Albumin (BSA) (B8894) was purchased from Sigma-Aldrich. 12% Fast-Cast® Stain-free® SDS-PAGE gel casting kit (1610184), 0.2 µm polyvinylidine fluoride (PVDF) Midi Trans-Blot Turbo Transfer Packs (170-4157) and Clarity® ECL (Enhanced chemiluminescence) peroxide reagent kit (1705061) were purchased from BioRad (South Africa).

2.2 Experimental Procedures

2.2.1 Tissue Culture of GT1-7 cells

Cells were cultured in DMEM supplemented with 10% FBS and 1% PenStrep, and maintained in a humidified incubator (Snijders Scientific, C01901) at 37 ºC and 5% CO_2 atmosphere.

2.2.1.1 Thawing and Culturing of Cells

Cryovials containing approximately $1x10^6$ cells in 1 mL FBS, with 10% DMSO, were thawed in 37 ºC warm water. The suspension was then slowly added to 4 mL pre-warmed media in a 15 mL falcon tube. The contents were spun down in a centrifuge (Eppendorf, 5804) for 4 min at 1500xg. The supernatant was discarded to remove DMSO and the pellet was resuspended in warm media and subsequently added to a T25 culture flask containing 5 mL fresh media. The media was changed every 2-3 days until the desired confluency (70-80%) was reached, after which cells were subcultured and seeded for experimental conditions indicated.

2.2.1.2 Sub-culturing of cells for Experiments

For passaging and sub-culturing of cells, media was removed and the cell monolayer was briefly rinsed with 1mL 0.25% trypsin-EDTA as recommended by ATCC. Once the initial trypsin was removed, 4 mL of fresh trypsin was added and left to incubate for 5 min until cells loosened. The trypsin was neutralised with FBS containing DMEM (2x volume of trypsin). The suspension was then centrifuged for 4 min at 1500 xg. The pellet was resuspended and cells were counted in a Neubauer Improved haemocytometer (Marenfield) to be seeded for various experiments.

2.2.1.3 Experimental Groups

To induce and determine autophagic dysfunctional states, as detailed in the experimental aims, GT1-7 cells were treated with the lysomotrophic reagent chloroquine diphosphate (CQ) with varying concentrations (ranging from 12.5 to 100 µM) for 6 and 24 h, respectively. Viability of cells was then determined using the WST-1 assay. The concentration that caused a significant decrease in cell viability after 24h, but not 6h, was selected for subsequent experiments.

For Western blot analysis, cell lysates were harvested every 2h over a period of 24h. In addition, select time points within the 24h period were chosen and treated with Bafilomycin A1

for 2 hours post chloroquine treatment to measure relative autophagic flux. These selected time points included 6h and 24h.

2.2.2 Reductive Capacity Assay

A WST-1 assay was used to measure the cellular reductive capacity in response to the chloroquine treatment. It has historically been used as a marker for cell viability in numerous studies by inferring cell death due to a lack of metabolic activity (Gomez *et al.*, 1997; Goodwin *et al.*, 1995). WST-1 is a tetrazolium-based salt that is reduced by primarily mitochondrial enzymes into water-soluble formazan crystals. The media containing the dissolved crystals can then be measured spectrophotometrically and viability be inferred.

In brief, GT1-7 cells were seeded into a 48-well plate at a density of 75 000 cells/well and left to grow in 200 µL media overnight. The following day, cells were treated over the required time period. Next, 10 µL of WST-1 reagent was added to each well and plates were incubated for a period of 2 hours, after which they were agitated in a shaking incubator (37 ºC, 200 RPM) for 5 min to dissolve the formazan crystals. Supernatants were spectrophotometrically read at a wavelength of 595 nm on a universal micro plate reader (EL800, Bio-Tek Instruments Inc.) and data were recorded using the KC Junior software. Absorbance values were expressed as a percentage of the control ± SEM.

2.2.3 Protein Determination

Once treatment protocols were completed, media was removed from T75 culture flasks, cells were immediately placed on ice and thoroughly washed 3x with cold PBS. Total protein of GT1-7 cells was extracted with a radio-immunoprecipitation (RIPA) lysis buffer containing Tris-HCl 50 mM; NaCl 150 mM, EDTA 1 mM, NP-40 1%, Na-deoxycholate 0.25%. The buffer was supplemented with 1 mM Sodium Orthovanadate (Na_3VO_4), 1 mM Sodium Fluoride (NaF), 1 mM PMSF (phenylmethylsulfonyl fluoride) and 1x cOmplete Protease Inhibitor Cocktail (as per manufacturers protocol), to inhibit both phosphatase and protease activity.

Protein content of GT1-7 cell lysates was quantified using the Bradford Reagent assay (Bradford, 1976).

2.2.4 Sample Preparation

Samples were prepared after protein content of lysates had been determined. Aliquots containing 50 µg/ µL of protein and Laemli's sample buffer (diluted in a 2:1 ratio) were

prepared. The aliquots were stored at -80 ºC and thawed when required. Prior to loading onto the gels, samples were thawed on ice and boiled at 95 ºC for 5 min to denature and linearize proteins.

2.2.5 SDS-PAGE and Western Blot Analysis

GT1-7 were added to wells of a 10-well 1 mm casted gel using a 12% Stain-free® Fast-Cast® SDS-PAGE kit. Proteins were separated using 250 V and 400 mA for an average time of 90 minutes. Once the electrophoresis was complete, proteins were transferred to a PVDF membrane using a Trans-Blot Transfer pack (GT1-7 cells) using the BioRad Trans-Blot Turbo electrotransfer system (BioRad, 170-4155), which is operated at 120V and 400mA for 7 minutes. The membrane was then incubated for 1 hour in 5% fat-free milk made up in Tris-buffered saline/0.1% Tween 20 (TBS-T) to prevent non-specific binding. Once the blocking procedure was complete, membranes were washed 3x 5 min with TBS-T and subjected to probing with the specific primary antibody at 4°C overnight. The following day, membranes were washed 3x 5 min with TBS-T and probed for 1 hour at room temperature with the corresponding secondary antibody. Membranes were washed 3x 5 min with TBS-T and exposed to ECL chemiluminescent reagent for 5 minutes. Developing bands were detected and captured using the ChemiDoc imaging system (ChemiDoc MP, Imaging System). Band intensities were normalised against total lane protein and quantified using the Bio-Rad Image Lab software.

2.2.5.1 Total Protein Loading Controls

BioRad Stain-free® technology allows for the normalisation of band intensities to total protein in respective lanes, which is due to a patented additive within the gel mixture (BioRad 2014). The additive reacts with tryptophan residues within protein sequences and allows their visualisation when exposed UV radiation. The Bio-Rad Image Lab software provides a user friendly interface to generate normalised data.

2.2.6 Transfection optimisation

An established protocol for optimised transfections in the GT1-7 cell line was used. This allowed for the highest transfection efficiency and cell viability after the electroporation process.

In brief, 500 000 cells were trypsinsed, counted and washed in PBS. Next, after being spun down the PBS was decanted and cells resuspended in 100 µL sterile Neon® Resuspension buffer containing 5 µg of GFP-Tau (P301L) DNA. Next, the suspension was aspirated into a gold plated Neon® Tip using a Neon® Pipette. The tip was then immersed into Neon® Electrolytic buffer inside the Neon® Pipette Station, and cells were electroporated at 1350 V for 1 pulse lasting 30 ms. Finally, cells were plated into 6-well dishes containing 14 mm round coverslips in fresh media without antibiotics and left to recover overnight. Following the recovery period cells were treated as required.

2.2.7 Confocal and SR-SIM Fluorescent Microscopy

2.2.7.1 Sample Preparation for SR-SIM and Confocal microscopy

In brief, 50 000 transfected or untransfected cells were seeded into 6-well dishes containing 5 mm round coverslips and 2 mL fresh media and left to grow overnight. The next day coverslips were treated according to the previously determined experimental groups. Once treatment had completed cells were fixed for 10 min in a 1:1 ratio of 4% w/v Paraformaldehyde: DMEM at 37ºC in an incubator. Coverslips were then washed 3x 5 min with cold PBS, after which they were incubated for 30 min in a blocking buffer made up of 5% v/v donkey serum in PBS. After blocking, cells were subjected to the required primary antibodies, and incubated overnight at 4 ºC. The following day cells were probed with corresponding secondary antibodies for 50 min, after which 50 uL of diluted Hoechst 33342 nuclear dye was added. Cells were then incubated in the secondary antibody/Hoechst mixture for a further 10 min. The coverslips were then washed 3x 5 min with PBS. After the last wash, PBS was decanted and slides mounted in an inverted manner onto a glass slide containing Dako® fluorescent mounting media and sealed with clear nail polish. Slides were then stored in a foil wrapped container at -20 ºC until analysis was required.

2.2.7.2 Confocal microscopy sample acquisition and processing

Confocal analysis was performed on fluorescently stained and transfected cells using the Zeiss LSM 780 system (Carl Zeiss Microimaging, Germany). Data of cells were collected by acquiring z-stacks, each with 10-12 image frames, and increments of ~0,975 µm step width. A LCI Plan-Apochromat 63x/1.4 Oil DIC M27 objective equipped with a Diode 405nm CW/PS (pulsed), 488 nm laser, 561 nm laser and GaAsP detector (32+2 PMT), was utilised.

Maximum intensity projections of z-stacks were processed and generated in the Zeiss Zen Black Software (2012) and utilised for subsequent experimental analysis.

2.2.7.3 SR-SIM microscopy sample acquisition and processing

For SR-SIM analysis of GFP-Tau transfected cells, thin (0.1 µm) z-stacks of high-resolution image frames were collected by utilizing an alpha Plan-Apochromat 60x/1.4 oil immersion DIC M27 ELYRA objective, using an ELYRA PS.1 system (Carl Zeiss Microimaging, Germany) equipped with a 488nm laser (100mW) in 5 rotations, 561nm laser (100mW) in 5 rotations and an Andor EM-CCD camera (iXon DU 885). Images were reconstructed using Zeiss Zen Black Software (2012) based on a structured illumination algorithm (Heintzmann & Cremer 1999). Analysis was performed on reconstructed super- resolution images in ZEN.

2.2.7.4 Co-localisation Analysis

Before co-localisation analysis was performed, single stains of cells using each primary antibody and its corresponding fluorescently tagged secondary antibody were imaged and pixel intensities were viewed on a scatter plot. The scatter plot was defined and generated by the Zeiss Zen Lite Black Edition Software (2012) as follows;

“All pixels having the same positions in both images are considered a pair. Of every pair of pixels (P1, P2) from the two source images, the intensity level of pixel P1 is interpreted as X coordinate, and that of pixel P2 as Y coordinate of the scatter diagram. The value of the pixel thus addressed is increased by one every time, up to the maximum number of pixels used. This way, each pixel of the scatter diagram is a value that shows how often a particular pair of pixels has occurred” (Zeiss Zen Black Edition Software, 2012).

Here, P1 and P2 represent two different colour channels captured on the same image. The single stains of the two separate fluorophores being analysed for co-localisation are represented by the X and Y axis respectively with the intensity of each of the pixels representing the value in the respective axis. The single stains allowed for the generation of threshold values to prevent a false positive reading when co-localisation analysis was performed on an image containing both the fluorophores. Furthermore, a colour lookup table at the bottom of the scatter plot indicates the frequency at which pixels occur in the same position.

Two different co-localisation coefficients were calculated using the Zeiss Zen Lite Black Edition Software. The calculated coefficients include the Manders’ Overlap Coefficient (MOC) and the co-localisation coefficient.

The MOC is mathematically defined as:

$$MOC = \frac{\sum_i Ch1_i * Ch2_i}{\sqrt{\sum_i (Ch1_i)^2 * \sum_i (Ch2_i)^2}}$$

The MOC is a parameter used to quantify co-localisation in image pairs, i.e. two different colour channels of the same image. It is insensitive to differences in intensities between the two channels, photo-bleaching or signal amplifier settings. The values range from 0 – 1 (0: no co-localisation, 1: all pixels co-localise).

The co-localisation coefficients are defined as:

$$c_1 = \frac{pixels_{Ch1.coloc}}{pixels_{Ch1.Total}} \qquad c_2 = \frac{pixels_{Ch2.coloc}}{pixels_{Ch2.Total}}$$

The C1 and C2 coefficients denote the relative number of co-localising pixels in channels 1 and 2 respectively, as percentage of the total number of pixels above threshold (Zeiss Zen Black Software, 2011). It indicates how much of each co-localising fluorophore or protein is represented relative to the total number of pixels.

2.2.7.5 Line Profile Intensities

Line Profile Intensities can be defined as the intensity profiles of two fluorescent molecules as determined by a straight line through the region of interest. This allows to elucidate a relationship between two labelled proteins, further supporting the extent of co-localisation data (Kleemann *et al*. 2014). The line profiles of the specified proteins were determined using Zeiss Zen Lite Black Edition Software (2012) (Kleemann *et al*. 2014).

2.2.8 STORM

Stochastic optical reconstruction microscopy (dSTORM) is a super resolution microscopy technique that allows the obtaining of fluorescent images beyond the diffraction limit. It is an extremely powerful technique in that it can resolve images to a resolution of 20 nm compared to SR-SIM which is limited to approximately 80 nm in xy resolution. In sharp contrast, confocal microscopy achieves an xy resolution of 200 nm.

2.2.8.1 Sample Preparation

Samples were similarly prepared as described in 2.2.7.1, except that cells were seeded into Mattek 35 mm Gridded Coverslip dishes. Furthermore, cells were fixed for a second time in 4% w/v paraformaldehyde solution post-secondary antibody incubation, and were exposed to 2 mL of redox buffer made up of 0.1% 2-Cysteamine in dH2O instead of being mounted.

2.2.8.2 Sample Acquisition and Processing

STORM was performed on a ZEISS LSM780 ELYRA PS1. Super-resolution microscope, equipped with an Alpha Plan-Apochromat 100x/1.46 Oil immersion objective, optimised for STORM. The 488nm ELYRA laser (100 mW) was used for excitation, while the BP 495-550 / LP750 reflector module was selected for emission detection. The microscope is equipped with an Andor EM-CCD (iXon DU 897) camera for STORM. The field of view was cropped to include only the desired area of interest, allowing the minimum exposure time of 15 ms and for each sample, 50 000 frames were recorded. STORM data was processed with the ZEN 2012 PALM package. For processing overlap was ignored, a mask size of 9 pixels and peak intensity to noise ratio of 5 was selected. Post-processing procedures included a drift correction.

2.2.9 Correlative Light and Electron Microscopy (CLEM)

Correlative Light and Electron Microscopy (CLEM) is an extremely powerful technique that allows the correlation of fluorescent microscopy image data with electron microscopy micrographs for the evaluation of protein localisation in the context of EM derived ultra-structural detail.

2.2.9.1 Sample Preparation

Samples were similarly prepared as described in 2.2.7.1. However, after the last PBS wash the coverslips were placed on grid and coated with elemental carbon using a carbon coater for Scanning Electron Microscope (SEM) analysis.

2.2.9.2 Sample Acquisition and Processing

The confocal microscopy data were acquired as described in 2.2.7.2. After carbon coating, samples were transferred to the Zeiss MERLIN Field Emission Scanning Electron Microscope

(Carl Zeiss Microimaging, Germany) with Zeiss SmartSEM for data acquisition using the Zeiss SE2 detector and further processed for correlation using the Zeiss Zen Black Software (2012).

2.3 Statistical Analysis

Statistica® 13 software was used for analysis of all generated data sets. Data were tested for normality after which the appropriate tests were performed. These included repeated measures one-way ANOVAs with Fishers Least Squared Difference (LSD) Post-Hoc tests. A p-value < 0.05 compared to the control was considered statistically significant.

Chapter 3: Results

3.1 Chloroquine treatment causes a significant reduction in cell viability after 24 hours

3.1.2 100 µM CQ causes a significant reduction in cell viability after 24 hours of exposure, but not after 6 hours

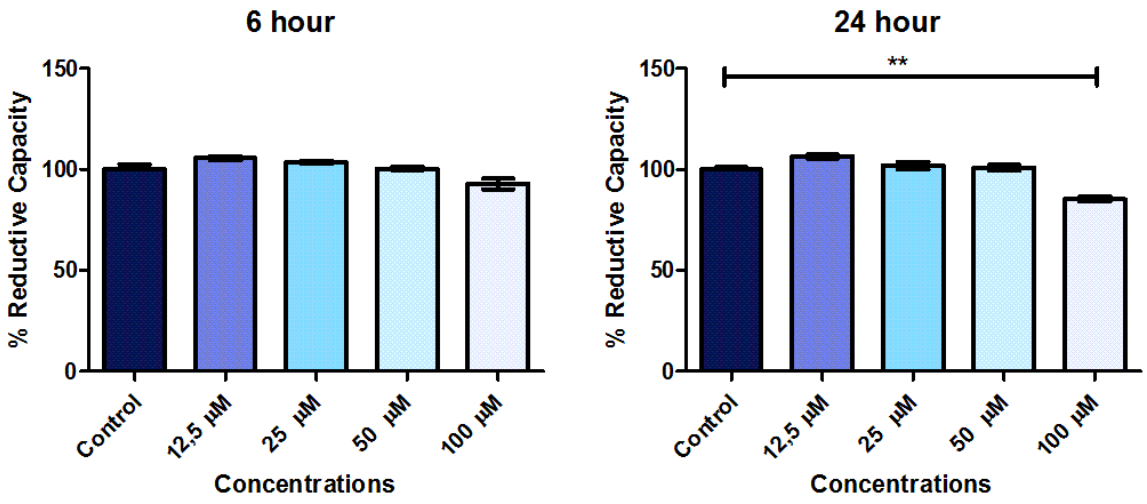

Figure 3.1: WST-1 reductive capacity assay of cells treated with CQ for 6 and 24 hours, respectively. *100 µM CQ was sufficient to cause a significant reduction in cell viability after 24 hours of CQ exposure, but not after 6 hours. All data are presented as a percentage of control (Mean± SEM). ** (p-value<0.005 vs control). N=3 independent experiments.*

To determine the desired concentration and time of exposure to CQ set out in the experimental aims, GT1-7 cells were exposed to increasing concentrations of the drug for 6 and 24 hours respectively. WST-1 reductive capacity was then utilised to assess cell viability of the cells at each time point and concentration. After 6 hours, reductive capacity initially increased slightly, but not significantly, relative to control when exposed to the 12.5 µM of CQ (105.6 ± 1.12%), but steadily declined in a dose dependent manner. This is likely an indication for mitochondrial stress in response to the treatment, rather than an increase in viability per se. Furthermore, no significant reduction in reductive capacity was observed at this time.

After 24 hours of CQ exposure, a similar trend was observed when reductive capacity initially increased relative to control at 12.5 µM of CQ (106.5 ± 0.95%), but steadily declined in a dose dependent manner. However, in contrast to the 6 hour time point, a significant reduction in reductive capacity relative to control was observed when cells were exposed to 100 µM of CQ [(85.35 ± 1.24%) ($p<0.005$ vs control)] for 24 hours.

Thus, in all subsequent experiments GT1-7 cells were exposed to 100 µM of CQ for 6 and 24 hours respectively.

3.2 Chloroquine treatment causes progressive autophagy dysfunction by inducing autophagosome synthesis and inhibiting autophagosome degradation

3.2.1 LC3-II protein levels significantly and progressively increase in response to CQ exposure

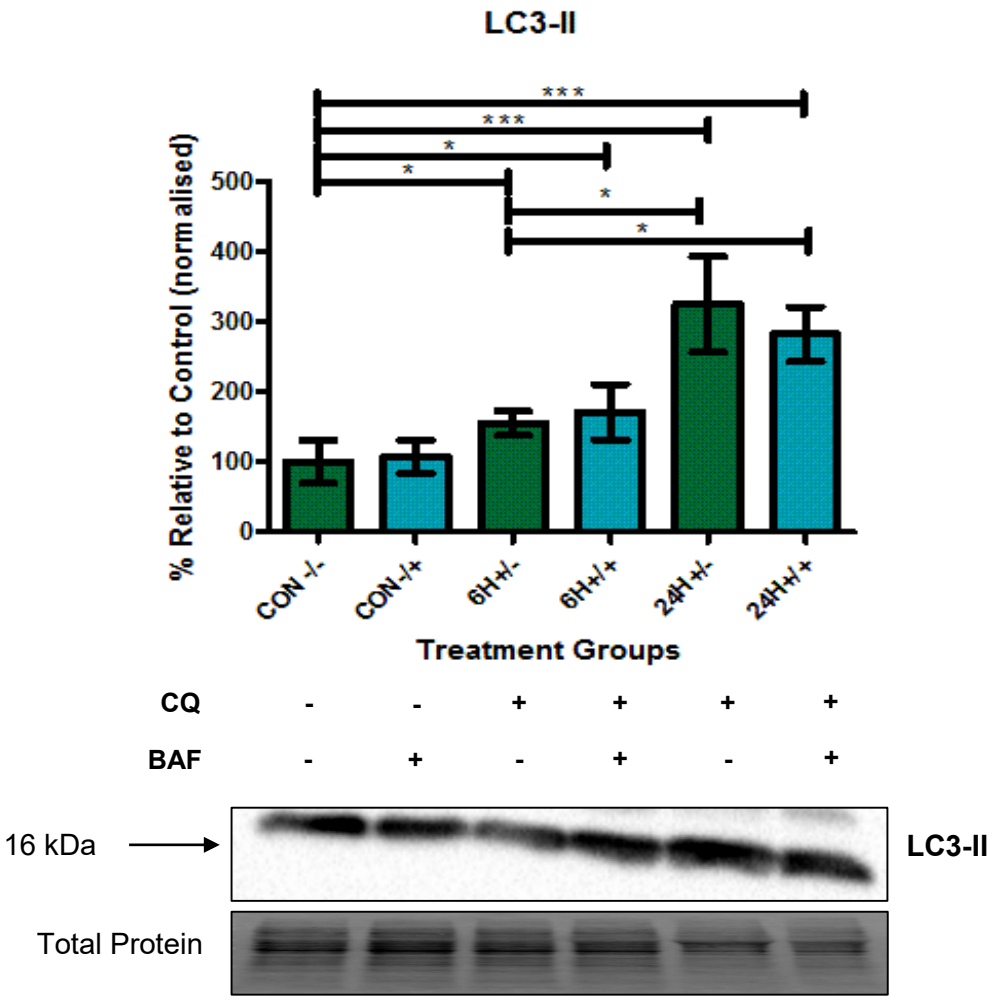

Figure 3.2: Western blot analysis of LC3-II protein levels in response to CQ and/or BAF. CQ led to a progressive accumulation of LC3-II over time, in the presence and absence of BAF, confirming autophagy dysfunction. Band Intensities normalised to total lane protein. All data are presented as a percentage of control (Mean ± SEM). * ($p<0.05$ vs control). *** ($p<0.0001$ vs control). N=5 independent experiments.

LC3 has two forms, the non-lipidated LC3-I and the lipidated LC3-II, which is incorporated into the forming autophagosomal membrane and can be used as a measurement of the abundance of autophagosomes within the cell at a given time. One can compare cytosolic LC3-II protein levels from cells treated with the autophagy inhibitor Bafilomycin A1 (BAF),

which prevents the fusion of autophagosomes and lysosomes, to untreated cells to measure the relative autophagic flux of a system – the rate of autophagosome synthesis versus degradation (Mizushima & Yoshimori 2007; Rubinsztein et al. 2009). Similarly, one can also test the effect of a therapeutic intervention on the relative autophagic flux of a system by simply treating cells in the presence or absence of BAF.

To confirm autophagy dysfunction, Western blot analysis was performed to assess the relative protein levels of LC3-II. The progressive accumulation of LC3-II in response to CQ exposure confirmed that autophagy was becoming dysfunctional over time (Fig 3.2 & 3.3).

In addition to CQ, cells were also in some cases exposed to BAF (400nM) for 2 hours post treatment to confirm that CQ was indeed causing complete inhibition of autophagosome degradation.

Our results (Fig 3.2) indicate that CQ caused progressive accumulation of LC3-II leading to a significant increase after 6 hours [(155.2 ± 17.23%) ($p<0.05$ vs control)] and 24 hours [(324.8 ± 68.25%) ($p<0.0001$ vs control)], respectively. When assessing the effect of BAF on the control cells in the absence of CQ, we see that there were no significant differences in LC3-II protein levels between the control cells (100 ± 30.65%) and cells treated with BAF (107.1 ± 23.15%), suggesting a very low rate of relative flux under homeostatic conditions (Fig 3.2). Similarly after 6 hours, no significant differences were observed in LC3-II accumulation in cells treated with CQ (155.2 ± 17.23%) when compared to cells treated with CQ and BAF (171.1 ± 39.73%) confirming that CQ was indeed causing maximal inhibition of autophagosome degradation at the time (Fig 3.2). In addition, it appears that chloroquine not only inhibits autophagy at this time of exposure, but also affects the flux by enhancing autophagosome synthesis (Rubinsztein et al. 2009). Finally, relative to 6 hours of CQ exposure, there was a significant increase ($p<0.05$) in LC3-II protein levels after 24 hours of CQ treatment as well as CQ and BAF treatment (Fig 3.2)

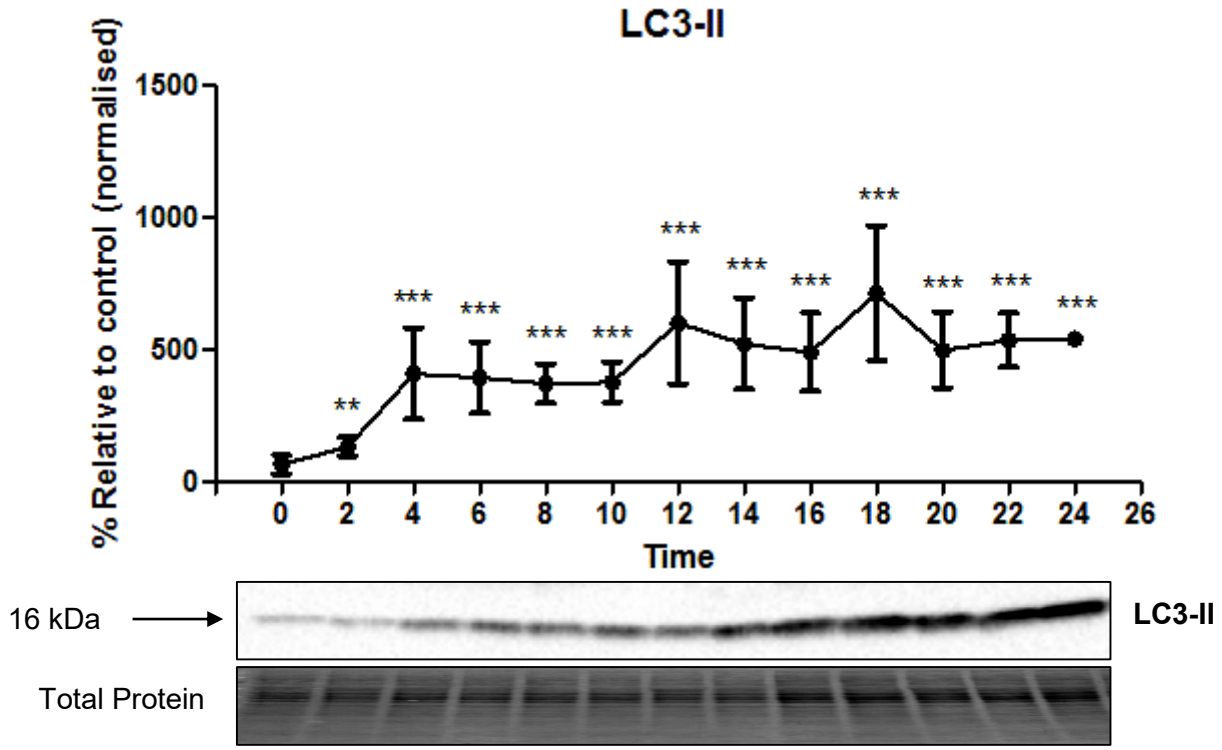

Figure 3.3: Western blot analysis of LC3-II protein levels in response to CQ-induced autophagy dysfunction over the course of 24 hours. *The data suggest progressive autophagy dysfunction due to the inhibition of autophagosome degradation. Band intensities normalised to total lane protein. All data are presented as a percentage of 0 hours (Mean ± SEM). ** (p<0.05 vs 0 hours) *** (p<0.0001 vs 0H). N=3 independent experiments*

LC3-II protein levels significantly increase after 2 hours of CQ exposure relative to 0 hours ($p<0.05$) and progressively and significantly increase ($p<0.0001$ vs 0 hours)] further over the course of 24 hours.

3.2.2 p62 protein levels significantly and progressively decrease in response to CQ exposure

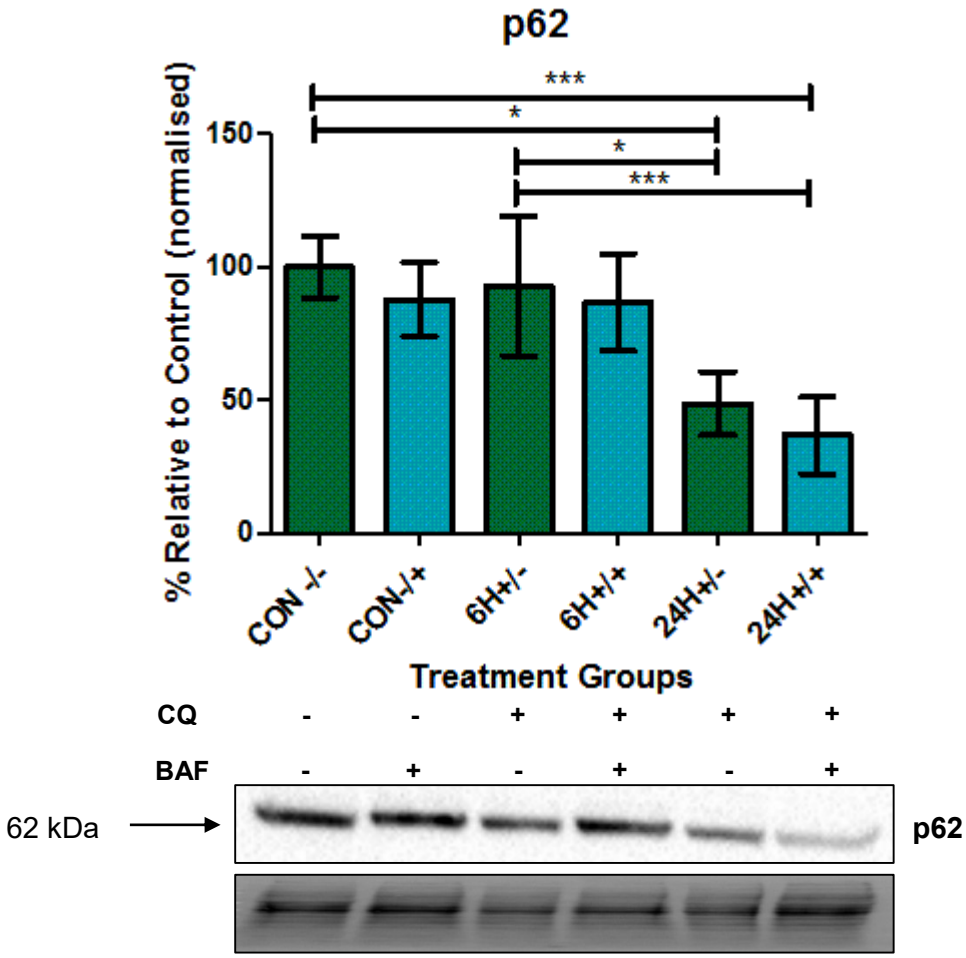

Figure 3.4: Western blot analysis of p62 protein levels in response to CQ and/or BAF. *CQ led to a progressive decline in p62 concentrations over time. The combined effect of CQ and BAF led to a further decrease in concentrations when compared to cells treated with CQ alone, at both 6 and 24 hours of CQ exposure. Band Intensities normalised to total lane protein. All data are presented as a percentage of control (Mean ± SEM). * (p<0.05 vs 0H). *** (p<0.0001 vs 0H).N=5 independent experiments*

p62 is an autophagy related adaptor protein that targets poly-ubiquinated proteins toward the forming autophagosome for selective degradation (Sahani et al. 2014). p62 not only directly interacts with LC3 residues but is also independently incorporated into the autophagosomal membrane and can therefore also be used as a marker for selective autophagy activity (Sahani et al. 2014). Our results (Fig. 3.4) indicate that CQ caused a progressive decline in p62 protein levels over time leading to a significant decrease relative to control after 24 hours [(48.74 ± 11.93%) ($p<0.05$ vs control)]. Similarly, a significant decrease was also observed between the control cells and cells treated with both CQ and BAF after 24 hours [(36.88 ± 14.46%) ($p<0.0001$ vs control)]. In addition, a significant decrease was also observed relative to 6 hours of CQ treatment after 24 hours of CQ ($p<0.05$) as well as CQ and BAF ($p<0.05$).

However, no significant differences were observed after 24 hours between cells treated with CQ and those treated with CQ and BAF.

3.3 CQ-induced autophagy dysfunction impacts microtubulin stability and structure

3.3.1 Acetylated α-Tubulin protein levels increase non-significantly in response to CQ exposure

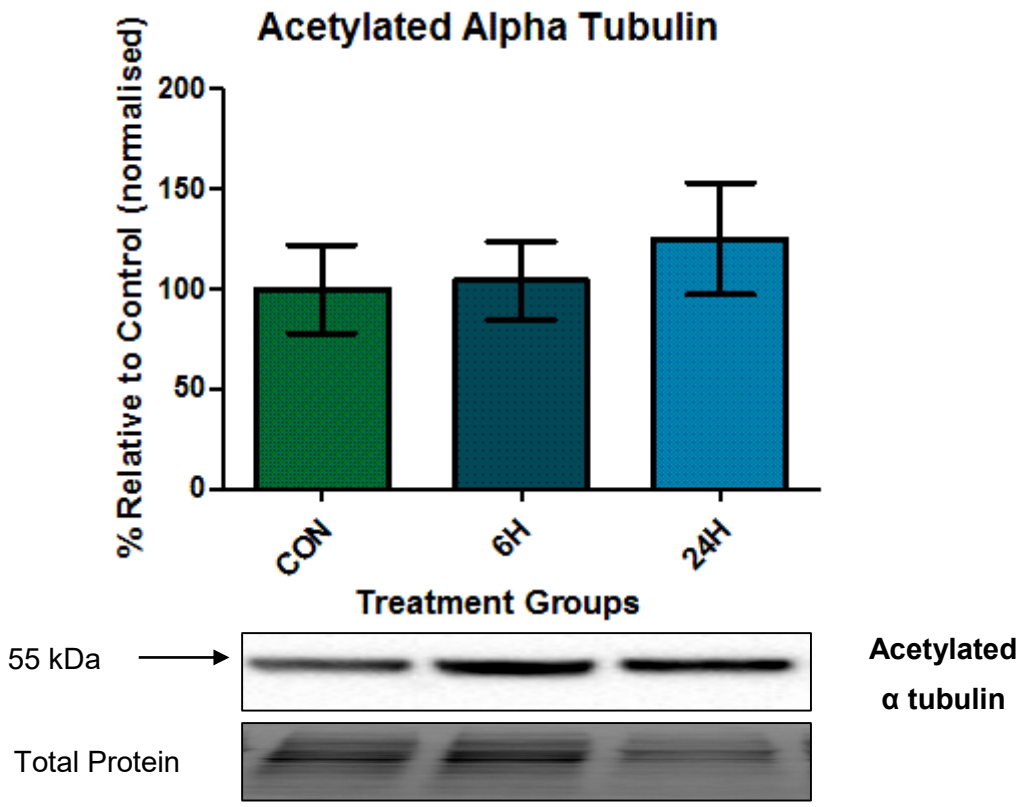

Figure 3.5: Western blot analysis of Acetylated α-tubulin protein levels *– a marker for stable tubulin, after 6 and 24 hours of CQ exposure. CQ-induced autophagy dysfunction led to a non-significant increase in acetylated tubulin over time. Band Intensities normalised to total lane protein. All data are presented as a percentage of control (Mean ± SEM). N=6 independent experiments*

Acetylated tubulin is considered an indicative marker of stable microtubules (Butler et al. 2007). Protein levels of acetylated α-tubulin were assessed in response to progressive CQ-induced autophagy dysfunction. Our results indicate that tubulin stability is impacted over time during autophagy dysfunction. Although it is not a trend leading to significance, the progressive increase in acetylated tubulin can be observed after both 6 hours (104.3 ± 19.75%) and 24 hours (125.2 ± 27.86%) of CQ exposure relative to the control (100 ± 22.1%).

3.3.2 CQ-induced autophagy dysfunction impacts acetylated α-tubulin

Super Resolution Structured Illumination microscopy (SR-SIM) and direct stochastic optical reconstruction microscopy (dSTORM) microscopy are super resolution techniques that resolve images to a maximum resolution of 80 nm and 20 nm, respectively. They are thus extremely powerful techniques to assess protein localisation and distribution.

Confocal, SR-SIM and dSTORM microscopy was utilised to assess the acetylated α-tubulin signal under control and after CQ-induced autophagy dysfunction. Under control conditions, microscopy analysis revealed that acetylated α-tubulin signal was diffusely distributed in the cytosol of cells, however, the signal consistently arranged into an intense network like morphology in the perinuclear region of the cell (Fig 3.6A, 3.7A & 3.8A).

After 6 hours of CQ exposure, acetylated α-tubulin became less diffusely distributed in the cytosolic compartments and processes, instead arranging into dense filamentous networks that distributed the expanse of the cell (Fig 3.6B, 3.7B & 3.8B).

After 24 hours of CQ exposure, minimal diffusely distributed acetylated α-tubulin signal was observed in cytosolic compartments or in processes. The majority of the signal arranged into dense filamentous structures in a network morphology (Fig 3.6C, 3.7C & 3.8C).

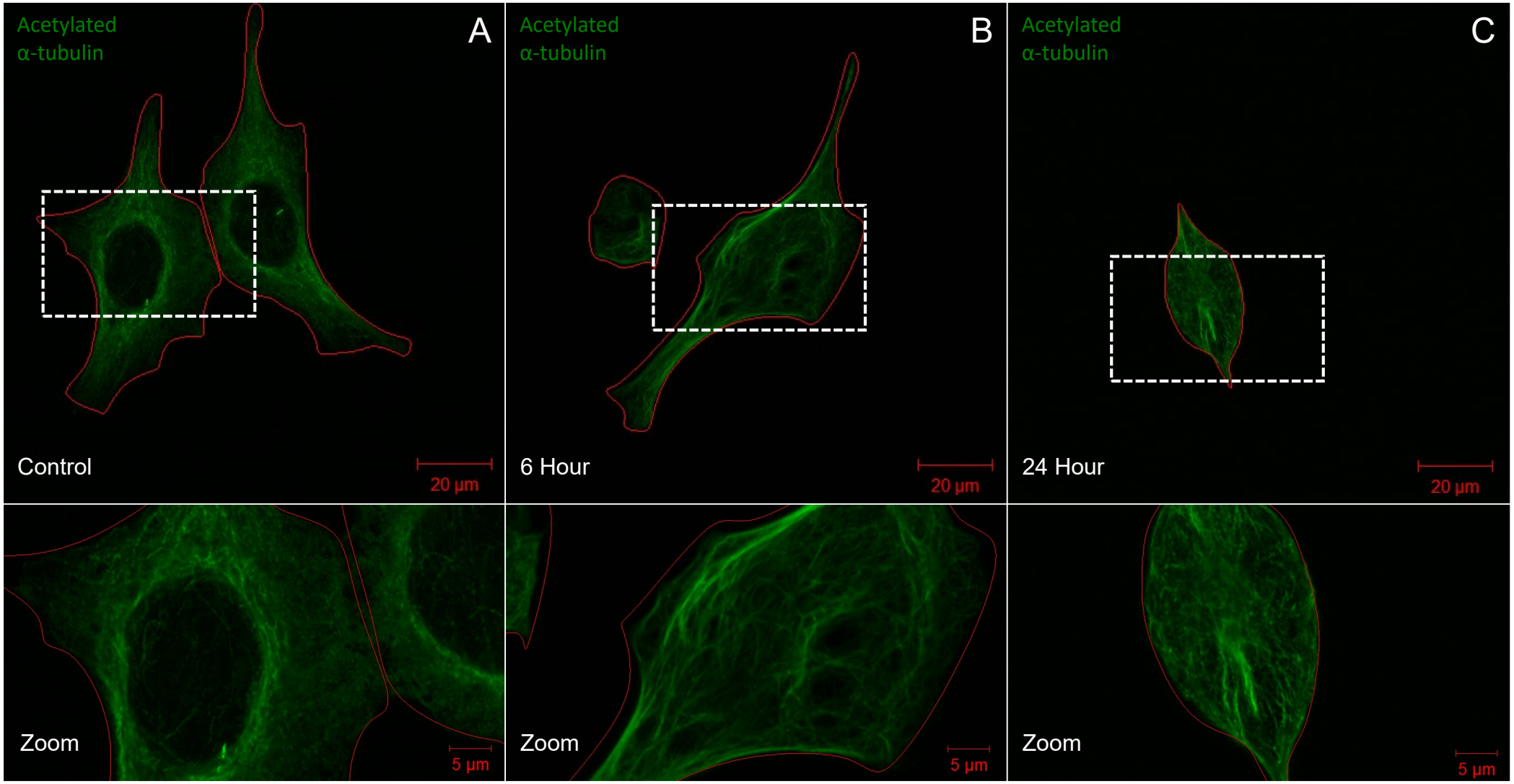

Figure 3.6: Confocal microscopy assessing acetylated α-tubulin signal distribution in response to CQ-induced autophagy dysfunction. *Acetylated α-tubulin (Alexa 488) (Green). N=3 independent experiment. Scale bar = 20 µm and 5 µm, respectively.*

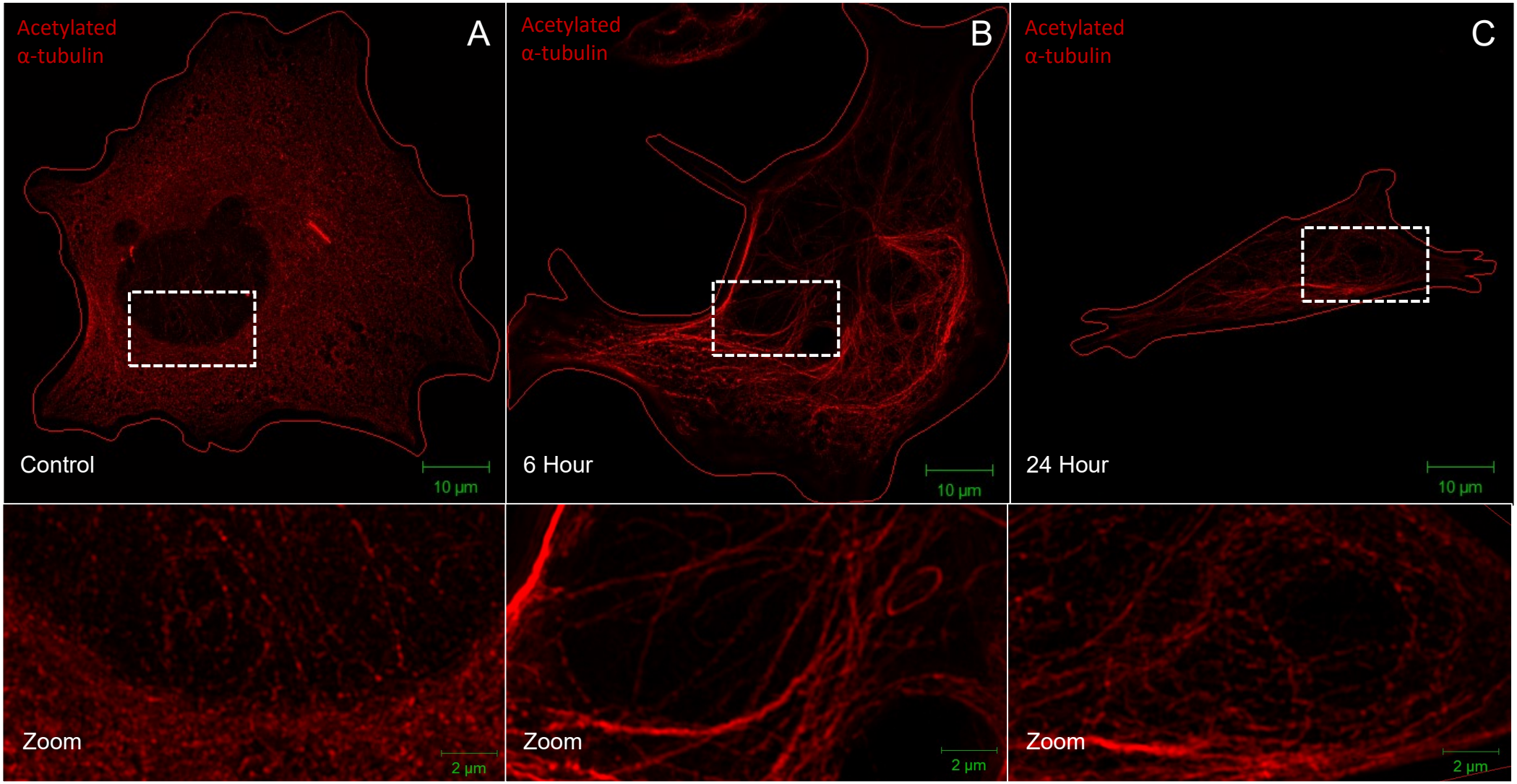

Figure 3.7: SR-SIM microscopy assessing acetylated α-tubulin signal distribution in response to CQ-induced autophagy dysfunction. *Acetylated α-tubulin (Alexa 568) (Red). N=3 independent experiment. Scale bar = 10 µm and 2 µm, respectively.*

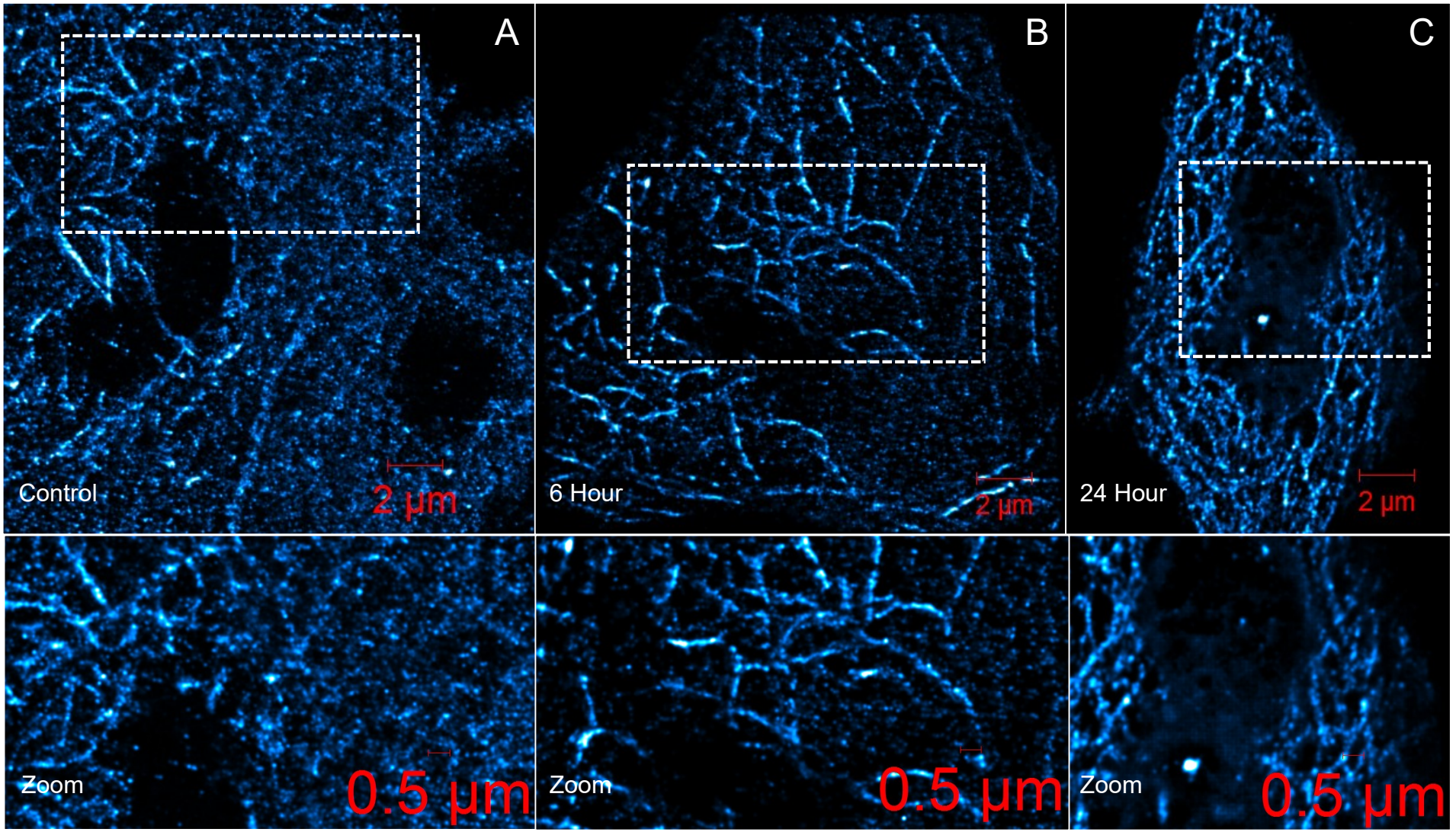

Figure 3.8: dSTORM microscopy assessing acetylated α-tubulin signal distribution in response to CQ-induced autophagy dysfunction. *Acetylated α-tubulin (Alexa 488) (Cyan). N=1 independent experiment. Scale bar = 2 µm and 0,5 µm, respectively.*

3.4 CQ-induced autophagy dysfunction causes a decrease in Tau protein levels and Tau aggregation

3.4.1 Total Tau protein levels in response to CQ exposure

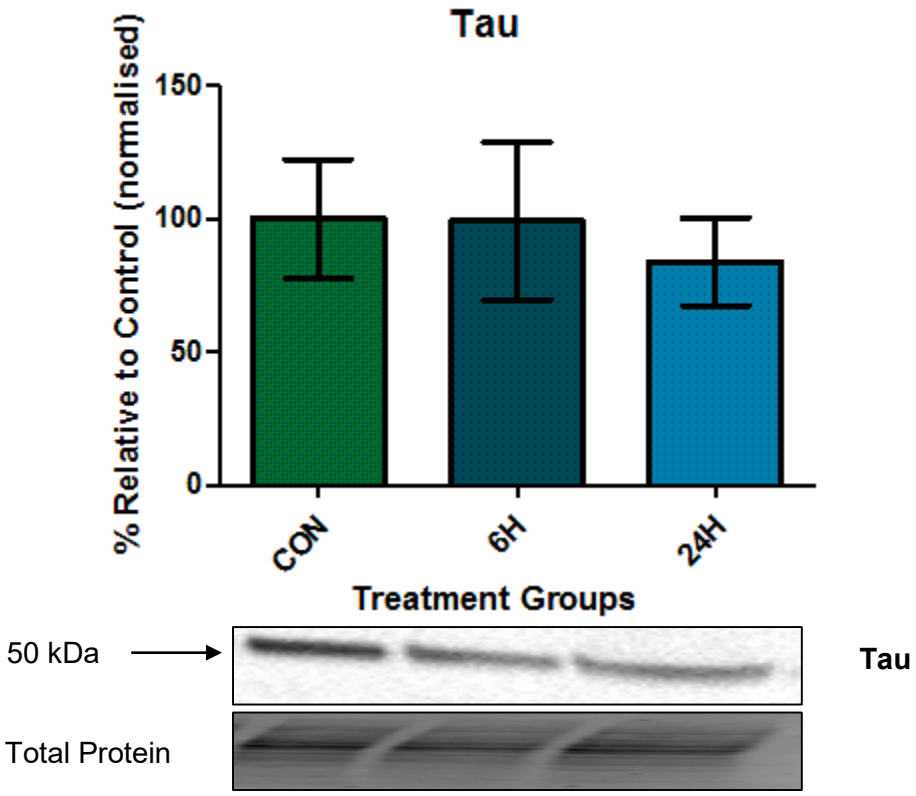

Figure 3.9: Western blot analysis of total Tau protein levels, after 6 and 24 hours of CQ exposure. *CQ-induced autophagy dysfunction cause a progressive, yet non-significant decrease in Tau protein levels. Band Intensities normalised to total lane protein. All data are presented as a percentage of control (Mean ± SEM). N=6 independent experiments.*

To assess the protein levels of total Tau in response to the CQ-induced autophagy dysfunction, an anti-CP27 antibody was used, which recognises the amino acid sequence between the 130-150 residues in human Tau, but also detects mouse total Tau as it shares ~88% sequence homology (Petry et al. 2014). Our results indicate that Tau is impacted by autophagy dysfunction over time as a decreasing trend in protein levels was observed. Although the trend is not one leading to significance, we observed progressive decline in total Tau protein levels relative to control cells (100 ± 22.29%) at 6 hours (99.36 ± 22.59%) and 24 hours (83.94 ± 16.55%), respectively.

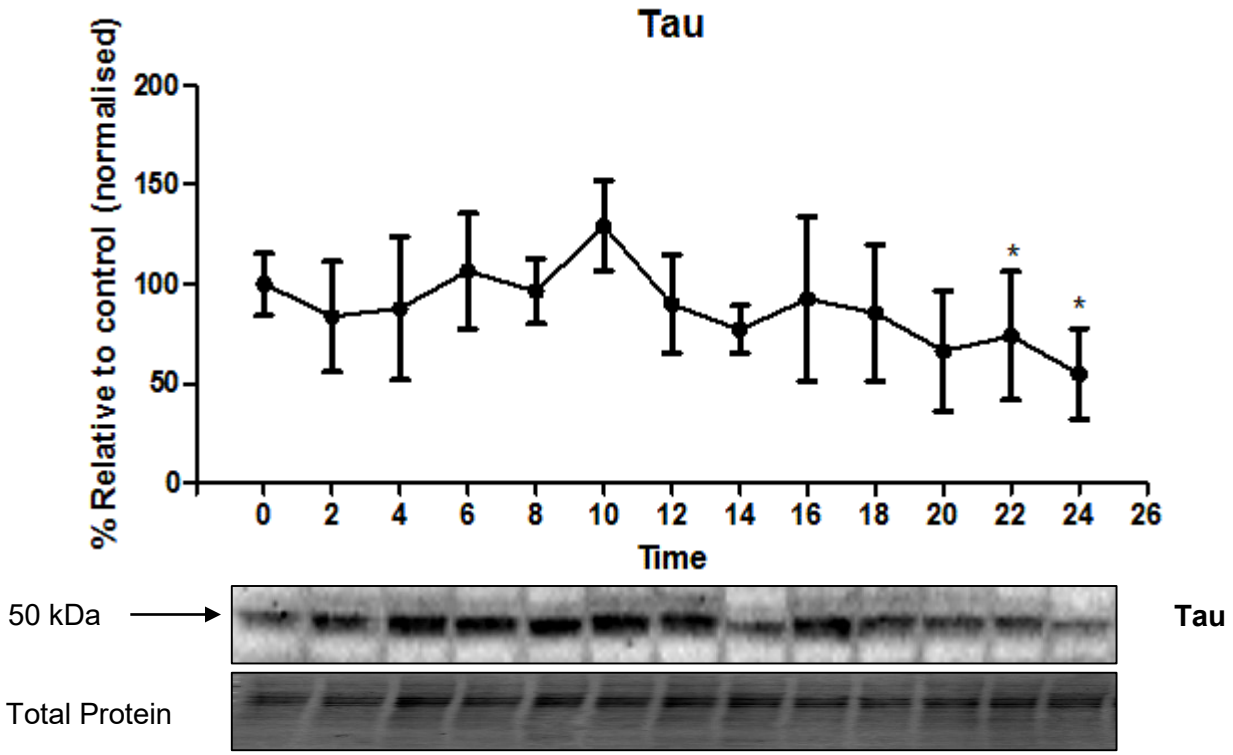

Figure 3.10: Western blot analysis of Tau protein levels in response to CQ-induced autophagy dysfunction over the course of 24 hours. *Tau protein levels progressively decrease over time in response to CQ exposure. All data are presented as a percentage of 0 hours (Mean ± SEM). *(p<0.05 vs 0 hours). N=3 independent experiments.*

Total Tau protein levels declined after 2 hours of exposure to CQ relative to 0 hours, which then increased after 10 hours, after which it progressively and gradually decreased during the rest of the 24 hour period, relative to 0 hours. Protein levels were significantly reduced relative to 0 hours after 22 hours ($p<0.05$) and 24 hours ($p<0.05$), respectively.

3.4.2 Tau progressively aggregates in response to CQ-induced autophagy dysfunction

To assess Tau signal distribution in relation to acetylated α-tubulin in cells, under control and experimental conditions, SR-SIM analysis was performed using cells transfected with GFP tagged human Tau (P301L) and stained with Alexa Fluor-568 against acetylated α-tubulin (Fig. 3.11). Under control conditions Tau signal was diffusely distributed within the cell, but diminished slightly around the nuclear region (Fig. 3.11A, C &D). Acetylated α-tubulin signal was diffusely distributed in the cell cytosol and periphery, particularly the processes, but became dense and more ordered around the perinuclear region manifesting as a clear microtubulin network pattern (Fig. 3.11B &D). After 6 hours of CQ-induced autophagy dysfunction Tau signal became less diffuse, instead arranging into aggregate-like regions in the cytosol (Fig. 3.11G & H). Similarly acetylated α-tubulin signal became less diffuse in the cytosolic regions, manifesting as highly dense network like microtubule structures (Fig. 3.11F &H). Furthermore, clear regions either devoid or with diminished signal were clearly resolved in the cytosol (Fig. 3.11H). After 24 hours of CQ-induced autophagy dysfunction, Tau signal was maintained in aggregate-like regions (Fig. 3.11K & L), but importantly the aggregated signal increasingly concentrated in cell processes (Fig. 20I &L). The acetylated α-tubulin signal show clear disruptions in the linear signal distribution (Fig. 3.11L). Moreover, the acetylated α-tubulin signal appeared clustered in the peripheral areas of the cell (Fig. 3.11J).

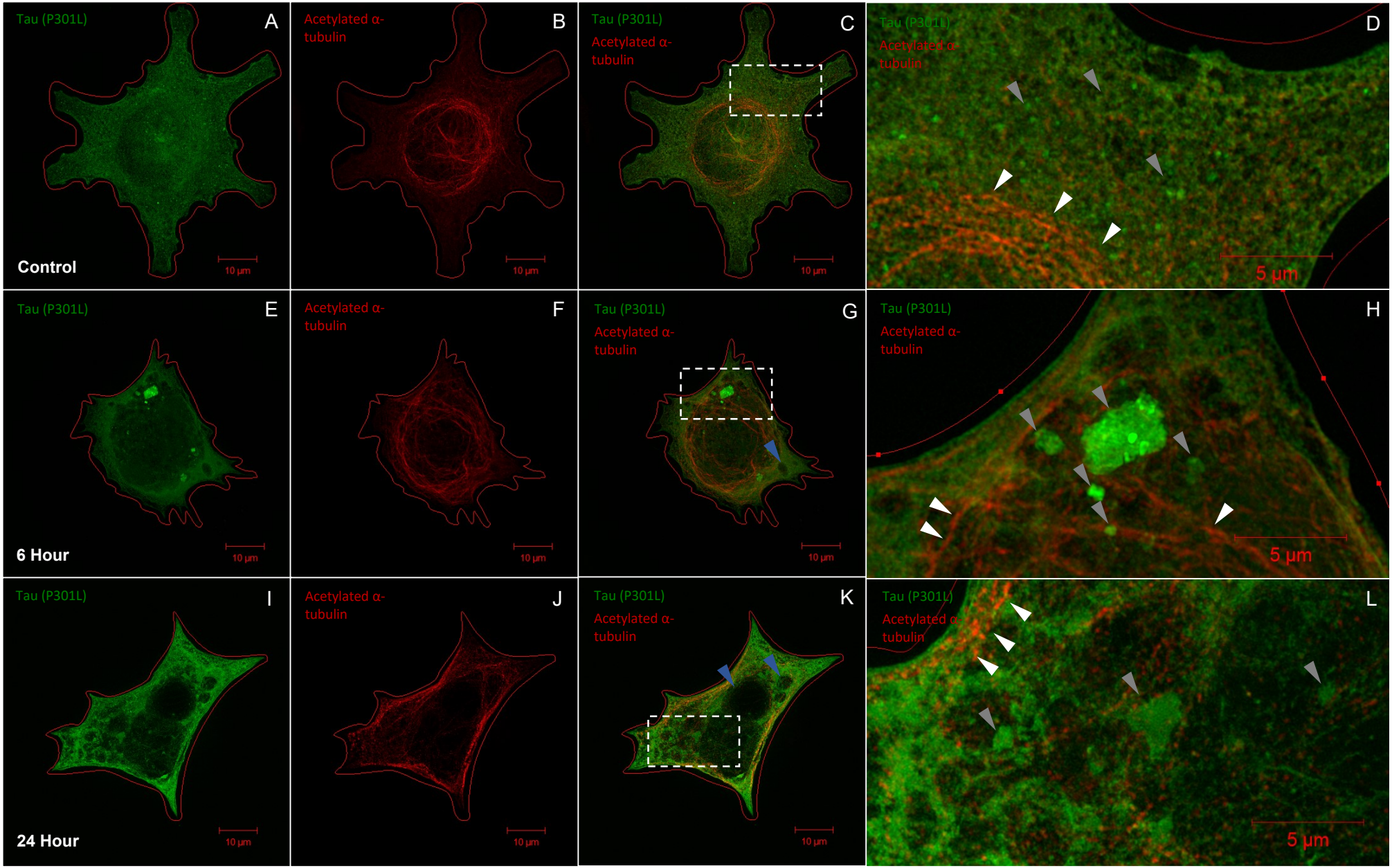

Figure 3.11: Distribution of Tau and acetylated α-tubulin signal under control conditions and during various stages of CQ-induced autophagy dysfunction. *Blue arrow heads indicate vacuole-like structures, white arrow heads indicate tubulin structure and grey arrow heads indicate Tau aggregation. Tau (GFP) and acetylated α-tubulin (Alex Fluor-568). N=3 independent experiments. Scale bar = 10 µm and 5 µm, respectively.*

3.5 CQ-induced autophagy dysfunction causes an increase in Tau phosphorylation, but not phosphorylated Tau aggregation

3.5.1 pTau protein levels increase in response to CQ exposure

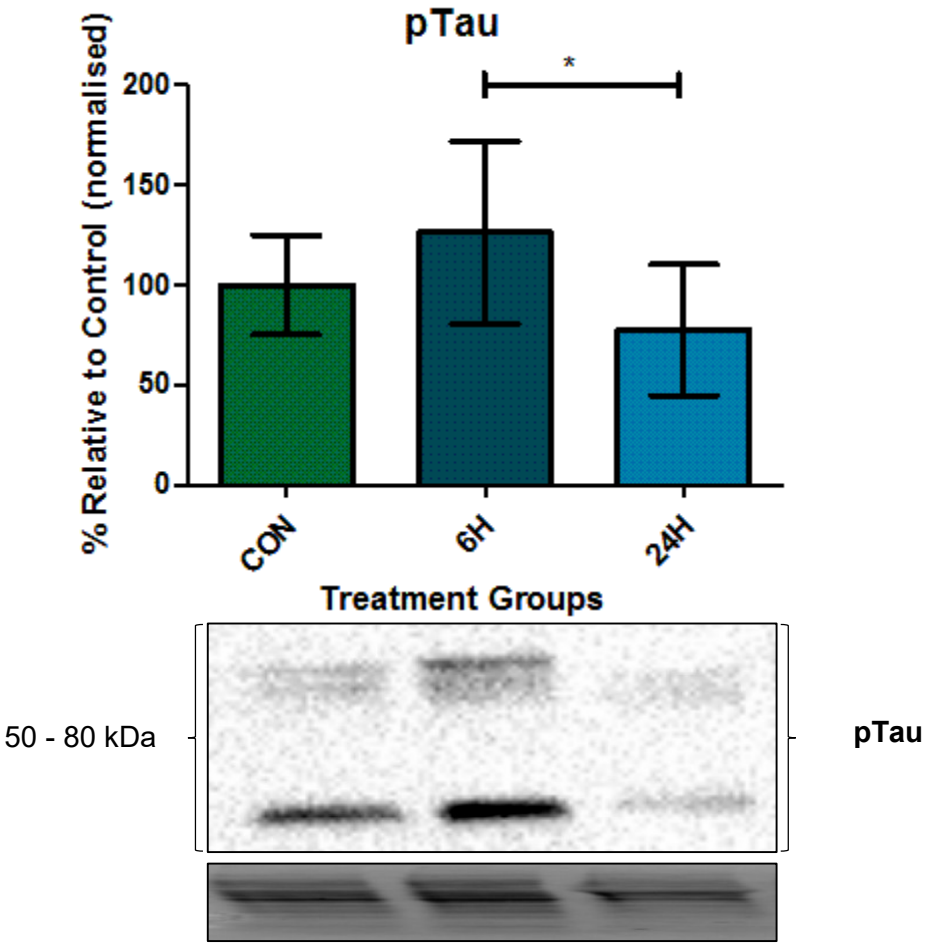

Figure 3.12: Western blot analysis of phosphorylated Tau (pTau) protein levels, after 6 and 24 hours of CQ exposure. *CQ-induced autophagy dysfunction caused a non-significant increase in pTau after 6 hours of exposure, but this was not maintained after 24 hours. Furthermore, concentrations significantly declined relative to 6 hours and non-significantly relative to control conditions. All data are presented as a percentage of control (Mean ± SEM). *(p<0.05 vs CON). N=6 independent experiments.*

To assess the effect of CQ-induced autophagy dysfunction on Tau phosphorylation we assessed phosphorylation at specific sites which included serine 400, threonine 403 and serine 404 residues. Tau with phosphorylation of the serine 404 residue has been associated with an impaired ability to facilitate microtubule polymerisation (Evans et al. 2000). When compared to control (100 ± 24.92%) Tau phosphorylation increased as an early event after 6 hours (126.4 ± 45.82%) of autophagy dysfunction, although this was not a significant difference. Furthermore, this increase in phosphorylation was not maintained after 24 hours

(77.49 ± 32.68%) of dysfunction, as a significant difference between 6 and 24 hours can be observed ($p<0.05$; 6H vs 24H) (Fig 3.12).

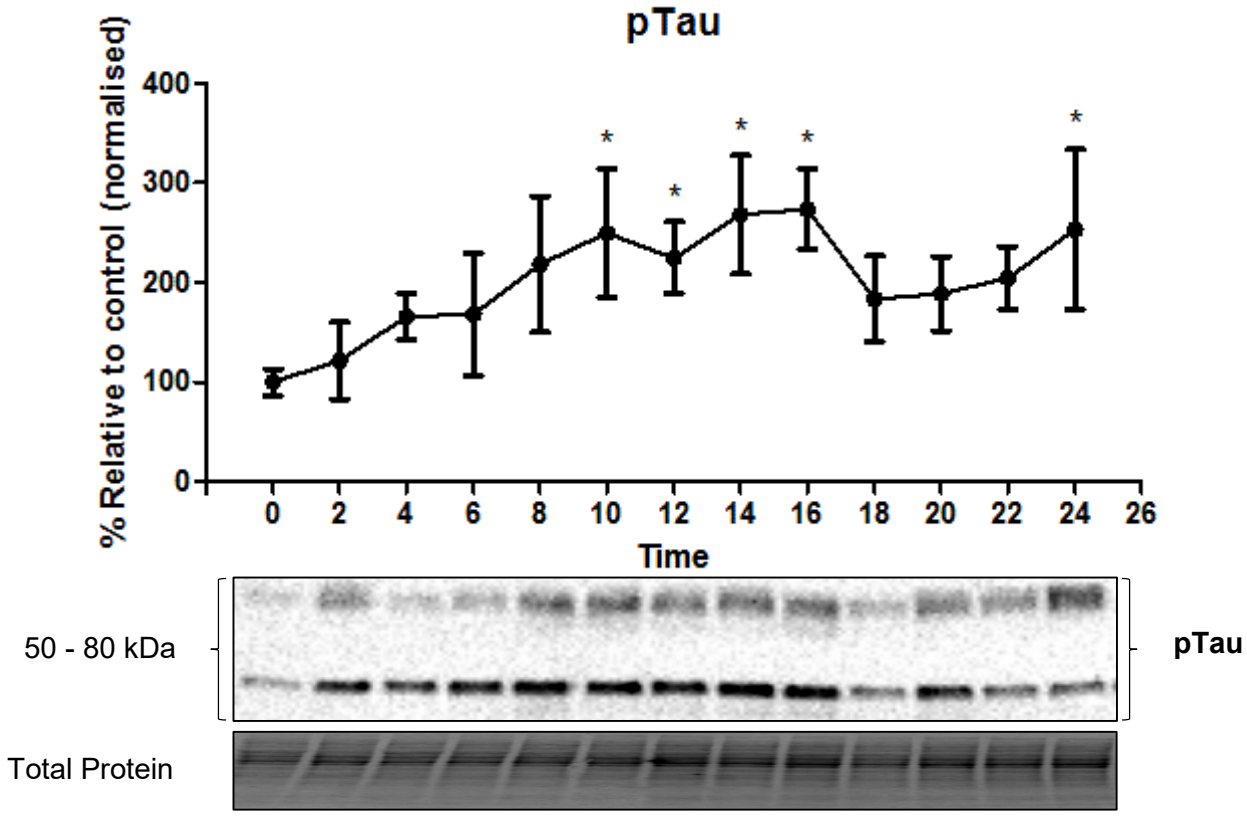

Figure 3.13: Western blot analysis of pTau protein levels in response to CQ-induced autophagy dysfunction over the course of 24 hours. *pTau protein levels progressively increase over time in response to CQ exposure. All data are presented as a percentage of 0 hours (Mean ± SEM). *($p<0.05$ vs 0 hours). N=3 independent experiments.*

In response to CQ exposure, phosphorylation of Tau progressively increased, reaching significance at 10 hours vs 0 hours ($p<0.05$) and remained significantly elevated after 16 hours, but decreased to non-significant levels after 18 hours relative to 0 hours. A non-significant decreasing trend was observed until 24 hours where the protein levels were significantly higher relative to 0 hours (Fig 3.13).

Although findings of a significant increase in pTau after 24 hours are in contrast to those observed in Fig 3.12, it is important to note that the sample size of this particular analysis was indeed smaller and therefore the standard error of the mean was larger – reducing the statistical power. Nonetheless, the majority of these findings are still in agreement with the analysis presented in Fig 3.12, particularly the increase in pTau protein levels observed after 6 hours of CQ exposure (Fig 3.12 & 3.13).

3.5.2 pTau localises within the nucleus, which is maintained during CQ-induced autophagy dysfunction

To assess pTau signal distribution in relation to acetylated α-tubulin in cells, under control and experimental conditions, confocal analysis was performed using cells stained with Alexa Fluor-488 against acetylated α-tubulin and Alexa Fluor-568 against pTau, and finally counterstained with Hoechst 33342 (Fig. 3.14). pTau signal was distributed very weakly in the cytosol regions. In fact, it appeared that the pTau signal was almost exclusively localised within the nucleus (Fig. 3.14B & D). After 6 hours of CQ exposure, no changes in of pTau signal distribution were observed – as the signal remained concentrated in the nucleus (Fig. 3.14F & H). Importantly, no signs of pTau signal aggregation were observed (Fig. 3.14H). After 24 hours of CQ exposure, no changes could be discerned in pTau signal relative to the control conditions and earlier point of CQ exposure (Fig. 3.14L).Of note, the nuclear signal distribution of pTau became progressively more condensed during the CQ-induced autophagy dysfunction especially at the late time point (24 hours), which may suggest cellular stress (Fig. 3.14D, H & L). Furthermore, the overall cell morphology indicated shrinkage over time and clear vacuolar-like structures were observed after 24 hours of autophagy dysfunction (Fig. 3.14L).

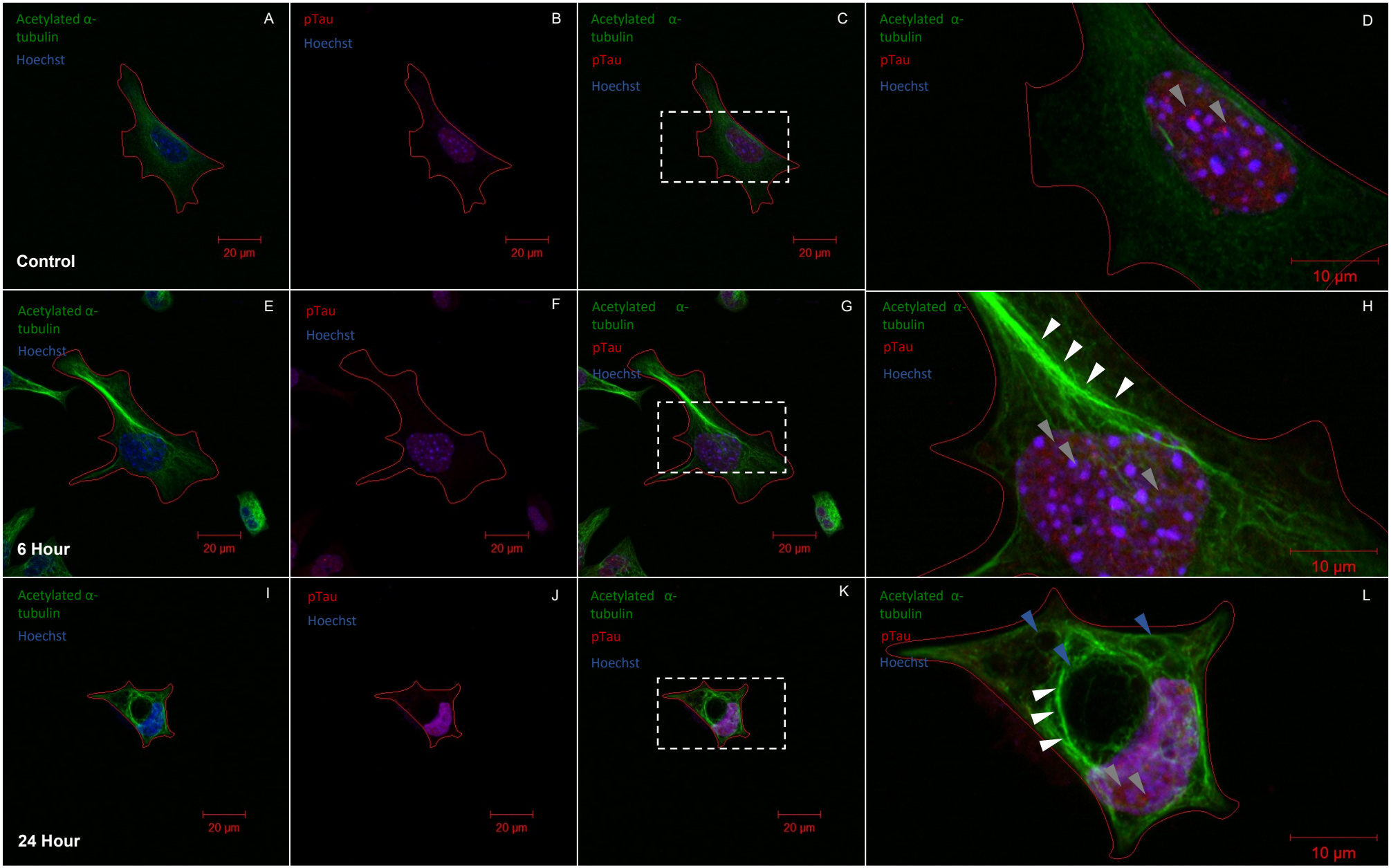

Figure 3.14: Distribution of pTau and acetylated α-tubulin signal under control conditions and during various stages of CQ-induced autophagy dysfunction*. N=3 independent experiments. Acetylated α-tubulin (Alexa Fluor-488), pTau (Alexa Fluor-568) and Hoechst 33342 (Blue). Blue arrow heads indicate vacuole-like structures, white arrow heads indicate tubulin structure and grey arrow heads indicate pTau distribution. Scale bar = 20 µm and 10 µm, respectively.*

3.6 CQ-induced autophagy dysfunction causes a non-significant increase Spastin protein levels and a change in Spastin cellular localisation

3.6.1 Spastin protein levels non-significantly increase in response to CQ exposure

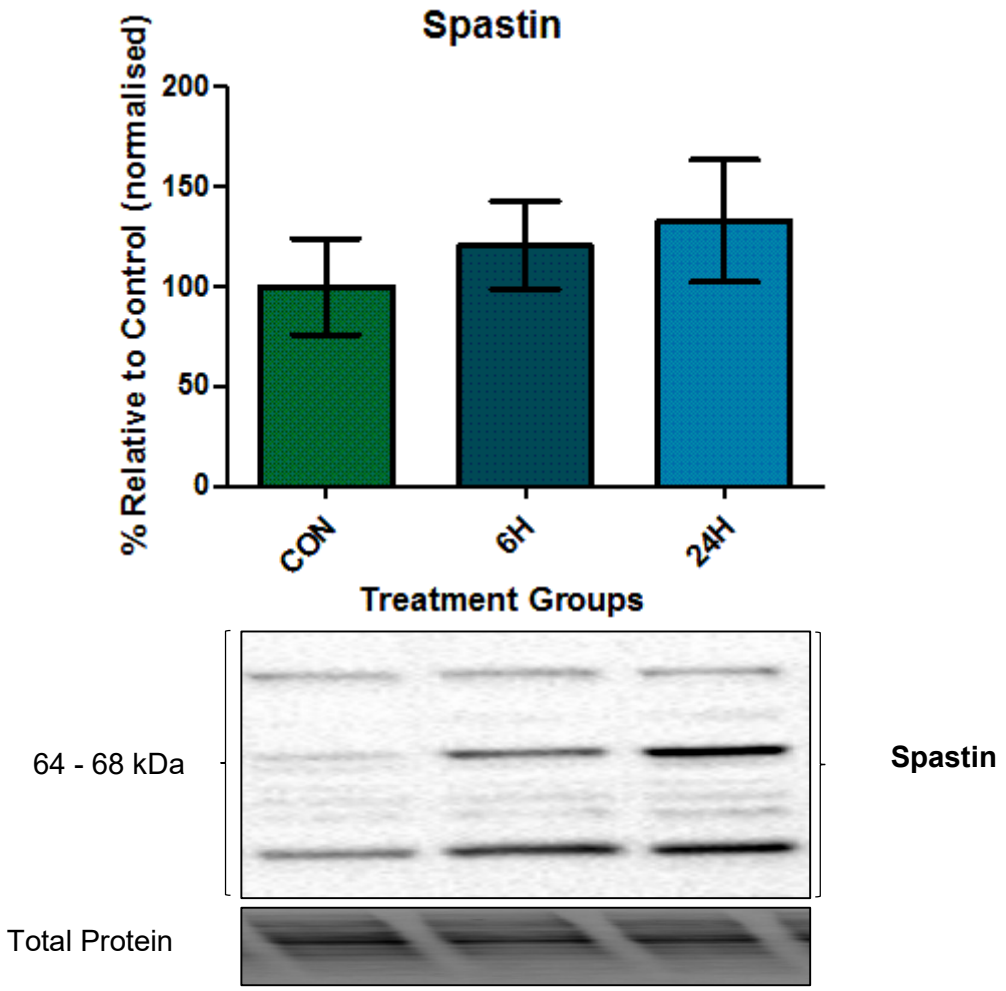

Figure 3.15: Western blot analysis of Spastin expression, after 6 and 24 hours of CQ exposure*. CQ-induced autophagy dysfunction caused a progressive, but non-significant increase in Spastin protein levels over time. Band Intensities normalised to total lane protein. All data are presented as a percentage of control (Mean ± SEM). N=6 independent experiments.*

CQ-induced autophagy dysfunction led to a progressive increase in Spastin protein levels over time. The trend did not lead to a significant increase, but clear differences can be observed between control cells (100 ± 24.15%) and those exposed to CQ for 6 hours (120.4 ± 22.12%) and 24 hours (132.8 ± 30.59%), respectively.

3.6.2 Spastin signal distributes throughout the cell and forms punctate and ordered structures around areas of euchromatin

To assess Spastin signal distribution in relation to stable microtubulin in cells, under control and experimental conditions, confocal analysis was performed using cells stained with Alexa Fluor-488 against acetylated α-tubulin and Alexa Fluor-568 against Spastin, counterstained with Hoechst 33342 (Fig. 3.16). Spastin signal was diffusely distributed in the cell cytosol, but showed strong signal as bright punctate structures around euchromatic DNA regions within the nucleus (Fig. 3.16D). After 24 hours of CQ exposure, Spastin signal remained diffusely distributed in the cytosol, but the punctate structures around euchromatin regions in the nucleus appeared to be reduced in number and intensity (Fig. 3.16H). Furthermore, vacuolar-like structures with reduced signal distribution were also visible. After 24 hours of CQ exposure, the overall cellular morphology showed a decrease in size, indicative of cellular stress. Regardless of the size of the cells, clustered acetylated α-tubulin signal could still be resolved (Fig. 3.16J & L). Spastin signal remained homogenously distributed in the cytosol, but the nuclear puncta were reduced in number, likely due to the nuclear condensation observed. Additionally, Spastin signal was observed in the cell periphery, partially extracellular area (Fig. 3.16L), suggesting membrane rupture and release of cytosolic constituents.

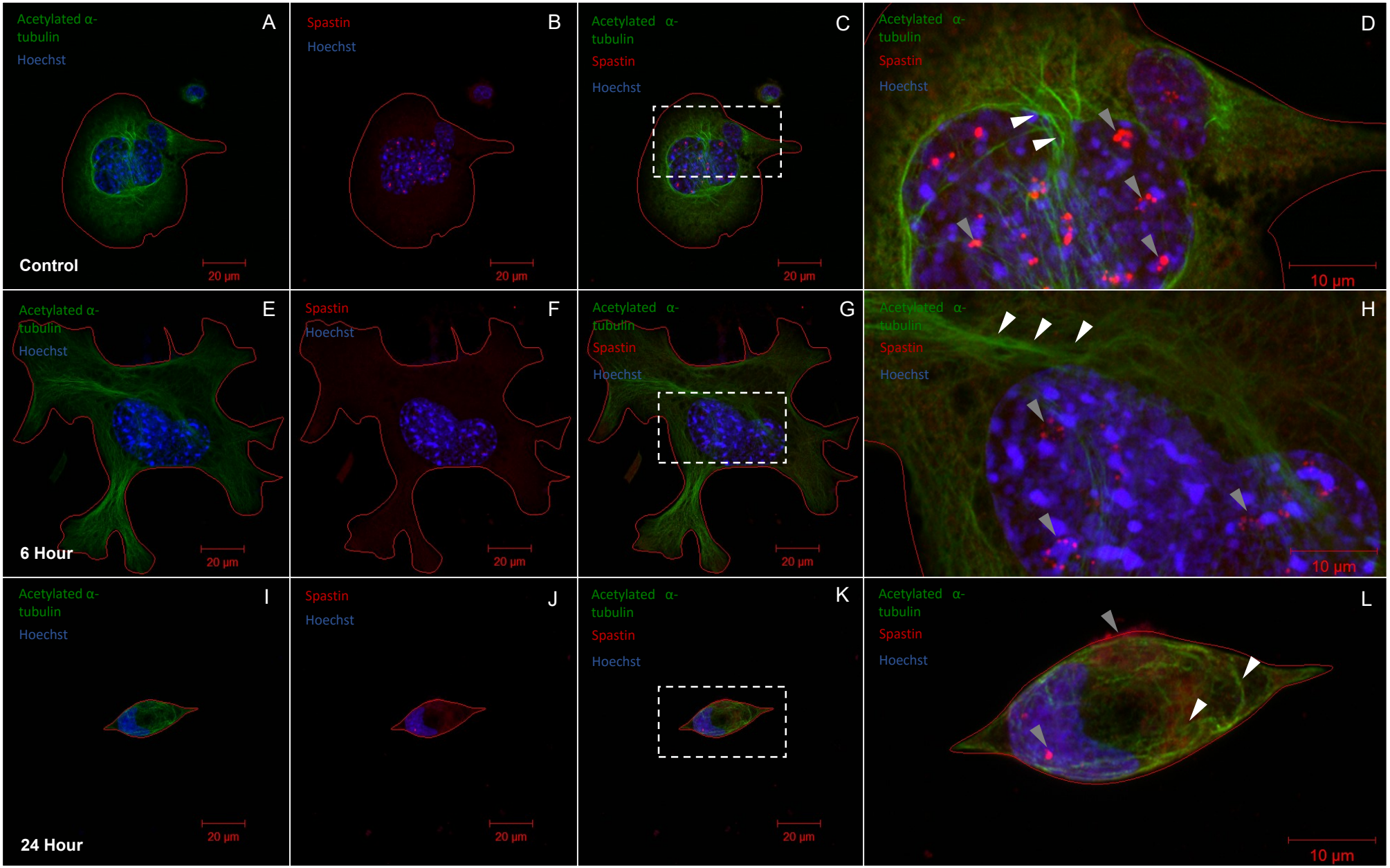

Figure 3.16: Distribution of Spastin and acetylated α-tubulin signal under control conditions and during various stages of CQ-induced autophagy dysfunction. *N=3 independent experiments. Acetylated α-tubulin (Alexa Fluor-488), Spastin (Alexa Fluor-568) and Hoechst 33342 (Blue). Blue arrow heads indicate vacuole-like structures, white arrow heads indicate tubulin structure and grey arrow heads indicate Spastin distribution. Scale bar = 20 µm and 10 µm, respectively.*

3.7 CQ-induced autophagy dysfunction causes a significant increase in Katanin p60 protein levels, but no change in Katanin p60 localisation

3.7.1 Katanin p60 protein levels progressively and significantly increase in response to CQ exposure

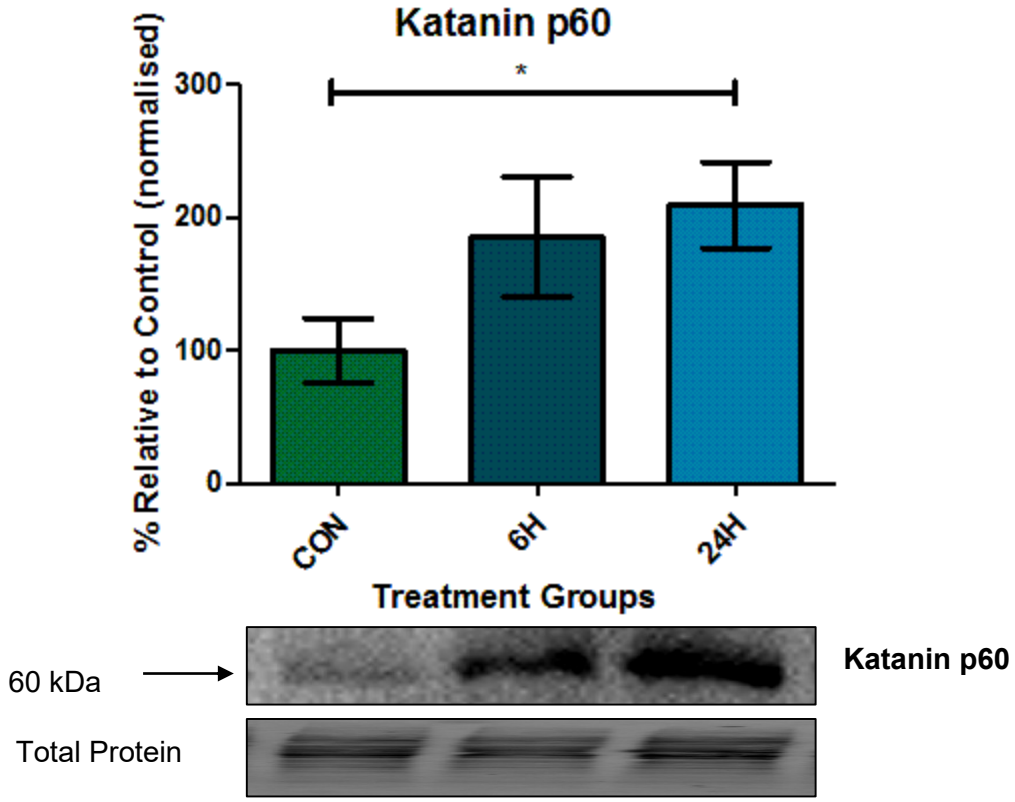

Figure 3.17: Western blot analysis of Katanin p60 expression, after 6 and 24 hours of CQ exposure. *CQ-induced autophagy dysfunction caused a progressive increase in Katanin p60 protein levels over time, leading to a significant increase relative to control after 24 hours of exposure. Band Intensities normalised to total lane protein. All data are presented as a percentage of control (Mean ± SEM). *(p<0.05 vs CON). N=6 independent experiments.*

CQ-induced autophagy dysfunction led to a progressive increase in Katanin p60 protein levels over time. A significant increase in Katanin p60 protein levels was observed after 24 hours [(209.4 ± 32.14%) ($p<0.05$)] of autophagy dysfunction relative to the control conditions (100 ± 24.03%). After 6 hours (185.1 ± 45.12%) of autophagy dysfunction the Katanin p60 protein levels markedly increased relative to the control with a probability strongly leaning towards significance ($p=0.06$).

3.7.2 Katanin p60 signal localised in the nucleus and increased in intensity in response to CQ-induced autophagy dysfunction

To assess Katanin p60 signal distribution in relation to acetylated α-tubulin in cells, under control and experimental conditions, confocal analysis was performed on cells stained with Alexa Fluor-488 against acetylated α-tubulin and Alexa Fluor-568 against Katanin p60, counterstained with Hoechst 33342 (Fig. 3.18). Under control conditions, Katanin p60 signal was diffusely distributed across the cell, with random regions containing puncta of intense signal. Furthermore, the signal also appeared more intense around euchromatin regions in the nuclei (Fig. 3.18D). After 6 hours of CQ, Katanin p60 signal appeared preferentially concentrated in areas occupied by euchromatin (Fig. 3.18H). Vacuolar-like structures are clearly visible after this time of CQ exposure (Fig. 3.18E). Results after 24 hours of CQ exposure remained similar to observed after 6 hours in both acetylated α-tubulin and Katanin p60 signal distribution (Fig. 3.18L). Of note, both nuclear and Katanin p60 signal was visible outside of the cell, suggesting cell death onset at this stage (Fig. 3.18L).

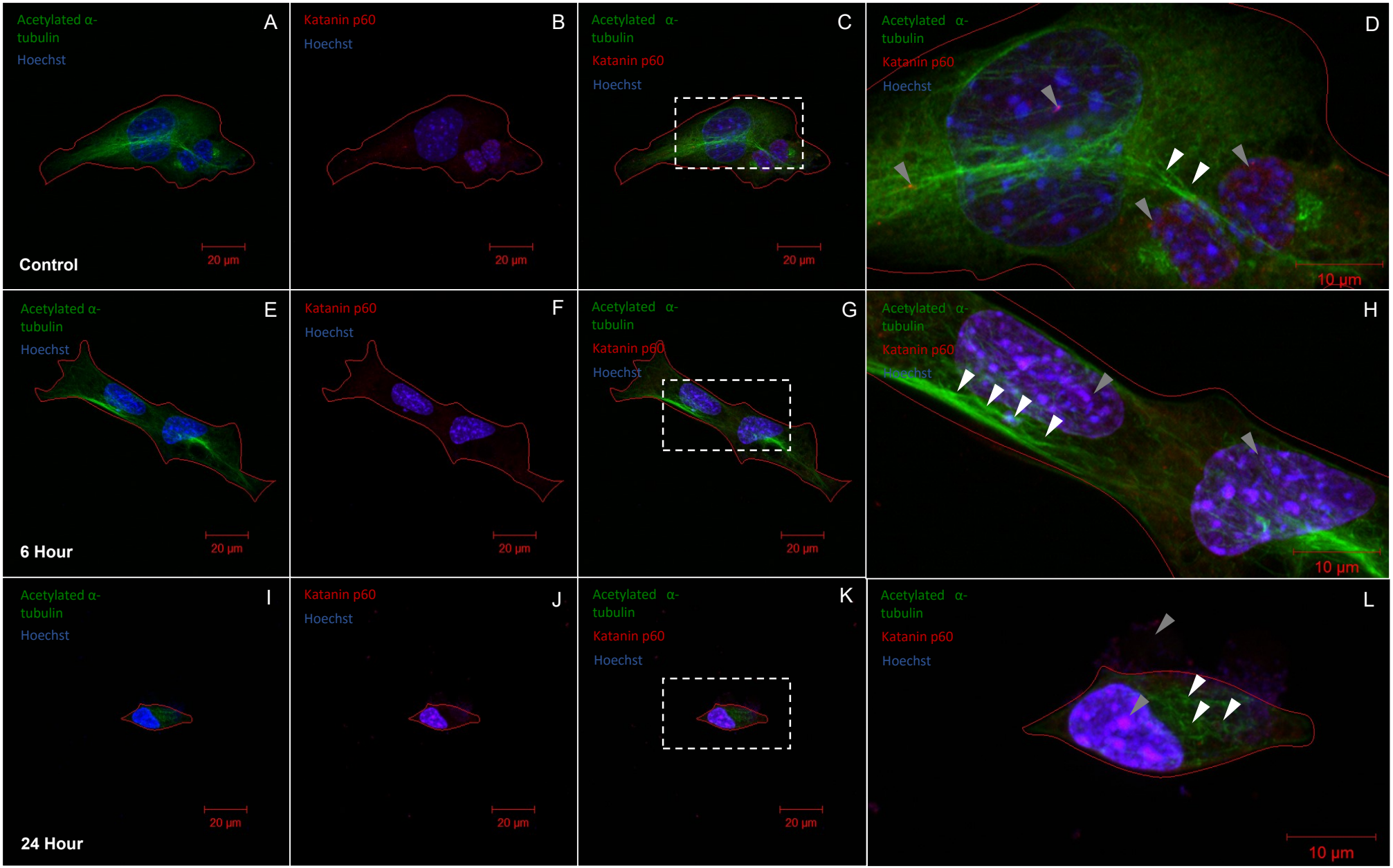

Figure 3.18: Distribution of Katanin p60 and acetylated α-tubulin signal under control conditions and during various stages of CQ-induced autophagy dysfunction*. N=3 independent experiments. Acetylated α-tubulin (Alexa Fluor-488), Katanin p60 (Alexa Fluor-568) and Hoechst 33342 (Blue). Blue arrow heads indicate vacuole-like structures, white arrow heads indicate tubulin structure and grey arrow heads indicate Katanin p60 distribution. Scale bar = 20 µm and 10 µm, respectively.*

3.8 Western Blot Summary Panels

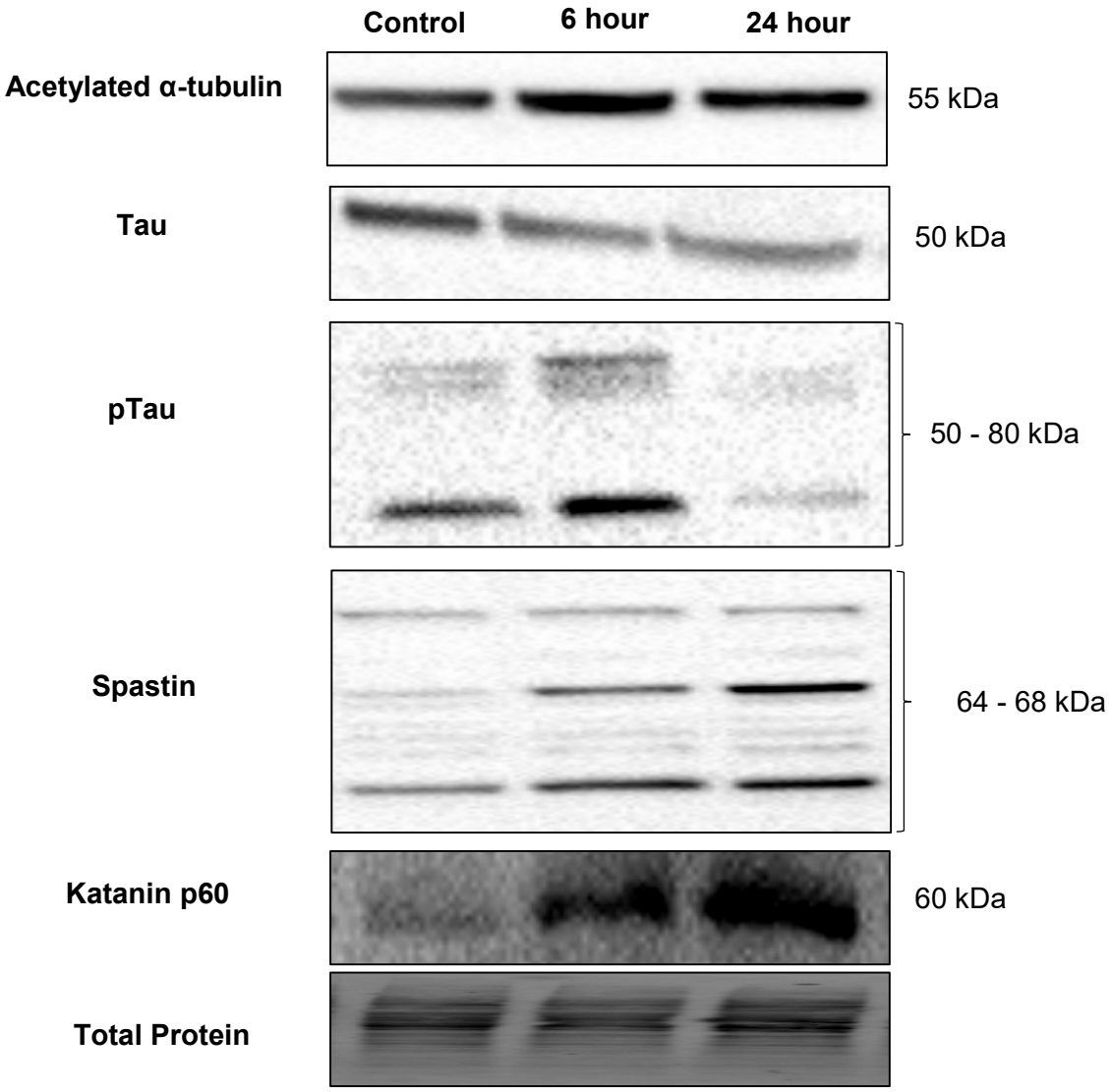

Figure 3.19: Representative blots of proteins assessed under control conditions and after of CQ exposure.

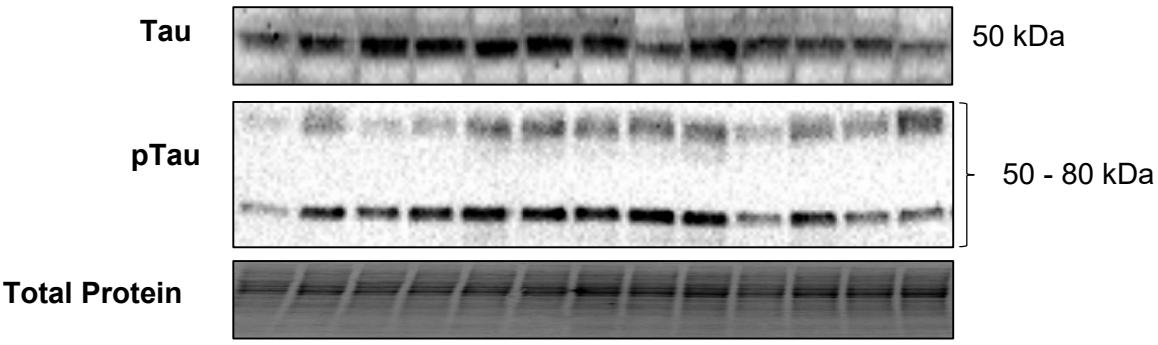

Figure 3.20: Representative blots of proteins assessed over 24 hours of CQ exposure.

3.9 CQ-induced autophagy dysfunction causes changes in co-localisation and line intensity profile intensities between acetylated α-microtubulin, microtubule associated proteins and severing enzymes

3.9.1 Tau co-localises with acetylated α-tubulin, which does not significantly change during CQ-induced autophagy dysfunction

3.9.1.1 Line profile intensities of Tau and acetylated α-tubulin

Line intensity profiles of both Tau and acetylated α-tubulin remained similar in both control and CQ-treated conditions. However, regional intensity hot spots of acetylated α-tubulin signal were observed in all conditions (Fig. 3.21B, F & J).

3.9.1.2 No significant changes in co-localisation are observed between Tau and acetylated α-tubulin

Manders Overlap Coefficient (MOC) revealed that under control conditions the co-localisation between Tau and acetylated α-tubulin signal was very strong with approximately 87% overlap between the signals (Table 3.1). Even after 6 and 24 hours of CQ exposure, respectively, the values remained near similar, showing a decreasing, but minor, trend over time. This suggests no change in co-localisation between Tau and acetylated α-tubulin over time. Under control conditions, Tau co-localisation with acetylated α-tubulin represented 62% of the total Tau above threshold. This increased slightly to 66% after 6 hours of CQ exposure, but subsequently fell below the control value to 55% after 24 hours (Table 3.1). However, none of the observed changes were significant relative to control conditions. Under control conditions, acetylated α-tubulin co-localising with Tau represented 84% of the total acetylated α-tubulin above threshold. This value increased to 88% after 6 hours of CQ exposure and after 24 hours further to 89% (Table 3.1). However, none of the observed changes were significant relative to control conditions. In summary and importantly, based on the co-localisation data (Table 3.1), Tau does not dissociate from acetylated α-tubulin in response to CQ-induced autophagy dysfunction.

Table 3.1: Co-localisation coefficients of Tau and acetylated α-tubulin. Data represented as Mean ± SEM.

	MOC	**Tau/Total**	**Acetylated α-tub/Total**
Control	0,87±0,02	0,62±0,08	0,84±0,05
6 Hour	0,85±0,03	0,66±0,08	0,88±0,05
24 Hour	0,83±0,03	0,55±0,08	0,89±0,04

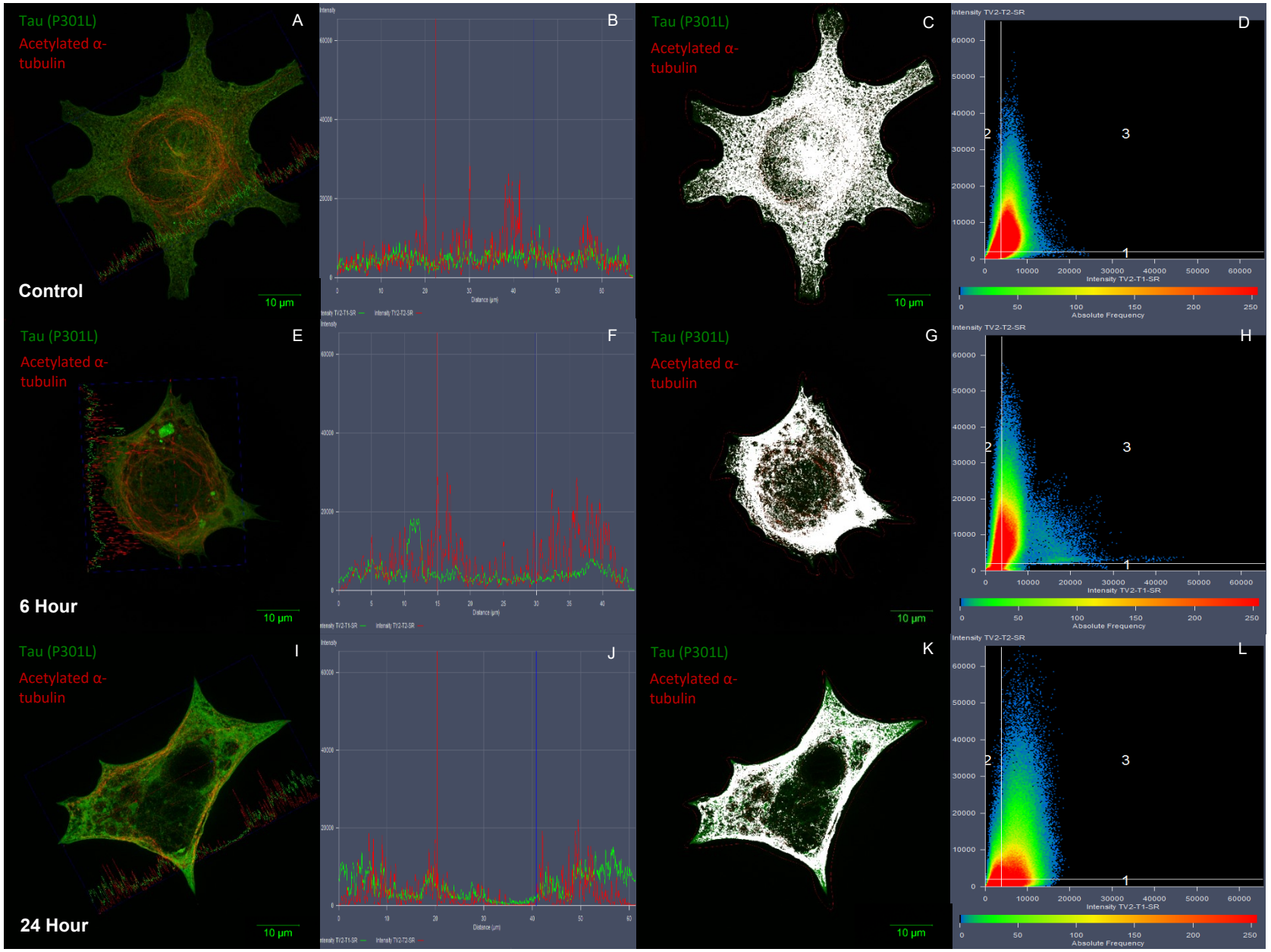

Figure 3.21: Co-localisation between Tau and acetylated α-tubulin under control conditions and after CQ treatment*. A scatter plot showing thresholded pixel distribution. N=3 independent experiments. Pixels seen in white fall above threshold, but do not necessarily indicate co-localisation. Tau (GFP), Acetylated α-tubulin (Alexa Fluor-568). Scale bar = 10 µm.*

3.9.2 pTau does not co-localise with acetylated α-tubulin under control conditions or during CQ-induced autophagy dysfunction

3.9.2.1 Line profile intensities of pTau and acetylated α-tubulin

The intensity profile of acetylated α-tubulin remained as discussed previously in 3.9.1.1, where regional intensity hotspots can be observed in areas of signal clustering, suggestive of protein aggregation (Fig. 3.22E & F). Under control conditions and during periods of CQ exposure, pTau signal intensity was consistently higher in the nucleus of the cell relative to the cytosolic regions – indicated by the vertical red and blue lines which denote the nucleus (Fig. 3.22B, F &J).

3.9.2.2 pTau co-localisation with acetylated α-tubulin does not occur in the cell processes or cytosol and is unaffected by CQ-induced autophagy dysfunction

The MOC revealed that under control conditions, the sum of the total acetylated α-tubulin and pTau pixels that fell above threshold, only 51% co-localised. This increased slightly to 66% after 6 hours of CQ exposure, but subsequently declined to 55% after 24 hours (Table 3.2). Importantly, this area co-localisation did not manifest in the cell processes or cytosol and no significant changes were observed relative to control conditions. Under control conditions, pTau co-localising with acetylated α-tubulin represented 79% of the total pTau signal falling above threshold. This increased to 88% after 6 hours of CQ exposure and fell slightly to 85% after 24 hours (Table 3.2). However, no significant changes were observed relative to control conditions. Under control conditions, acetylated α-tubulin co-localising with pTau represented 13% of total acetylated α-tubulin signal falling above threshold. This did not significantly change relative to control conditions after 6 or 24 hours of CQ exposure (Table 3.2). To summarise, pTau and acetylated α-tubulin co-localisation did not occur in the cell processes or cytosol and no significant changes were observed after CQ-induced autophagy dysfunction. Importantly, it should be noted that the threshold regions observed, represent a fairly small area of the total cell in the control conditions and after 6 hours of CQ exposure (Fig. 3.22C, G & K). Importantly, these data suggest that pTau co-localisation with acetylated α-tubulin is unaffected by CQ-induced autophagy dysfunction.

Table 3.2: Co-localisation coefficients of pTau and acetylated α-tubulin. Data represented as Mean ± SEM.

	MOC	**pTau/Total**	**Acetylated α-tubulin/Total**
Control	0,51±0,04	0,79±0,12	0,13±0,03
6 Hour	0,60±0,05	0,88±0,04	0,12±0,03
24 Hour	0,55±0,07	0,85±0,11	0,12±0,04

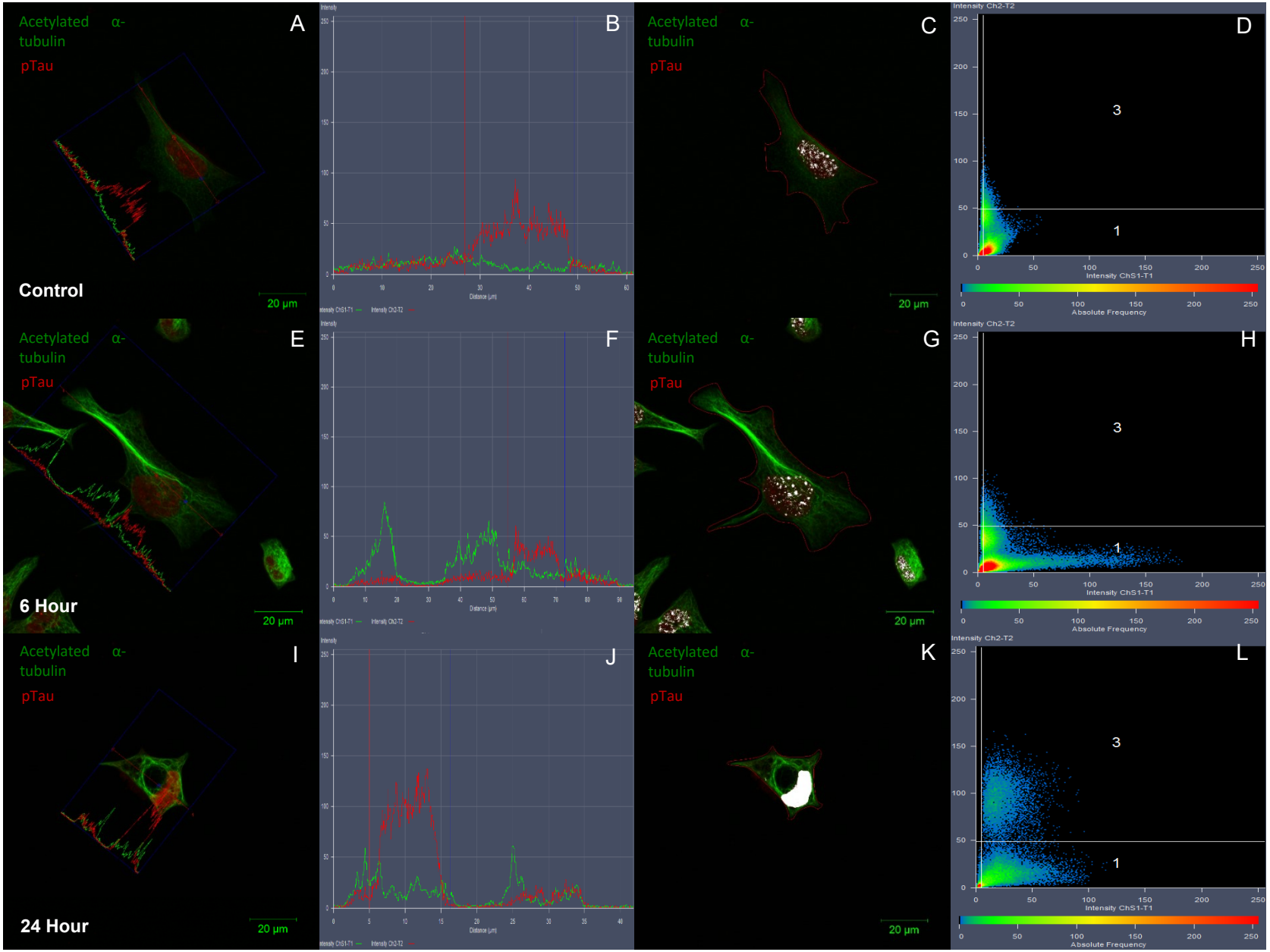

Figure 3.22: Co-localisation between pTau and acetylated α-tubulin under control conditions and after CQ treatment. *A scatter plot showing thresholded pixel distribution. N=3 independent experiments. Pixels seen in white fall above threshold, but do not necessarily indicate co-localisation. Acetylated α-tubulin (Alexa Fluor-488), pTau (Alexa Fluor-568). Scale bar = 20 µm.*

3.9.3 Spastin co-localises with acetylated α-tubulin, which significantly and progressively increases in response during CQ-induced autophagy dysfunction

3.9.3.1 Line profile intensities of Spastin and acetylated α-tubulin

Spastin signal intensity remained fairly constant under control conditions and during periods of CQ exposure (Fig. 26B, F & J).

3.9.3.2 Spastin co-localisation with acetylated α-tubulin progressively and significantly increases during CQ-induced autophagy dysfunction

The MOC revealed that Spastin and acetylated α-tubulin co-localise under control conditions with 68% co-localisation, which progressively and significantly increases to 88% after 24 hours of CQ exposure. (Table 3.3). Under control conditions, Spastin co-localising with acetylated α-tubulin represented 96% of the total Spastin signal that fell above the threshold. This remained constant even after 6 and 24 hours of CQ exposure, respectively (Table 3.3). Under control conditions, acetylated α-tubulin co-localising with Spastin represented 86% of the total acetylated α-tubulin pixels falling above threshold. This decreased slightly to 71% after 6 hours of CQ exposure, but increased significantly to 93% relative to control after 24 hours (Table 3.3). In summary, Spastin and acetylated α-tubulin co-localise under control conditions and progressively co-localise in response to CQ-exposure, to eventual significance after 24 hours suggesting an increase in Spastin activity. Of note, these data further suggest that Spastin is always associated with acetylated α-tubulin regardless of CQ-exposure (Table 3.3).

Table 3.3 Co-localisation coefficients between Spastin of acetylated α-tubulin. Data represented as Mean ± SEM. *(p<0.05 vs control)

	MOC	Spastin/Total	Acetylated α-tubulin/Total
Control	0,68±0,04	0,96±0,01	0,86±0,03
6 Hour	0,72±0,04	0,99±0,00	0,71±0,05
24 Hour	0,81±0,01*	0,99±0,00	0,93±0,02*

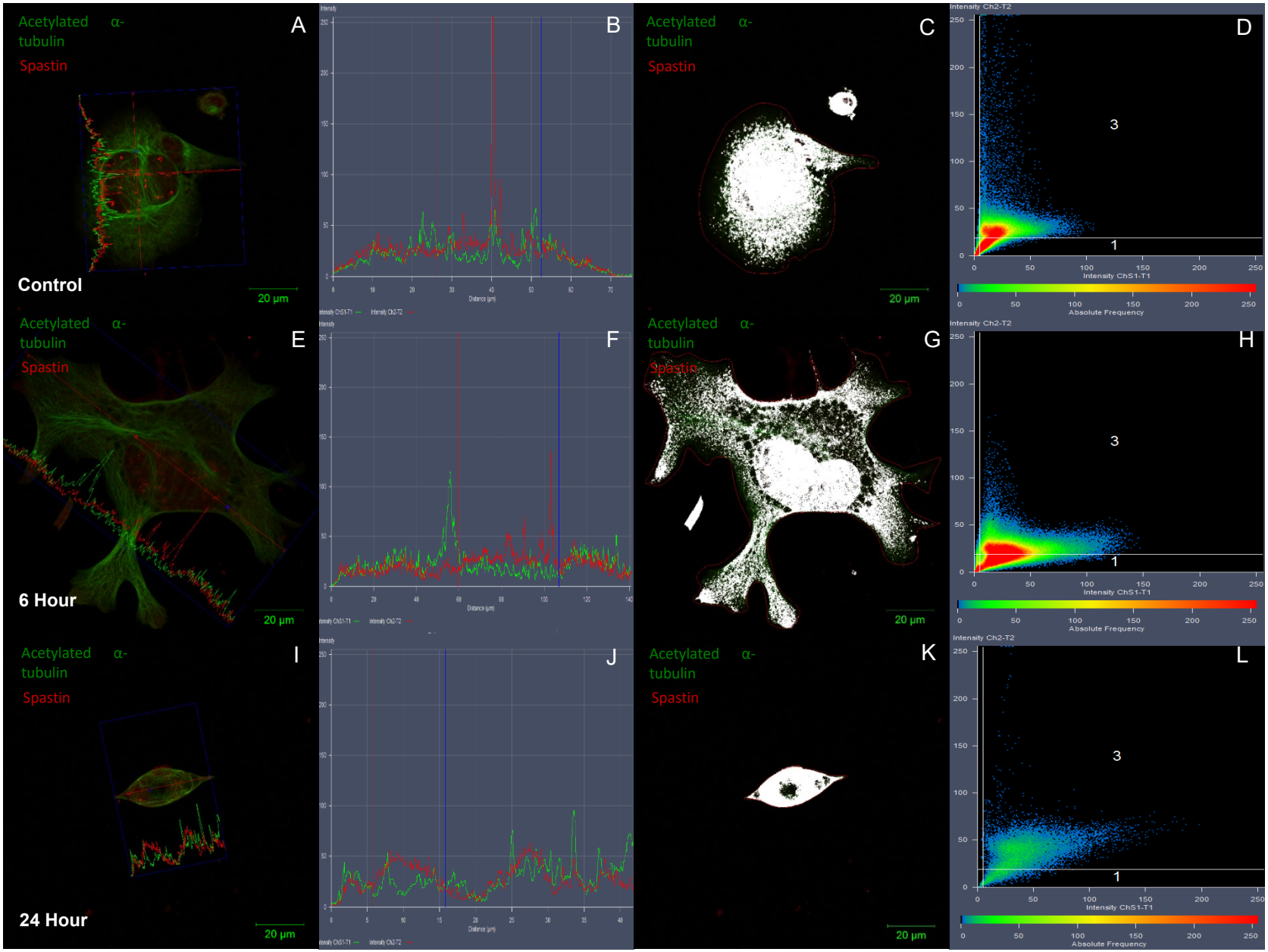

Figure 3.23: Co-localisation between Spastin and acetylated α-tubulin under control conditions and after CQ treatment. *A scatter plot showing thresholded pixel distribution. N=3 independent experiments. Pixels seen in white fall above threshold, but do not necessarily indicate co-localisation. Acetylated α-tubulin (Alexa Fluor-488), Spastin (Alexa Fluor-568). Scale bar = 20 µm.*

3.9.4 Katanin p60 does not co-localise with acetylated α-tubulin in cell processes or cytosol

3.9.4.1 Line profile intensities of Katanin p60 and acetylated α-tubulin

The intensity profile of acetylated α-tubulin remained as discussed previously in 3.2.1.1, where spikes in the signal intensity can be seen in areas of signal bundling (Fig. 3.24E & F). Katanin p60 signal intensity appeared diffusely expressed under control conditions, however after 6 and 24 hours of CQ exposure, respectively, there appears to be a spike in signal intensity within the nuclear regions of the cells (Fig. 3.24F & J).

3.9.4.2 Katanin p60 co-localisation with acetylated α-tubulin does not occur in the cell processes or cytosol and is unaffected by CQ-induced autophagy dysfunction

The MOC revealed that under control conditions 63% of acetylated α-tubulin and Katanin signal co-localised of the total signal that fell above the threshold. This decreased to 57% after 6 hours of CQ exposure and down further to 56% after 24 hours (Table 3.4). Importantly, this co-localisation did not occur in cell processes or cytosol and no significant changes were observed relative to control. Under control conditions, Katanin co-localising with acetylated α-tubulin represented 95% of the total Katanin p60 signal falling above threshold. This remained fairly constant even after 6 and 24 hours of CQ exposure, respectively (Table 3.4). Under control conditions and after 6 of CQ exposure, acetylated α-tubulin co-localising with Katanin p60 represented less than 5% of total acetylated α-tubulin signal falling above threshold. This increased significantly to 23% after 24 hours of CQ exposure (Table 3.4). To summarise, Katanin p60 and acetylated α-tubulin co-localise, but not in cell processes or cytosol and no significant changes were observed after CQ-exposure. Moreover, a significant change was observed in the amount of co-localisation of acetylated α-tubulin with Katanin p60, but this did not occur in cell processes or cytosol (Fig. 3.24C, G & K). These data thus suggest that co-localisation between Katanin p60 acetylated α-tubulin is unaffected by CQ-induced autophagy dysfunction.

Table 3.4: Co-localisation coefficients of Katanin p60 and acetylated α-tubulin. Data represented as Mean ± SEM. *(p<0.05 vs control).

	MOC	Katanin/Total	Acetylated α-tubulin/Total
Control	0,63±0,03	0,95±0,03	0,01±0,01
6 Hour	0,57±0,03	0,94±0,03	0,03±0,01
24 Hour	0,56±0,02	0,97±0,01	0,23±0,06*

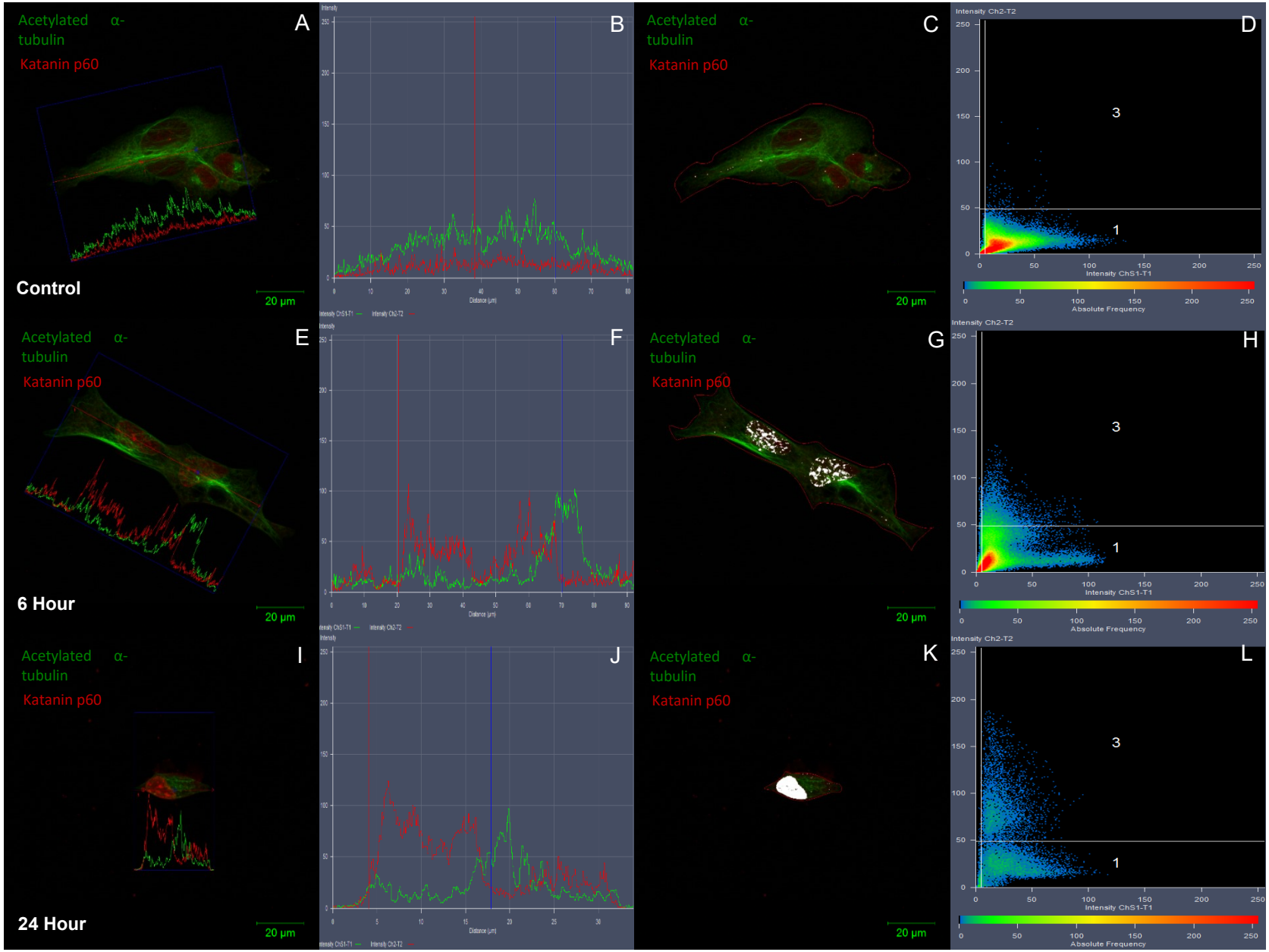

Figure 3.24: Co-localisation between Katanin p60 and acetylated α-tubulin under control conditions and after CQ treatment. *A scatter plot showing thresholded pixel distribution. Pixels seen in white fall above threshold, but do not necessarily indicate co-localisation. Acetylated α-tubulin (Alexa Fluor-488), Katanin p60 (Alexa Fluor-568). N=3 independent experiments. Scale bar = 20 µm.*

3.10 CQ-induced autophagy dysfunction causes an observable change in cellular topology and ultrastructure

Correlative Light and Electron Microscopy (CLEM) is an extremely powerful technique that allows the correlation of fluorescent microscopy with electron microscopy and allows the evaluation of protein ultrastructure and cellular topology. In our experimental analysis we utilised confocal laser microscopy to assess Alexa 568 against acetylated α-tubulin counterstained with Hoechst 33342, and scanning electron microscopy as correlative techniques.

Under control conditions, CLEM analysis revealed that acetylated α-tubulin signal was diffusely distributed in the cytosol of cells, however, the signal consistently arranged into an intense network like morphology around the perinuclear region of the cell (Fig 3.25A – D).

After 6 hours of CQ exposure, acetylated α-tubulin became less diffusely distributed in the cytosolic compartments and processes, instead arranging into dense filamentous structures around clear voids that formed in the cellular structure (Fig 3.25E – H)

After 24 hours of CQ exposure, the general cellular morphology decreased in size and cells visibly stressed. Minimal diffusely distributed acetylated α-tubulin signal was observed in cytosolic compartments or in processes. Majority of the signal arranged into dense filamentous structures in the cellular processes as well as forming network like patterns around vacuolar structures. Furthermore, breaks were observed in the parts of the networks (Fig 3.25I – L)

In summary, the results suggest that CQ-induced autophagy dysfunction impacts cellular morphology by affecting acetylated α-tubulin signal distribution and possibly in response to the formation of autophagic vacuoles.

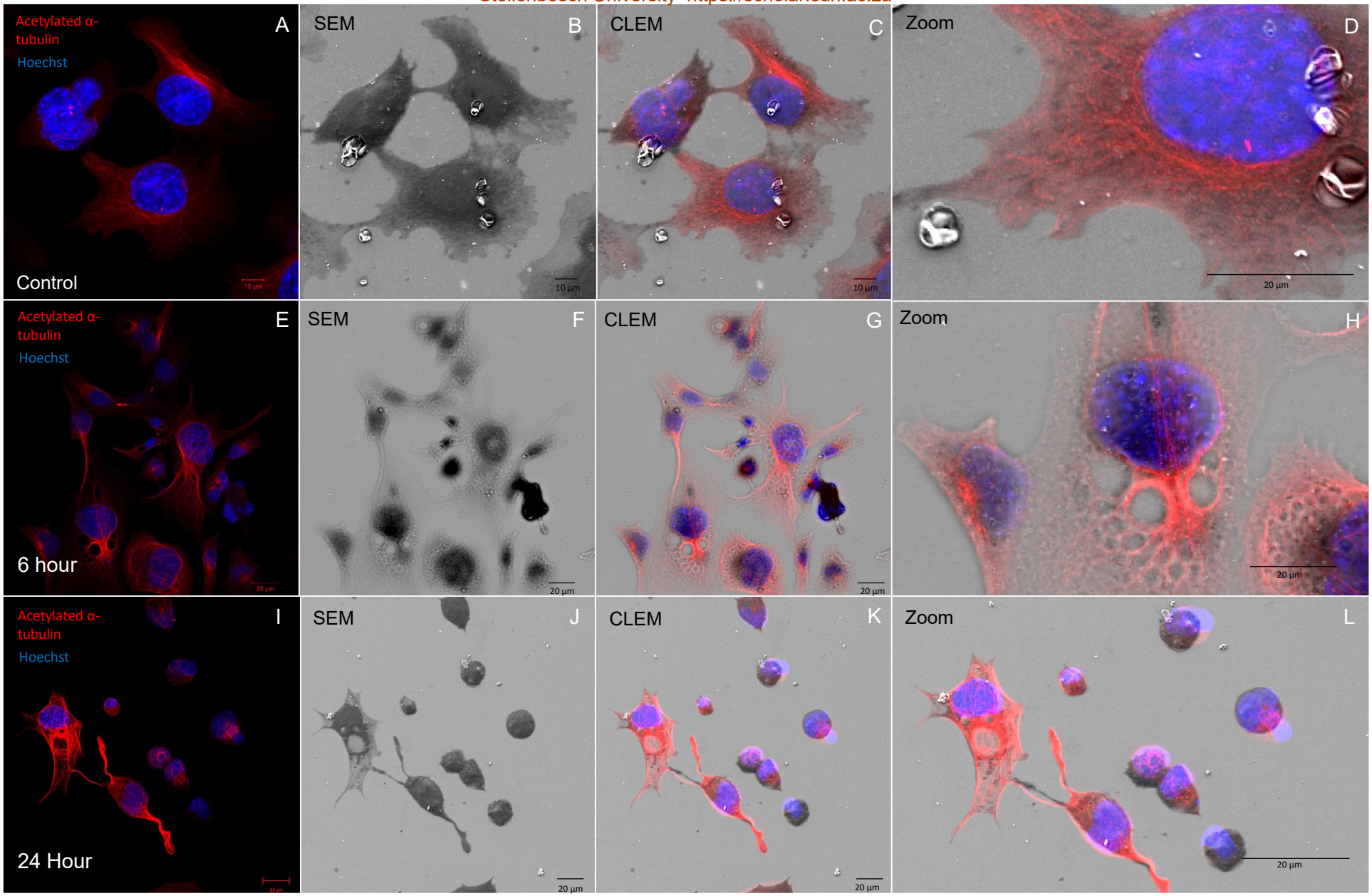

Figure 3.25: CLEM analysis of SEM and confocal microscopy assessing acetylated α-tubulin signal distribution in response to CQ-induced autophagy dysfunction. *Acetylated α-tubulin (Alexa 568), Hoechst 33342 (Blue). N=1 independent experiment. Scale bar = 10 µm and 20 µm, respectively.*

Chapter 4: Discussion

The microtubulin network is an important part of the cytoskeleton, acting as a track for vesicle and organelle transport (Mitchison & Kirschner 1984). It is a very dynamic structure, changing its shape according to the cell's requirements – shrinking and growing, i.e. treadmilling, during specific periods such as cell division, process formation and neuronal migration (Desai & Mitchison 1997). Tau is an important microtubule associated protein that serves to stabilise this network during these dynamic changes, with phosphorylation regulating its binding affinity for microtubulin (Avila et al. 2004). In Alzheimer's disease Tau becomes hyperphosphorylated and permanently dissociates from the network, aggregating into insoluble and cytotoxic structures termed Neurofibrillary Tangles (Braak & Del Tredici 2014). At the same time, microtubules decrease in mass and density and this negatively impacts the ability of the cell to maintain functional axonal transport (Braak et al. 1994). There is no mechanistic evidence to suggest that Tau dissociation directly causes this loss in microtubulin mass and it is not clear when Tau dissociation occurs within the disease pathogenesis (Sudo & Baas 2011; Jean & Baas 2013). Subsequent studies have suggested that Tau may in fact protect the microtubule from proteins which directly cleave it (Mandelkow et al. 2004). Katanin and Spastin are the most characterised severing enzymes that are known to cleave the microtubule and further research has proven that their activity is affected by the presence of Tau on the microtubule (Qiang et al. 2006; Yu et al. 2008). The pathological mechanisms upstream to the onset of Tau hyperphosphorylation still remain largely unknown. Autophagy plays a vital role in maintaining the turnover of Tau and numerous studies have suggested that inhibition of autophagy leads to an increase in Tau aggregation and phosphorylation (Lee et al. 2013; Krüger et al. 2012; Wang et al. 2009; Wang & Mandelkow 2012; Hamano et al. 2008). However, the underlying mechanisms that govern Tau aggregation and subsequent microtubulin instability are neither fully understood nor characterized. In addition, it is not known to what extent autophagy dysfunction influences the pathological changes associated with microtubule destabilisation, Tau aggregation and proteotoxicity.

Here we hypothesized that autophagy disruption causes Tau to accumulate intracellularly and on the microtubulin network. Accumulated Tau associated with the microtubule becomes hyperphosphorylated, reducing its binding affinity and ultimately causing its dissociation. This in turn increases microtubule susceptibility to severing enzymes such as Spastin and Katanin, causing its fragmentation and dysfunction. It is further hypothesized that these events occur prior to the onset of cell death.

We treated GT1-7 cells with the autophagy inhibitor Chloroquine diphosphate (CQ) to induce a state of autophagy disruption. To confirm autophagy dysfunction we utilised Western blot

analysis to assess LC3 and p62 protein levels in response to the treatment intervention in the presence and absence of Bafilomycin A1 (BAF). To determine the effects of CQ-induced autophagy dysfunction on microtubulin stability we assessed acetylated α-tubulin protein levels – a marker for stable microtubules – utilising Western blot analysis and visualised its structure and distribution using confocal, super-resolution structured illumination (SR-SIM) and STORM microscopy. To determine the effects of CQ-induced autophagy dysfunction on Tau phosphorylation and aggregation we assessed relative protein levels of total Tau and pTau utilising Western blot analysis and measured co-localisation between Tau and acetylated α-tubulin, as well as pTau and acetylated α-tubulin, utilising SR-SIM and confocal microscopy. Finally, to determine the effects of CQ-induced autophagy dysfunction on severing enzymes, we performed Western blot analysis to assess Spastin and Katanin p60 protein levels and visualised and measured the extent of co-localisation with acetylated α-tubulin.

Here we will discuss and interpret our results in the context of available literature. Finally we will conclude with proposed mechanisms underlying the effect of autophagy dysfunction and the pathological changes associated with Tau aggregation and subsequent microtubulin destabilisation.

4.1 The effect of CQ treatment on autophagy function

4.1.1 CQ treatment causes a significant reduction in cell viability

Functional disruption of autophagy leads to the aberrant accumulation of undigested protein and is implicated in the clinical pathogenesis of numerous neurodegenerative diseases including Alzheimer's disease (Hara et al. 2006; Loos et al. 2013; Nixon 2013)

Chloroquine (CQ) is an autophagy inhibitor that exerts its effects by accumulating in lysosomes and raising the luminal pH, inhibiting the vacuolar type H+-ATPase pump and thus preventing functional acidification (Llewellyn et al. 2015). From our results we determined that 100 μM CQ was sufficient to induce a significant reduction in viability of GT1-7 cells after 24 hours of treatment, but mild enough to induce a modest non-significant reduction after 6 hours (Fig 3.1). This finding was in agreement with our experimental aims which allowed us to assess any changes in the defined parameters prior to and during the onset of cell death. Furthermore, these time points also served translationally as a model system that mirrors the clinical representation of a pre-symptomatic undiagnosed AD patient and a diagnosed AD patient – at which time a significant amount of neuronal death has occurred and symptoms have manifested.

The concentration of CQ used is in agreement with a study that investigated the effects of CQ on ubiquinated protein and p62 degradation (Myeku & Figueiredo-Pereira 2011). However, a recent review has highlighted that treating cells with more than 50 μM of CQ for 4 hours can induce p53-mediated caspase-independent cell death in mouse tissue (Sharifi et al. 2015; Maclean et al. 2008). Although, another study suggests that CQ-mediated cell death occurs in both a caspase- and p53-independent manner, instead of inducing cell death through the accumulation of autophagic vacuoles. Here, however, human glioblastoma cell line models were used and the exact molecular mechanisms underlying the cell death onset remained to be elucidated (Geng et al. 2010). This basis of these studies indicate the probable mode of cell death occurring after 24 hours of CQ exposure and highlights the severity of the insult.

4.1.2 CQ treatment leads to a progressive accumulation of LC3-II protein

CQ treatment led to a progressive accumulation of LC3-II over time (Fig 3.2 & 3.3), confirming autophagosome accumulation and therefore autophagy dysfunction. CQ has consistently been shown to inhibit autophagy in both in vitro and in vivo studies (Murakami et al. 1995; Murakami et al. 1998; Bendiske & Bahr 2003; Shacka et al. 2006; Hamano et al. 2008; Yoon et al. 2010). Assessing LC3-II protein levels in response to treatment, in the presence or absence of Bafilomycin A1 (BAF), was used to indicate the effect of CQ on the relative autophagic flux – the rate of autophagosome synthesis vs autophagosome degradation – of the system. BAF is most often referenced in literature as only inhibiting autophagy through the prevention of fusion between autophagosomes and lysosomes, but in fact it additionally also prevents lysosome acidification through inhibition of the vacuolar type H+-ATPase pump (Klionsky et al. 2008). It is reasoned that the specific mode of action is determinant on the time of exposure (Klionsky et al. 2008). The relative autophagic flux of GT1-7 cells under basal conditions appeared to be very low, as evidenced by the minor increase in LC3-II protein levels in cells treated with BAF (400 nM) when compared to the untreated control cells LC3-II protein levels (Fig 3.2). This is not unusual for neurons, as measuring autophagic flux in this tissue type has historically been recognised as challenging due to the unexpected responses of generally used autophagy modulators and the contentious scrutiny of published results (Mizushima 2003; Rubinsztein & Nixon 2010). It is generally thought that the flux in neurons is high due their high metabolic needs (Nixon & Yang 2011).

Several reasons may explain these results. Initially, it was thought that the concentration of BAF used was not sufficient, however, it is significantly higher than the concentrations used in the literature, which ranges from 1 nM – 200 nM (Pivtoraiko et al. 2010; Shacka et al. 2006; Li et al. 2012). The amount of time that the cells were exposed to BAF (120 min) may have

been insufficient, however, prior work by others has shown that BAF elicits effects at lower doses for even shorter exposure times (Shacka et al. 2006; Klionsky et al. 2008). Furthermore, we exposed the cells to BAF after the CQ treatment concluded, which may have allowed the cells to recover. However, this is an unlikely factor due to the increase in the LC3-II protein levels in cells treated with both CQ and BAF at 6 hours compared to cells treated with CQ alone (Fig 3.2). BAF has been shown to be a more potent autophagy inhibitor than CQ, even at lower concentrations compared to that utilised in the present study (Ni et al. 2011; Sahani et al. 2014). In addition, BAF has also been shown to attenuate CQ-induced cell death, but does not attenuate CQ-induced autophagy inhibition (Shacka et al. 2006). Lastly, it has been shown that BAF may also inhibit the proteasome and endosome trafficking, amongst other processes (Klionsky et al. 2008)

A major drawback of assessing autophagic flux using Western blotting is that it is less suitable to actually measure flux, which is defined as the rate of autophagy mediated degradation over time (Rubinsztein et al. 2009; Klionsky et al. 2012). There is no parameter of time moving forward when considering the flux of the system in this manner, merely a change in the system at one point in time relative to another. Therefore Western blot results of LC3-II should be interpreted with caution and should always reported as relative change, since a continuous measurement is not taken (Loos et al. 2014).

According to the results observed in cells following 6 hours of CQ treatment compared to the cells following 6 hours of CQ treatment and BAF, there is an increase in LC3-II accumulation (Fig 3.2). Although this is not a significant difference, it may suggest that CQ not only inhibits autophagosome degradation, but also enhances autophagosome formation (Rubinsztein et al. 2009). Furthermore, because of the modest additive effect of CQ in the presence of BAF on LC3-II accumulation, it supports the notion that not only is the relative rate of total autophagic turn-over in GT1-7 cells low at basal conditions, but also that CQ most likely induces maximal inhibition of autophagy after 6 hours of exposure.

After 24 hours of CQ exposure, we observed a significant increase in LC3-II protein levels relative to control, suggesting major autophagosome accumulation. At this time a significant reduction in cell viability was observed after 24 hours of CQ exposure and given that both CQ and BAF are extremely cytotoxic it is possible that the cumulative toxicity had an effect on LC3-II protein levels. In summary, these findings demonstrate the ability of the intervention employed to impact autophagy function by inhibiting autophagosome degradation, therefore establishing a powerful model system.

4.1.3 CQ treatment leads to a progressive decrease in p62 protein

CQ-induced autophagy dysfunction led to a progressive decrease in p62 protein levels over time (Fig 3.4). The decrease was enhanced when cells were treated with BAF after both 6 hours and 24 hours of CQ exposure, respectively. This suggests that p62 is either being degraded even when autophagy was being functionally disrupted, or its synthesis ceased.

There are multiple reasons to explain these results. Briefly, the sequestosome1/p62 targets poly-ubiquinated proteins to the forming autophagosome for selective degradation by acting as an adaptor protein between LC3-II residues and the tagged protein (Barth et al. 2010). It is therefore used as a marker for selective autophagy activity, but it is also viewed as an autophagy target itself (Barth et al. 2010). Furthermore, p62 also has a role in the proteasome pathway (UPS) and its expression is also regulated at a transcriptional level by oxidative stress and other signalling pathways, such as Ras or NFκ-B, that are independent of autophagy (Moscat & Diaz-meco 2009; Myeku & Figueiredo-Pereira 2011). Therefore taking the literature in account, interpretation of our p62 results should be approached with caution.

The fact that p62 protein levels continued to decline in the presence of both CQ and BAF may have multiple reasons (Fig 3.4). Firstly, since p62 is also a UPS target, it may be as a result of a compensatory increase in UPS activity in response to CQ-mediated autophagy inhibition. Indeed, it has been shown that inhibition of autophagy can lead to compensatory responses by the UPS (Ding et al. 2007). Secondly, it may not necessarily be an increase in p62 degradation that we observed, but a decline in p62 transcription. This explanation seems plausible since it is known that p62 transcription is affected by autophagy-independent signalling (Barth et al. 2010). However, Sahani and colleagues have shown that p62 mRNA levels remained unchanged in Mouse Embryonic Fibroblasts (MEFs) in response to CQ treatment, even though they also observed a time dependent decrease in p62 protein levels (Sahani et al. 2014). Lastly, the results may suggest that CQ does not completely inhibit autophagy. Indeed, others have shown that CQ does not completely inhibit p62 degradation even in the presence of LC3-II accumulation (Sahani et al. 2014; Gomez-Sanchez et al. 2016). However, this scenario remains unlikely simply because the cells additionally treated with BAF displayed a similar decrease in p62 protein levels (Fig 3.4). Of note, it may also be a decrease in protein poly-ubiquitination that caused p62 protein levels to decline, although this too remains unlikely as it has been shown that CQ treatment in fact increases protein poly-ubiquitination (Myeku & Figueiredo-Pereira 2011).

In summary, although the results in p62 protein levels in response to CQ treatment may suggest incomplete inhibition of autophagy-mediated p62 degradation, it is clear that the mechanisms governing p62 protein levels and activity are highly complex. Furthermore, our

LC3-II Western blot results are in strong agreement with literature that autophagy was indeed successfully and progressively inhibited. Finally, we also suspect that the increased induction of autophagosome synthesis may be a compensatory response by the cell due to the stress brought about by the abundance of undigested autophagosomes.

4.2 The effect of progressive CQ-induced autophagy dysfunction on microtubulin stability and structure

4.2.1 CQ-induced autophagy dysfunction impacts microtubulin stability over time

Acetylated tubulin is considered as an indicative marker of stable microtubules (Butler et al. 2007). CQ treatment led to a progressive, but non-significant increase in acetylated α-tubulin protein levels over time (Fig 3.5). These results indicate that tubulin stability may be impacted by CQ-induced autophagy dysfunction. A limited number of studies performed by others on CQ-mediated changes in acetylated α-tubulin protein levels, observed that acetylated α-tubulin protein levels progressively declined in rat brain slices treated with CQ (Bendiske et al. 2002; Bendiske & Bahr 2003; Butler et al. 2007). Acetylated α-tubulin is required for the fusion of lysosomes and autophagosomes and serves as the preferential recruitment and binding site for motor proteins (Bulinski 2007; Dompierre et al. 2007; Xie et al. 2010). CQ deacidifies lysosomes, but does not prevent fusion, so it is plausible to suggest that the increase in acetylated α-tubulin may be due to the accumulation of autophagosomes and subsequent fusion with lysosomes. Indeed, a study conducted on proteotoxicity in cardiomyocytes observed that cells synergistically increase acetylation of α-tubulin when autophagy is induced in response to protein aggregation (Mclendon et al. 2014). Tubulin acetylation is also required for starvation-induced autophagy by modulating the assembly of autophagic cargo along the microtubule during nutrient deprivation (Geeraert et al. 2010).

In summary, acetylated α-tubulin protein levels increased suggesting that CQ-induced autophagy dysfunction causes tubulin to stabilise, which is likely a compensatory response of the cell to stress.

4.2.2 CQ-induced autophagy dysfunction disrupts microtubulin structural organisation

Changes were observed in acetylated α-tubulin signal distribution from a diffuse cytoplasmic and well-organised perinuclear structure under control conditions to a densely structured,

aggregated network over the course of CQ exposure in confocal (Fig 3.6), SR-SIM (Fig 3.7), dSTORM (Fig 3.8) and CLEM (Fig 3.25) derived image data. The increase in condensed structured signal and the non-significant increase in acetylated α-tubulin protein levels over time suggest that it is newly polymerised tubulin, instead of the modification of existing tubulin networks (Fig 3.6 - 3.8 & 3.25). CLEM analysis (Fig 3.25G & H) revealed that some of the vacuole-like structures observed during fluorescent microscopy analysis of cells (Fig 3.11G&K, 3.14K), were in indeed vacuolar structures that formed within the cytoplasm, suggesting major impact of the CQ treatment on lysosomal morphology. CLEM also made clear that the tubulin network re-arranged, surrounding these sometimes large, vacuolar structures. This clearly demonstrates the impact that CQ-induced autophagy has on microtubulin cytoskeletal dynamics. In addition, we consistently observed a reduction in cell size over time in response to CQ exposure, which appears contradictory to the notion of newly polymerised stable tubulin networks. Of note, a similar study found that proteasome inhibition led to an increase in acetylated α-tubulin protein levels as well as polymerisation in multiple cell lines, which included neurons (Poruchynsky et al. 2008). Although the acetylated α-tubulin signal became more structurally condensed over time, changes in the structural morphology of the network were observed, resulting in aggregate like formations after 24 hours of CQ exposure. Additionally, these changes also manifested and displayed as breakages in acetylated α-tubulin structure and clustering of individual fibrillar structures, specifically within cellular processes (Fig 3.11J; 3.14G&H; 3.18H). These changes may have impacted overall morphology leading to the observed reduction in cell size.

Our results have relevance in terms of clinical translation as they are supported by a study that found a significant increase in acetylated α-tubulin relative to total α-tubulin ratios in AD brain tissue compared to age-matched controls – although it should be noted that the overall α-tubulin protein levels were also found to be significantly reduced (Zhang et al. 2015). In agreement with these authors, we suspect that the increased acetylated α microtubulin protein levels may be an adaptive response to compensate for a loss in microtubule mass, but additionally we suggest that autophagy dysfunction may contribute to the increased levels of acetylated α-tubulin.

Of note, acetylation of α-tubulin has been shown to improve axonal transport and this has furthermore been exploited in AD treatment development with the anti-neoplastic drug Paclitaxel (Shemesh & Spira 2011). Paclitaxel is used in the treatment of a multitude of cancers, where it induces microtubule stabilisation by enhancing acetylation of tubulin and in doing so reduces the proliferative ability of neoplastic cells (Marcus et al. 2005; Shemesh & Spira 2011). The drug has been shown to stabilise microtubules in in vivo and in vitro models of tauopathy and at low doses, mitigates the cytotoxic effects of Tau pathology on vesicular

transport (Zhang et al. 2005; Shemesh & Spira 2011). However, the ability of the drug to cross the blood-brain barrier (BBB) is low and therefore its development as a treatment for neurodegenerative diseases has declined in recent years, but several derivatives and paclitaxel hybrid molecules have been investigated as alternatives (Ballatore et al. 2007). Recently, Epothilone D (EpoD) a drug that elicits the same microtubulin stabilising effect of paclitaxel, but which can cross the BBB, has been show to improve axonal transport and cognitive impairment in a mouse model for tauopathy (Zhang et al. 2012). It has further been investigated in a clinical trial for therapeutic use in AD, however, the trial ended in 2013 and use of EpoD as an AD therapy was subsequently discontinued (See Trial#: NCT01492374). It is of interest in this context, that the overall acetylation status may control autophagy. However, whether the indicated drugs indeed indirectly impact autophagy remains unclear.

In summary, our results suggest that the increase in acetylated α-tubulin protein levels and aggregation caused by CQ-induced autophagy dysfunction may be a response by the cell to compensate for the loss in microtubule mass in order to preserve structural functionality of the microtubulin network and to improve the axonal transport, which may have been impaired due to the accumulation of autophagosomes.

4.3 The effect of progressive CQ-induced autophagy dysfunction on Tau and pTau protein levels, localisation and co-localisation with stable microtubulin

4.3.1 CQ-induced autophagy dysfunction leads to a non-significant decrease in Tau protein levels

Endogenous total Tau protein levels progressively, but non-significantly declined, in response to CQ-induced autophagy dysfunction (Fig 3.9 & 3.10). This suggests that total Tau is not only being degraded, but the enhanced degradation may take place as a response to autophagy dysfunction brought about by CQ exposure. Our results are contradictory to the available literature, where it has been consistently found that Tau protein levels progressively increase in response to CQ treatment in in vitro, in vivo and ex vivo studies (Murakami et al. 1998; Oyama et al. 1998; Takeuchi 2001; Bendiske et al. 2002; Bendiske & Bahr 2003; Hamano et al. 2008; Wang et al. 2009; Torres et al. 2012). However, autophagy is not the only proteolytic pathway within mammalian systems and therefore our results of reduced total Tau protein levels in the wake of CQ-induced autophagy dysfunction may point towards alternative degradation pathways (Lee et al. 2013). Indeed, Tau has many isoforms, as well as truncated variants, which are found to be degraded through both the UPS and the ALP, as well as other

systems (Lee et al. 2013). Generation of truncated forms of Tau at Asp421 have been identified to be critical to the formation of NFTs, in fact, this appears to occur very early in the NFT evolution (Guillozet-Bongaarts et al. 2005). Truncation of Tau at Asp421 increases its fibrillogenic properties and its protein levels are abnormally high in the AD brain (Dolan & Johnson 2010). Furthermore, others have found that truncated Asp421 Tau is preferentially degraded through the ALP, whereas full length Tau was preferentially degraded through the UPS (Dolan & Johnson 2010). However, degradation of full length Tau has recently received major attention, with numerous studies providing evidence for both ALP and UPS driven degradation (Lee et al. 2013). In light of our findings it is clear that autophagy functionality affects the dynamics of Tau degradation, whether this is a direct or indirect effect remains to be fully elucidated.

In order to quantify total Tau protein levels we utilised the CP27 antibody for Western blot analysis which provides an advantage by detecting a sequence in human Tau that is conserved across all isoforms and which shares ~88% sequence homology with murine Tau variants, ranging from amino acid sequence 130 to 150 (Petry et al. 2014). However, a disadvantage is that CP27 cannot detect all truncated forms of Tau because not all the truncated variants express the target sequence, especially Tau (Asp421). Of note, an important observation was that both p62 and total Tau protein levels decreased in response to CQ exposure (Fig 3.4 & 3.9), which further adds to the speculation of compensatory induction of UPS activity. Indeed, Babu and colleagues have shown that Tau degradation through the UPS is dependent on p62 recognition of K63 specific poly-ubiquitination chains. Furthermore, others have also shown that inhibiting autophagy in rat brain slices resulted in an upregulation of calpain-dependent proteolysis of Tau (Zhang et al. 2009).

In summary, although a decrease in Tau protein levels was witnessed during CQ-induced autophagy dysfunction, it was not a trend leading towards significance. Nonetheless, it is clear that a degree of total Tau degradation was taking place. Interpreting these results in context of the decrease in p62 protein levels may indicate a compensatory upregulation of UPS dependent proteolysis of Total Tau. Further work is thus required to assess the effect of CQ-induced autophagy dysfunction on poly-ubiquitination of Tau as well as targeting of Tau by p62, which can be performed with the aid of co-immunoprecipitation studies. Assessing Tau and p62 mRNA levels utilising qPCR techniques may also elucidate potential effect of CQ-induced autophagy dysfunction on gene transcription.

4.3.2 CQ-induced autophagy dysfunction causes progressive aggregation of Tau, without inducing dissociation from stable microtubulin

In order to assess Tau localisation we utilised SR-SIM microscopy to visualise Tau, using a transfected GFP-Tau construct. In spite of the reduced protein levels of endogenous Tau, we demonstrated that transfected GFP-Tau progressively aggregated over time during CQ exposure (Fig. 3.11H & L). Furthermore, after 6 hours of CQ-exposure the aggregates formed within vacuolar-like structures resembling autophagosomes (Fig 3.11H). This result is consistent with findings by Murakami and others in the brain slices of a CQ-treated rat model (Murakami et al. 1998).

Importantly, despite the reduction in endogenous Tau protein levels and progressive aggregation of GFP-Tau in response to CQ-induced autophagy dysfunction, no significant differences in co-localisation was observed between stable microtubulin and GFP-Tau over time, suggesting no dissociation of Tau took place (Table 3.1). However, although GFP-Tau did not dissociate from acetylated α-tubulin, it did progressively aggregate in response to the CQ-induced autophagy dysfunction, suggesting upregulation of GFP-Tau synthesis rather than an aggregation of dissociated GFP-Tau. Furthermore, GFP-Tau accumulated preferentially in the cell periphery and processes over time (Fig. 3.11). Similarly, Zempel and Mandelkow found that exposure of primary neurons to oligomeric Aβ mediated the missorting of newly synthesized Tau into somatodendritic compartments (Zempel & Mandelkow 2014), supporting our findings. Of note Tau mRNA has been shown to non-randomly localise as discrete granules of RNA along neuronal axons (Aronov et al. 2002), which may suggest a mechanism of newly synthesized Tau, as discussed above. Tau synthesis has been shown to be enhanced through Insulin-dependent activation of the mTOR/PI3K pathway (Nemoto et al. 2011). Additionally, the study confirmed that it was indeed enhanced protein synthesis rather than an increase in gene transcription through the use of cyclcohexamide, a protein synthesis inhibitor, and actinomycin D, an inhibitor of gene transcription (Nemoto et al. 2011). However, the molecular mechanisms underlying the regulation of Tau synthesis still remain largely unknown, although it has been demonstrated that some cellular factors such as fibroblast growth factor (FGF) enhance its synthesis, these aspects deserve further study (Medina & Avila 2014).

Of note, in a model for Tau pathology in AD, some have documented what they suggest to be critical steps in Tau-mediated neurodegeneration (Baas & Qiang 2005). It is suggested that excess Tau initially binds to microtubules and prevents microtubule-Kinesin binding, which hinders axonal transport (Baas & Qiang 2005). Tau is then hyperphosphorylated which decreases its affinity causing dissociation, which in turn triggers recruitment of severing

enzymes to the microtubules and subsequently leads to fragmentation and destabilisation of the network (Qiang et al. 2006). In our results Tau co-localised with acetylated α-tubulin and remained co-localised during autophagy dysfunction, suggesting no dissociation of Tau from microtubulin (Table 3.1) (Fig 3.21). We further observed breakages in the microtubulin structure during late CQ-induced autophagy dysfunction despite no changes in Tau co-localisation with acetylated α-tubulin (Fig 3.11J; 3.14G&H; 3.18H), which suggests that the destabilisation of acetylated α-tubulin structure was occurring independent of Tau association.

In summary, our results show that CQ-induced autophagy dysfunction causes Tau to aggregate in cell processes, but at the same time preserves and maintains co-localisation with acetylated α-tubulin networks. Furthermore, the association of Tau with acetylated α-tubulin networks did not prevent their destabilisation that may have been induced by autophagy dysfunction.

4.3.3 CQ-induced autophagy dysfunction causes an increase in Tau phosphorylation as an early event, but does not maintain the phosphorylation status

In order to quantify pTau protein levels we utilised Western blot analysis with an antibody that recognises phosphorylation of Tau on the Ser400/403/Ser404 amino acid residues. CQ-induced autophagy dysfunction caused a non-significant increase in Tau phosphorylation after 6 hours, relative to the control, but this was not maintained and subsequently declined to levels lower than those of control conditions after 24 hours (Fig 3.12). In a separate time course using Western blot analysis, pTau protein levels were also quantified in response CQ every two hours for 24 hours (Fig 3.13). These results contrastingly suggested that the pTau significantly increase relative to the 0H control after 6 and 24 hours. However, it should be noted that the sample size for this experiment was small and the standard error of the mean was large – reducing the statistical power. Nonetheless the trend observed after 6 hours of CQ exposure is similar to the 6 hour group in 3.5.1, which had a larger sample size (Fig 3.12). Furthermore, the trend seen after 16 hours is non-significantly decreasing which shows similarity with our previous findings (Fig 3.12).

Others have shown that CQ-induced autophagy perturbations caused Tau to accumulate and aggregate, but found no significant differences in phosphorylation (Hamano et al. 2008). What remains unknown is whether the increase in phosphorylation we observed was directly due to CQ-induced autophagy dysfunction or an indirect activation of enzymes known to phosphorylate Tau such as AMPK.

A plausible explanation for enhanced AMPK activity lies in the effect of CQ has on enhanced autophagy induction. AMPK, a metabolic sensor, is central to autophagy induction during starvation and periods of stress. It is activated through phosphorylation and induces autophagy through the mTOR-dependent pathway (Singh & Cuervo 2011). AMPK has been found to be abnormally activated in NFT-bearing neurons in AD and has furthermore been directly shown to phosphorylate Tau and mediate Tau pathology in vivo (Vingtdeux et al. 2011; Domise et al. 2016).

4.3.4 CQ-induced autophagy dysfunction does not impact pTau aggregation, localisation or changes in co-localisation with stable microtubulin

We observed no aggregation of pTau after 6 hours of CQ-induced autophagy dysfunction despite an increase in protein levels, albeit non-significant (Fig 3.12). To our surprise, we consistently observed that pTau primarily localised in the nucleus under control conditions, which was preserved after 6 and 24 hours of CQ exposure, respectively (Fig 3.12). Furthermore, no significant differences were observed in co-localisation between pTau and stable acetylated α-tubulin (Table 3.1), suggesting that pTau does not dissociate from microtubulin upon autophagy failure. The area of co-localisation appeared to increase and more a more structured pattern formed over time (Fig. 3.22C, G &K). However, one needs to consider that the cell size progressively decreased over time causing condensation of all fluorescent signals, which may impact the area of co-localisation. Furthermore, no co-localisation was observed in cytosolic areas rich in acetylated α-tubulin signal (Fig 3.22).

Given that Tau is a microtubule associated protein and that phosphorylation modulates its binding affinity, we expected that pTau would not co-localise with tubulin per se, but would localise within close proximity. The fact that pTau localised in an organised dot-like fashion within the nucleus around euchromatin (Fig 3.14D, H & L), suggests that it may have transcription factor-like properties. Indeed, Tau has previously been detected in the nucleus, where it is suggested to have a protective effect on DNA in response to heat shock stress and to be putatively involved in normal nucleolar organisation (Sjöberg et al. 2006; Sultan et al. 2011). Furthermore, a comprehensive study on the protein profiles of different Tau isoforms in the murine brain revealed that the 1R/2N Tau variant was predominantly expressed in cell nuclei (Liu & Gotz 2013). Since GT1-7 cells are murine derived, these data support our observation. It also provides a possibility for our observation of pTau localisation (Fig 3.14D, H & L), suggesting that this isoform is preferentially phosphorylated even under control conditions.

Furthermore, we speculate that the reason for its localisation in the nuclear region is due to the dynamic properties of nucleus, which includes constant remodelling due processes such cell division and protein synthesis. These processes are mostly dependent on the microtubulin network, especially chromatin separation, which may require the network to undergo similar remodelling events (van der Vaart et al. 2009). Thus it may explain the observed constant protein levels of pTau in this region. Taken together, the provided evidence supports the notion of constant nuclear pTau localisation.

Finally, Tau possesses multiple serine and threonine sites capable of being phosphorylated and the antibody we utilised only recognised 3 of these sites, Ser400, Thr403 and Ser404. Phosphorylation of Tau at Ser404 is associated with an inhibited ability to promote microtubule assembly, which is supportive of our experimental findings (Evans et al. 2000). Future studies may hence additionally assess other sites of phosphorylation in response to CQ-induced autophagy dysfunction.

In summary, Tau phosphorylation increased after 6 hours of CQ exposure, which may be due to an increase in AMPK activity caused by CQ-induced autophagosome synthesis. However, the phosphorylation was not maintained after 24 hours of CQ exposure. Furthermore, pTau did not form aggregates in the cell, but instead localised within the nucleus under control conditions and after CQ-exposure, which we suggest may be a protective effect, potentially impacting DNA in response to stress. Further work is thus required to elucidate the role of pTau during autophagy dysfunction, which may include Western blot analysis of cell lysate nuclear fractions or chromatin immunoprecipitation (ChIP).

4.4 The effect of progressive CQ-induced autophagy dysfunction on Spastin protein levels, localisation and co-localisation with stable microtubulin

4.4.1 CQ-induced autophagy dysfunction causes progressive, but non-significant accumulation of Spastin

Spastin is a hexameric protein that possesses the capability of cleaving the microtubule through the hydrolysis of ATP. Mutations in the SPG4 gene which encodes for Spastin, are the cause of 40% of Autosomal dominant – Hereditary Spastic Paraplegia (AD-HSP) cases (Charvin et al. 2003). In a murine model for the disease it was shown that mutated Spastin caused gross focal swellings in cortical neuron axons resulting in transport deficits (Tarrade et al. 2006).

In our model of CQ-induced autophagy dysfunction, Spastin protein levels progressively increased over time, however, it was not a trend leading to significance. There is no contextual literature to indicate how the turnover of Spastin is mediated. However, taking into account that the increase in protein levels was not significant, it is likely an indirect effect of autophagy dysfunction rather than an indication that autophagy plays a role in Spastin turnover itself.

4.4.2 CQ-induced autophagy dysfunction causes no changes in Spastin localisation, but leads to a progressive and significant increase in co-localisation with stable microtubulin

Under control conditions, Spastin diffusely localised in the cytosol and cell processes, but also formed punctate structures arranging in proximity to euchromatin in the nucleus (Fig 3.23). The signal in the cytosol remained unchanged after 6 and 24 hours of CQ-induced autophagy dysfunction, respectively. However, the punctate structures in the nucleus progressively decreased in intensity and frequency after CQ-induced autophagy dysfunction. Spastin has mainly two isoforms, M1 and M87. M87 is mainly cytosolically localised, whilst M1 favours ER and nuclear localisation. In our experiments the antibody used to assess Spastin localisation detected the total protein, however, we suspect that the punctate structures observed in the nucleus may indeed be the M1 isoform based on findings by others (Charvin et al. 2003; Claudiani et al. 2005; Solowska et al. 2008). Further work is required to confirm if the punctate structures are indeed the M1 isoform, which may include Western blot analysis using cellular nuclear fractions.

Under control conditions, there is moderate co-localisation between Spastin and stable microtubulin in the cytosol and processes of the cell. After CQ-induced autophagy dysfunction the co-localisation progressively increased to significance after 24 hours (Table 3.3). Interestingly, Spastin always appeared to co-localise with stable tubulin regardless of whether the cells were exposed to CQ or not (Table 3.3). However, observing the significant increase in stable microtubulin co-localising Spastin relative to control (Table 3.3) and taking into account the overall increase in acetylated α-tubulin protein levels, it indicates that the increase in co-localisation between Spastin and stable microtubulin is due to an increased acetylated α-tubulin protein levels.

This result allows us to deduce two aspects. Firstly, Spastin can interact with the microtubule whether Tau is bound to the network or not, unlike Katanin p60. Indeed, this finding is consistent with the literature which shows that Spastin activity is not inhibited by the presence of Tau on the microtubule (Sudo & Baas 2010). Secondly, it would appear that Spastin is recruited by acetylated α-tubulin which is in contrast to previous studies, showing Spastin

preferentially binds to and severs polyglutamylated microtubulin when compared to acetylated microtubulin (Lacroix et al. 2010; Zempel et al. 2013; Zempel & Mandelkow 2015). However, in these studies the polyglutamylation was induced through Aβ exposure and we did not investigate microtubulin polyglutamylation in this nor any other post-translational modification in context of CQ-induced autophagy dysfunction. Furthermore, one of these studies also showed that the Aβ exposure caused Tau missorting which subsequently led to the mislocalisation of the enzyme TTLL6 (Tubulin-Tyrosine-Ligase-Like 6) into neuronal dendrites. TTLL6 pathologically caused polyglutamylation of microtubulin, which induced Spastin recruitment and cleavage of the network (Zempel & Mandelkow 2015). In summary, although we did not directly measure Spastin activity in response to CQ-induced autophagy dysfunction, the increase in co-localisation between Spastin and acetylated α tubulin does infer an increase in its activity. Furthermore, the changes in acetylated α-tubulin ultrastructure observed after 24 hours of CQ exposure (Fig 3.6 - 3.8 & 3.25), in which breaks in fibrillar structures were apparent and the overall cell morphology became smaller, support the notion that Spastin activity was indeed increased.

4.5 The effect of progressive CQ-induced autophagy dysfunction on Katanin p60 protein levels, localisation and co-localisation with stable microtubulin

4.5.1 CQ-induced autophagy dysfunction causes a significant and progressive accumulation of Katanin p60 over time

Utilising Western blot analysis we quantified Katanin p60 protein levels in response to CQ-induced autophagy dysfunction. Katanin p60 protein levels progressively increased relative to control conditions in response to CQ-induced autophagy dysfunction, significantly so after 24 hours of CQ exposure (Fig 3.17). This suggests that either autophagy plays a role in the turn-over of Katanin p60 or its protein levels are indirectly affected by CQ-induced autophagy dysfunction. To the best of our knowledge there is no available literature to support our findings. However, recent research provides evidence that suggests that Katanin p60 turn-over is in fact mediated by proteasome degradation through targeting by the C terminus of Hsp70-interacting protein (CHIP) (Yang et al. 2013). These findings may point towards the possibility of Katanin targeted to the autophagy machinery. Whether indeed Katanin is cargo for macroautophagy could be confirmed with Bafilomycin A1 treatment since it prevents autophagosome and lysosome fusion – Katanin p60 protein levels should increase. Furthermore, the effect of CQ-induced autophagy dysfunction of Katanin p60 synthesis and gene transcription should be assessed through the use of cyclcohexamide and actinomycin D

to further confirm that Katanin p60 is indeed an autophagy target and the results observed are not due to enhanced protein synthesis or gene transcription.

The Katanin p60 protein levels in neurons are high, so that stoichiometrically it should be able to cleave all the microtubules in cell at any given time, which has put to question how its activity is regulated (McNally et al. 2002). In xenopus egg extracts it was found that Katanin p60's activity could be modulated by XMAP230 – a MAP4 homolog – and cyclinB/cdk1, which tied its regulation to the cell cycle (Vale 1991; McNally et al. 2002). Furthermore, they found that Katanin p60 activity was also higher in cells undergoing mitosis when compared to cells in interphase and this was related to the cells phosphorylation status (McNally et al. 2002). However, Katanin has so far not been found capable of being phosphorylated and this has led others to investigate other microtubule associated proteins (Baas & Qiang 2005). In a provocative study, Qiang and colleagues investigated Tau as a possible mediator of Katanin p60 activity in neurons due to the importance of phosphorylation in regulating its binding capacity. Furthermore, this speculation was additionally based on the findings of their previous experiments where Katanin p60 was over-expressed in cultured neurons and it was observed that microtubules in axons and dendrites, which are richer in Tau relative to somatic compartments, were more resistant to cleavage (Qiang et al. 2006).

These data suggest to consider the effect of a significant increase in Katanin p60 protein levels may have on the microtubulin network and cellular structure.

4.5.2 CQ-induced autophagy dysfunction causes no changes in Katanin p60 localisation or significant differences in co-localisation with stable microtubulin

Visualisation of Katanin p60 revealed minor localisation within the cytoplasm, with a predominant localisation in the nucleus. After 6 and 24 hours of CQ-induced autophagy dysfunction, Katanin p60 appeared preferentially localised in the nucleus of the cells (Fig 3.18). This is indeed a surprising finding, since even under control conditions one would expect to observe higher protein levels in the cytosol and processes according to the literature (Yang et al. 2013). Furthermore, no co-localisation between Katanin and stable tubulin was observed in the cytosol under control conditions or after CQ exposure for 6 or 24 hours, respectively (Fig 3.25). However, more acetylated α-tubulin co-localised with Katanin p60 after 24 hours of CQ exposure relative to control, remaining low nonetheless at 23% co-localisation and represented a small and localised area of the cell (Table 3.4) (Fig 3.24). The significance was likely due to the progressive increase in both Katanin p60 and acetylated α-tubulin protein levels.

Although we observed no co-localisation between Katanin p60 and stable tubulin in the cytosol under control conditions or after CQ exposure, this may be explained by our prior results of no changes in co-localisation between Tau and stable tubulin before or after treatment. Since GFP-Tau did not dissociate from stable tubulin and by taking literature into account (Qiang et al. 2006; Baas & Qiang 2005), it appears that Tau indeed prevented Katanin 60 from binding to the network. Furthermore, where Katanin p60 did appear to co-localise with acetylated α-tubulin was in the nucleus – confirming Tau's ability to inhibit Katanin p60 activity because pTau, which has reduced binding affinity, also only co-localised with acetylated α-tubulin in the nucleus (Fig 3.21). Katanin p60 has also been shown to preferentially be recruited by acetylated α-tubulin in vitro in fibroblasts, but the experimental enhancement of α-tubulin protein levels in neurons yielded no preferential recruitment or enhanced cleavage of Katanin p60 in axons and dendrites rich in Tau (Sudo & Baas 2010). Tau was further shown to inhibit Katanin p60 activity when it was overexpressed in the fibroblasts and negated the recruitment effect of enhanced acetylated α-tubulin protein levels (Sudo & Baas 2010).

Furthermore, our findings that Katanin p60 predominantly localises in the nucleus is supported by the literature since it has been shown that Katanin p60 plays a critical role in cell division, specifically in the process of cytokinesis – the division of cytoplasm – by contributing to the controlled microtubule instability occurring during mitosis as well as in the assembly, in synergy with Katanin p80, of microtubulin spindle poles (McNally et al. 2000; Matsuo et al. 2013). Katanin p60 protein levels in neurons is also further developmentally regulated – declining with age and spiking during milestones such neurogenesis (Yu et al. 2005). GT1-7 cells are immortalised hypothalamic neurons which continuously divide and therefore do not naturally differentiate. If Katanin p60 protein expression and activity is so closely tied to the cell cycle, this would provide an explanation for its predominant nuclear localisation. Therefore, for subsequent experiments it would beneficial to assess the effect of CQ-induced autophagy dysfunction on terminally differentiated neurons.

In summary, we report that although CQ-induced autophagy dysfunction caused a progressive and significant increase in Katanin p60 protein levels relative to control conditions, it did not lead to significant co-localisation between Katanin p60 and stable microtubulin in the cell processes, even under control conditions. When interpreting this result in the context of co-localisation between Tau and stable microtubulin, it suggests that Tau inhibited the ability of Katanin p60 to bind to microtubulin even under conditions of enhanced protein levels of acetylated α-tubulin, which has been shown to preferentially recruit Katanin p60.

4.6 Summary of findings

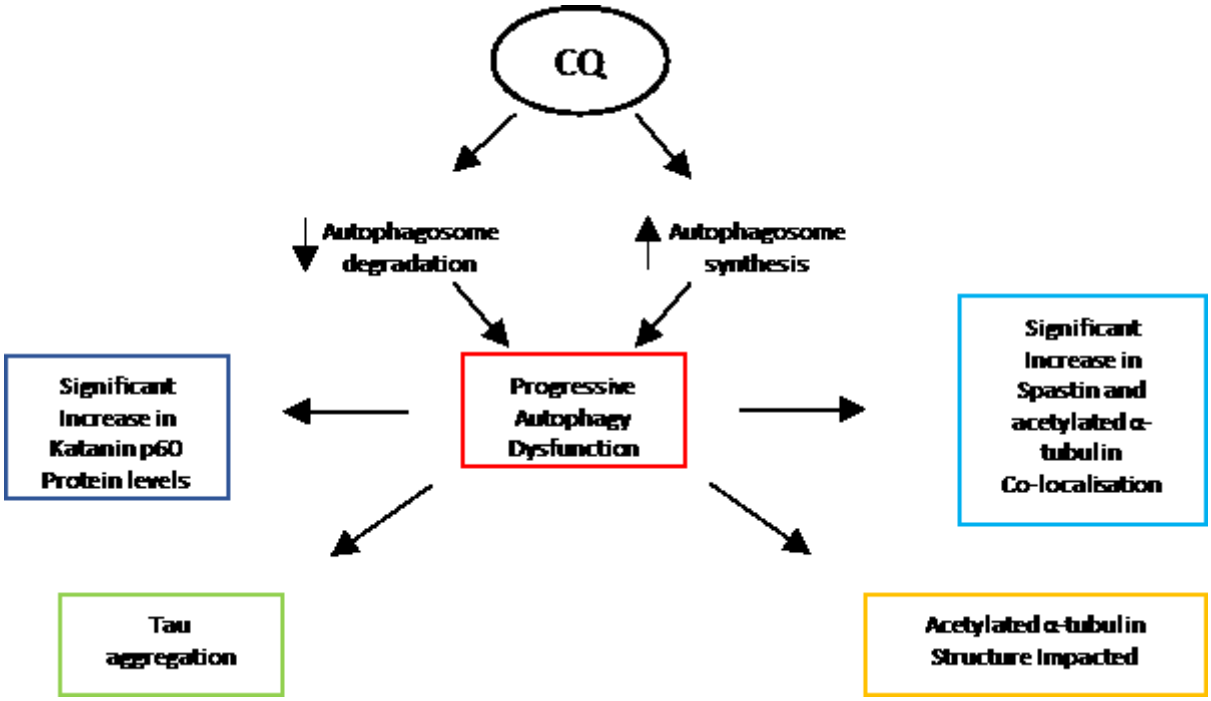

Figure 4.1: Summary of main findings. *CQ induces autophagy dysfunction by inhibiting autophagosome degradation. In response to autophagy dysfunction, Tau forms aggregates, but does not dissociate from acetylated α-tubulin. Katanin p60 protein levels significantly increase, but it does not associate with acetylated α-tubulin under control conditions or during autophagy dysfunction. Spastin increasingly co-localises with acetylated α-tubulin during autophagy dysfunction, which is suggestive of enzymatic cleavage. Consequently, the structure of acetylated α-tubulin is negatively impacted, manifesting in network breakages and possibly destabilisation.*

Chapter 5: Conclusion

Alzheimer's disease is an insidious neurodegenerative disease of the brain which has a highly complex aetiology with many underlying molecular mechanisms that remain largely uncharacterised. Hallmark characteristics of the disease pathology manifest as the deposition of insoluble protein aggregates, which are detrimental to neuronal health (Musiek & Holtzman 2015). NFTs are composed mainly of hyperphosphorylated Tau, a protein which facilitates the dynamic polymerisation and maintenance of microtubule networks. Under homeostatic conditions, phosphorylation modulates Tau's affinity for microtubulin, but in AD Tau is hyperphosphorylated causing it to permanently dissociate from the network and aggregate into NFTs. Proteolytic processes such as autophagy, which normally aid in the clearance of these aggregations, also become dysfunctional during the disease evolution (Nixon & Yang 2011). Furthermore, Tau dissociation leaves the microtubulin network vulnerable to induced destabilisation mediated by the enzymes Katanin p60 and Spastin – leading to deficits in axonal transport and contributing to the declining neuronal health (Ahmad et al. 2000; Yu et al. 2005; Qiang et al. 2006; Yu et al. 2008; Sudo & Baas 2010; Sudo & Baas 2011).

The underlying mechanisms that govern Tau hyperphosphorylation, aggregation and subsequent microtubulin instability are neither fully understood nor characterized in current literature. In addition, it is not known to what extent autophagy dysfunction influences the pathological changes associated with microtubule destabilisation, Tau aggregation and proteotoxicity.

Here we report that CQ induces progressive autophagy by inhibiting autophagosome degradation (Fig 4.1). The progressive autophagy dysfunction does indeed cause Tau to aggregate, but contrastingly causes Tau protein levels to non-significantly decrease. Tau phosphorylation does non-significantly increase initially, but Tau located on the network is not affected and subsequently does not dissociate. Surprisingly the microtubule network becomes more dense and structured over time, but eventually starts destabilising after 24 hours of autophagy dysfunction, manifesting in fragmentation. Katanin p60 protein levels increase, but this does not lead to increased binding and cleavage of the microtubule network, which is likely due the negating effects of the presence of Tau on the network (Fig 5.1A). Spastin protein levels non-significantly increase, but progressively and significantly co-localise with the acetylated α-tubulin, which suggests that Spastin-mediated cleavage may be the cause of microtubulin destabilisation observed after prolonged autophagy dysfunction (Fig 5.1B). This further suggests that Spastin's activity is not affected by the presence of Tau on the microtubule network, but is affected by autophagy dysfunction. Our findings further provide

evidence that autophagy plays a critical role in not only the turnover of Katanin p60, but also the microtubulin instability witnessed in AD affected neurons.

However, and most importantly, we show that these molecular events associated with progressive autophagy dysfunction occur prior to the onset of cell death. Therefore, we provide not only potentially novel drug targets, but also identify a therapeutic window which highlights that treatment interventions should be implemented early in the disease pathogenesis when the molecular perturbations are occurring and not at symptom onset, when most of the damage has already occurred.

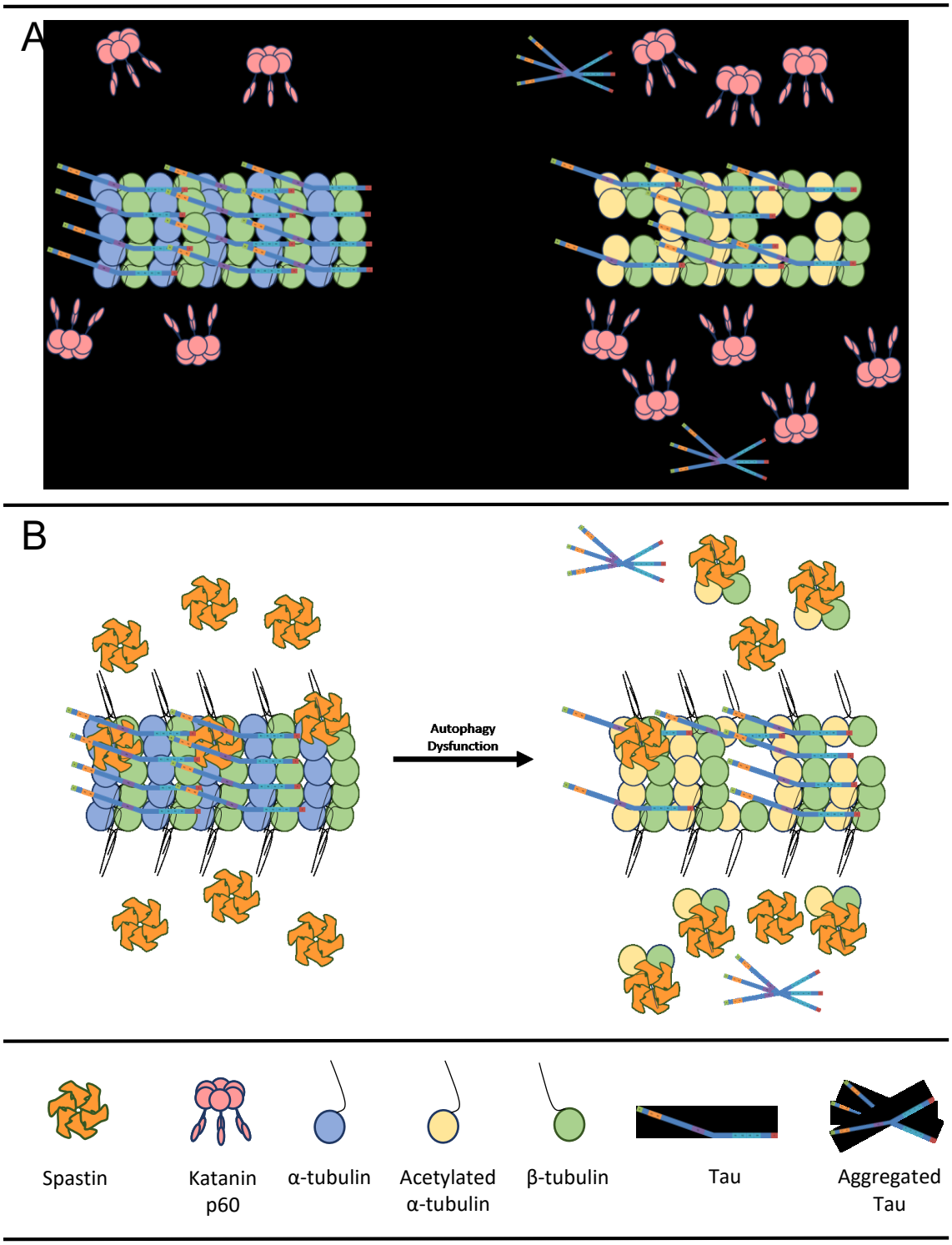

Figure 5.1: Potential molecular mechanisms underlying microtubulin instability associated with CQ-induced autophagy dysfunction. *(A) Proposed molecular mechanism underlying changes in Katanin p60 activity during CQ- induced autophagy dysfunction. (B) Proposed molecular mechanism underlying changes in Spastin activity during CQ-induced autophagy dysfunction.*

Chapter 6: Limitations and Future recommendations

This study has identified previously unknown relationships between progressive autophagy dysfunction and microtubulin instability that can be associated with the Alzheimer's disease aetiology. Therefore, replicating our experiment in an in vivo rodent model and confirming our in vitro results will strengthen the study as a viable model for Alzheimer's disease.

However, to rule out off target effects of chloroquine the study should be replicated in another autophagy dysfunctional model such as an Atg5-/- or Atg7-/- knockout in vitro or in vivo model or by genetically silencing beclin-1 or Atg5 in GT1-7 cells to render autophagy dysfunctional. Furthermore, Aβ-induced Tau pathology can be investigated using an APP overexpression model.

Assessing whether the same changes occur in primary tissue may present a novel diagnostic technique for early disease progression. For instance, if the same perturbations in autophagy dysfunction induced Spastin-mediated cleavage of the microtubule network are observed in non-invasively obtained tissue samples from a suspected Alzheimer's patient – such as fibroblasts from a skin sample – it would provide a novel and non-invasive diagnostic tool for Alzheimer's disease. This would have to entail isolating fibroblasts, back differentiating it into induced pluripotent stem cells (IPSCs) and then differentiating into neurons, since the microtubule polarity of fibroblasts and neurons are vastly different.

Furthermore, assessing the protein levels of Spastin and Katanin in post-mortem brain tissue of Alzheimer's disease patients relative to age matched controls may reveal previously unknown pathological molecular perturbations in the aetiology of the disease.

References

A. Armstrong, R., 2014. A critical analysis of the “amyloid cascade hypothesis.” *Folia Neuropathologica*, 3(3), pp.211–225. Available at: http://www.termedia.pl/doi/10.5114/fn.2014.45562 [Accessed October 31, 2014].

Ahmad, F.J. et al., 2000. An essential role for katanin in severing microtubules in the neuron. *Journal of Cell Biology*, 145(2), pp.305–315. Available at: http://www.jcb.org/cgi/doi/10.1083/jcb.145.2.305.

Ahmad, F.J. et al., 2006. Effects of dynactin disruption and dynein depletion on axonal microtubules. *Traffic*, 7(5), pp.524–537.

Ahmad, F.J. & Baas, P.W., 1995. Microtubules released from the neuronal centrosome are transported into the axon. *Journal of cell science*, 108 (Pt 8, pp.2761–2769.

Akhmanova, A. & Steinmetz, M.O., 2010. Microtubule +TIPs at a glance. *J Cell Sci*, 123(Pt 20), pp.3415–3419. Available at: http://jcs.biologists.org/cgi/doi/10.1242/jcs.062414 [Accessed November 24, 2015].

Allison, R. et al., 2013. An ESCRT-spastin interaction promotes fission of recycling tubules from the endosome. *Journal of Cell Biology*, 202(3), pp.527–543. Available at: http://jcb.rupress.org/cgi/content/long/202/3/527 [Accessed January 22, 2016].

Alonso, A.C. et al., 1994. Role of abnormally phosphorylated tau in the breakdown of microtubules in Alzheimer disease. *Proceedings of the National Academy of Sciences*, 91(12), pp.5562–5566. Available at: http://www.scopus.com/inward/record.url?eid=2-s2.0-0028227962&partnerID=tZOtx3y1 [Accessed May 18, 2016].

Asthana, J. et al., 2013. Inhibition of HDAC6 deacetylase activity increases its binding with microtubules and suppresses microtubule dynamic instability in MCF-7 cells. *Journal of Biological Chemistry*, 288(31), pp.22516–22526. Available at: http://www.pubmedcentral.nih.gov/articlerender.fcgi?artid=3829339&tool=pmcentrez&rendertype=abstract.

Auld, D.S. et al., 2002. Alzheimer’s disease and the basal forebrain cholinergic system: relations to beta-amyloid peptides, cognition, and treatment strategies. *Progress in neurobiology*, 68(3), pp.209–245.

Avila, J., 1992. Microtubule functions. *Life Sciences*, 50(5), pp.327–334.

Avila, J. et al., 2004. Role of Tau Protein in Both Physiological and Pathological Conditions. *Physiological Reviews*, 84(2), pp.361–384. Available at: http://physrev.physiology.org/content/84/2/361\nhttp://physrev.physiology.org/content/84/2/361.full.pdf\nhttp://physrev.physiology.org/content/84/2/361.short\nhttp://www.ncbi.nlm.nih.gov/pubmed/15044677.

Baas, P.W. & Qiang, L., 2005. Neuronal microtubules: When the MAP is the roadblock. *Trends in Cell Biology*, 15(4), pp.183–187. Available at: http://www.sciencedirect.com/science/article/pii/S0962892405000383 [Accessed February 1, 2016].

Ballatore, C., Lee, V.M.-Y. & Trojanowski, J.Q., 2007. Tau-mediated neurodegeneration in Alzheimer’s disease and related disorders. *Nature reviews. Neuroscience*, 8(9), pp.663–72. Available at: http://www.ncbi.nlm.nih.gov/pubmed/17684513 [Accessed November 3, 2014].

Bancher, C. et al., 1989. Accumulation of abnormally phosphorylated τ precedes the formation of neurofibrillary tangles in Alzheimer’s disease. *Brain Research*, 477(1–2), pp.90–99. Available at: http://www.scopus.com/inward/record.url?eid=2-s2.0-0024587074&partnerID=tZOtx3y1 [Accessed May 16, 2016].

Barth, S., Glick, D. & Macleod, K.F., 2010. Autophagy: Assays and artifacts. *Journal of Pathology*, 221(2), pp.117–124.

Becker, E.B.E. & Bonni, A., 2004. Cell cycle regulation of neuronal apoptosis in development and disease. *Progress in neurobiology*, 72(1), pp.1–25. Available at: http://www.ncbi.nlm.nih.gov/pubmed/15019174.

Bendiske, J. et al., 2002. Intracellular Deposition , Microtubule Destabilization , and Transport Failure : An "' Early '" Pathogenic Cascade Leading to Synaptic Decline. *Journal of Neuropathology & Experimental Neurology*, 61(7), pp.640–650.

Bendiske, J. & Bahr, B.A., 2003. Lysosomal activation is a compensatory response against protein ... *Journal of neuropathology and experimental neurology*, 62(May), pp.451–463.

BioRad, Western Blot Normalization Using Image Lab ™ Software Quick Start Guide. , pp.2–5.

Bjorky, G. et al., 2005. p62/SQSTM1 forms protein aggregates degraded by autophagy and has a protective effect on huntingtin-induced cell death. *Journal of Cell Biology*, 171(4), pp.603–614. Available at: http://www.jcb.org/cgi/doi/10.1083/jcb.200507002 [Accessed November 9, 2014].

Bonnet, C. et al., 2001. Differential Binding Regulation of Microtubule-associated Proteins MAP1A, MAP1B, and MAP2 by Tubulin Polyglutamylation. *Journal of Biological Chemistry*, 276(16), pp.12839–12848.

Boxer, A.L. et al., 2013. Frontotemporal degeneration, the next therapeutic frontier: Molecules and animal models for frontotemporal degeneration drug development. *Alzheimer's and Dementia*, 9(2), pp.176–188. Available at: http://linkinghub.elsevier.com/retrieve/pii/S1552526012017505.

Braak, F., Braak, H. & Mandelkow, E.-M., 1994. A sequence of cytoskeleton changes related to the formation of neurofibrillary tangles and neuropil threads. *Acta Neuropathologica*, 87(6), pp.554–567. Available at: http://www.scopus.com/inward/record.url?eid=2-s2.0-0028362458&partnerID=tZOtx3y1 [Accessed May 18, 2016].

Braak, H. & Braak, E., 1991. Neuropathological stageing of Alzheimer-related changes. *Acta neuropathologica*, 82(4), pp.239–259. Available at: http://link.springer.com/10.1007/BF00308809 [Accessed October 19, 2014].

Braak, H. & Del Tredici, K., 2014. Are cases with tau pathology occurring in the absence of A?? deposits part of the AD-related pathological process? *Acta Neuropathologica*, 128(6), pp.767–772.

Braak, H. & Del Tredici, K., 2015. The preclinical phase of the pathological process underlying sporadic Alzheimer's disease. *Brain*, 138(10), pp.2814–2833.

Bulinski, J.C., 2007. Microtubule Modification: Acetylation Speeds Anterograde Traffic Flow. *Current Biology*, 17(1), pp.18–20.

Butler, D. et al., 2007. Microtubule-stabilizing agent prevents protein accumulation-induced loss of synaptic markers ☆. , 562, pp.20–27.

Carter, C.L. et al., 2012. Sex and Gender Differences in Alzheimer's Disease: Recommendations for Future Research. *Journal of Women's Health*, 21(10), pp.1018–1023. Available at: http://online.liebertpub.com/doi/abs/10.1089/jwh.2012.3789 [Accessed November 1, 2014].

Caselli, R.J. & Reiman, E.M., 2012. Characterizing the preclinical stages of Alzheimer's disease and the prospect of presymptomatic intervention. *Advances in Alzheimer's Disease*, 3(SUPPL. 1), pp.405–416. Available at: http://www.scopus.com/inward/record.url?eid=2-s2.0-

84872584059&partnerID=tZOtx3y1 [Accessed November 1, 2014].

Cash, D.M. et al., 2013. The pattern of atrophy in familial alzheimer disease: Volumetric MRI results from the DIAN study. *Neurology*, 81(16), pp.1425–1433. Available at: http://www.scopus.com/inward/record.url?eid=2-s2.0-84888264549&partnerID=tZOtx3y1 [Accessed January 7, 2016].

Cassimeris, L., 1993. Regulation of microtubule dynamic instability. *Cell Motility and the Cytoskeleton*, 26(4), pp.275–281. Available at: http://biochemsoctrans.org/lookup/doi/10.1042/BST0371007.

Cataldo, A.M. et al., 2000. Endocytic Pathway Abnormalities Precede Amyloid β Deposition in Sporadic Alzheimer's Disease and Down Syndrome. *The American journal of pathology*, 157(1), pp.277–286. Available at: http://dx.doi.org/10.1016/S0002-9440(10)64538-5.

Cavallaro, S., 2015. Cracking the code of neuronal apoptosis and survival. *Cell Death and Disease*, 6(11), p.e1963. Available at: http://www.nature.com/doifinder/10.1038/cddis.2015.309 [Accessed February 8, 2016].

Charvin, D. et al., 2003. Mutations of SPG4 are responsible for a loss of function of spastin, an abundant neuronal protein localized in the nucleus. *Human Molecular Genetics*, 12(1), pp.71–78.

Chen, D. et al., 2008. Multiple pathways differentially regulate global oxidative stress responses in fission yeast. *Molecular biology of the cell*, 19(1), pp.308–317.

Claudiani, P. et al., 2005. Spastin subcellular localization is regulated through usage of different translation start sites and active export from the nucleus. *Experimental Cell Research*, 309(2), pp.358–369. Available at: http://www.sciencedirect.com/science/article/pii/S0014482705002788 [Accessed February 11, 2016].

Connell, J.W. et al., 2009. Spastin couples microtubule severing to membrane traffic in completion of cytokinesis and secretion. *Traffic*, 10(1), pp.42–56.

Cuervo, A.M., 2010. Chaperone-mediated autophagy: Selectivity pays off. *Trends in Endocrinology and Metabolism*, 21(3), pp.142–150. Available at: http://linkinghub.elsevier.com/retrieve/pii/S1043276009001623.

Dehmelt, L. & Halpain, S., 2005. The MAP2/Tau family of microtubule-associated proteins. *Genome biology*, 6(1), p.204. Available at: http://www.pubmedcentral.nih.gov/articlerender.fcgi?artid=549057&tool=pmcentrez&rendertype=abstract.

Desai, A. & Mitchison, T.J., 1997. Microtubule Polymerization Dynamics. *Annual Review of Cell and Developmental Biology*, 13(1), pp.83–117. Available at: http://www.annualreviews.org/doi/abs/10.1146/annurev.cellbio.13.1.83.

Deter, R.L., Baudhuin, P. & De Duve, C., 1967. Participation of lysosomes in cellular autophagy induced in rat liver by glucagon. *Journal of Cell Biology*, 35(2), pp.C11–C16. Available at: http://www.ncbi.nlm.nih.gov/pmc/articles/PMC2107130/ [Accessed November 3, 2014].

Ding, W.-X. et al., 2007. Linking of autophagy to ubiquitin-proteasome system is important for the regulation of endoplasmic reticulum stress and cell viability. *The American journal of pathology*, 171(2), pp.513–24. Available at: http://www.pubmedcentral.nih.gov/articlerender.fcgi?artid=1934546&tool=pmcentrez&rendertype=abstract.

Dixit, R. et al., 2008. Differential Regulation of Dynein and. *Science (New York, N.Y.)*, 319(February), pp.8–11.

Dolan, P.J. & Johnson, G.V.W., 2010. A caspase cleaved form of tau is preferentially degraded through the autophagy pathway. *Journal of Biological Chemistry*, 285(29), pp.21978–21987.

Domise, M. et al., 2016. AMP-activated protein kinase modulates tau phosphorylation and tau pathology in vivo. *Scientific Reports*, 6(February), p.26758. Available at: http://www.nature.com/articles/srep26758.

Dompierre, J.P. et al., 2007. Histone Deacetylase 6 Inhibition Compensates for the Transport Deficit in Huntington ' s Disease by Increasing Tubulin Acetylation. *Journal of Neuroscience*, 27(13), pp.3571–3583.

Dráberová, E. et al., 2011. Microtubule-severing ATPase spastin in glioblastoma: increased expression in human glioblastoma cell lines and inverse roles in cell motility and proliferation. *Journal of neuropathology and experimental neurology*, 70(9), pp.811–26. Available at: http://www.pubmedcentral.nih.gov/articlerender.fcgi?artid=3400501&tool=pmcentrez&rendertype=abstract.

DuBoff, B., Feany, M. & G??tz, J., 2013. Why size matters - balancing mitochondrial dynamics in Alzheimer's disease. *Trends in Neurosciences*, 36(6), pp.325–335. Available at: http://www.sciencedirect.com/science/article/pii/S0166223613000404.

Eckert, T., Le, D.T. Van, et al., 2012. Spastin's Microtubule-Binding Properties and Comparison to Katanin. *PLoS ONE*, 7(12), pp.1–17.

Eckert, T., Link, S., et al., 2012. Subunit interactions and cooperativity in the microtubule-severing AAA ATPase spastin. *Journal of Biological Chemistry*, 287(31), pp.26278–26290.

Elmore, S., 2007. Apoptosis: a review of programmed cell death. *Toxicologic pathology*, 35(4), pp.495–516. Available at: http://tpx.sagepub.com/content/35/4/495.full.

Evans, D.B. et al., 2000. Tau phosphorylation at serine 396 and serine 404 by human recombinant tau protein kinase II inhibits tau's ability to promote microtubule assembly. *Journal of Biological Chemistry*, 275(32), pp.24977–24983.

Flaherty, D.B. et al., 2000. Phosphorylation of Human Tau Protein by and cdk5 Are Key Participants. , 472(July), pp.463–472.

De Forges, H., Bouissou, A. & Perez, F., 2012. Interplay between microtubule dynamics and intracellular organization. *International Journal of Biochemistry and Cell Biology*, 44(2), pp.266–274. Available at: http://linkinghub.elsevier.com/retrieve/pii/S1357272511003074.

Geeraert, C. et al., 2010. Starvation-induced hyperacetylation of tubulin is required for the stimulation of autophagy by nutrient deprivation. *Journal of Biological Chemistry*, 285(31), pp.24184–24194.

Geng, Y. et al., 2010. Chloroquine-induced autophagic vacuole accumulation and cell death in glioma cells is p53 independent. *Neuro-Oncology*, 12(5), pp.473–481. Available at: http://www.pubmedcentral.nih.gov/articlerender.fcgi?artid=2940627&tool=pmcentrez&rendertype=abstract.

Godyn, J. et al., 2016. Therapeutic strategies for Alzheimer's disease in clinical trials. *Pharmacological Reports*, 68(1), pp.127–138.

Goldstein, L.S.B. & Yang, Z., 2000. M ICROTUBULE -B ASED T RANSPORT S YSTEMS IN N EURONS : The Roles of Kinesins and Dyneins. , pp.39–71.

Gomez-Sanchez, R. et al., 2016. mRNA and protein dataset of autophagy markers (LC3 and p62) in several cell lines. *Data in Brief*, 7, pp.641–647. Available at:

http://dx.doi.org/10.1016/j.dib.2016.02.085.

Gorman, A.M., 2008. Neuronal cell death in neurodegenerative diseases: Recurring themes around protein handling: Apoptosis Review Series. *Journal of Cellular and Molecular Medicine*, 12(6A), pp.2263–2280.

Grenningloh, G. et al., 2004. Role of the Microtubule Destabilizing Proteins SCG10 and Stathmin in Neuronal Growth. *Journal of Neurobiology*, 58(1), pp.60–69.

Guillozet-Bongaarts, A.L. et al., 2005. Tau truncation during neurofibrillary tangle evolution in Alzheimer's disease. *Neurobiology of Aging*, 26(7), pp.1015–1022.

Gunawardena, S., Yang, G. & Goldstein, L.S.B., 2013. Presenilin controls kinesin-1 and dynein function during APP-vesicle transport in vivo. *Human Molecular Genetics*, 22(19), pp.3828–3843.

Hamano, T. et al., 2008. Autophagic-lysosomal perturbation enhances tau aggregation in transfectants with induced wild-type tau expression. *European Journal of Neuroscience*, 27(5), pp.1119–1130. Available at: http://www.ncbi.nlm.nih.gov/pubmed/18294209 [Accessed May 12, 2015].

Hamano, T. et al., 2009. Concentration-dependent effects of proteasomal inhibition on tau processing in a cellular model of tauopathy. *International Journal of Clinical and Experimental Pathology*, 2(6), pp.561–573. Available at: http://www.pubmedcentral.nih.gov/articlerender.fcgi?artid=2713451&tool=pmcentrez&rendertype=abstract.

Hara, T. et al., 2006. Suppression of basal autophagy in neural cells causes neurodegenerative disease in mice. *Nature*, 441, pp.885–889.

Hardy, J.A. & Higgins, G.A., 1992. Alzheimer's disease: The amyloid cascade hypothesis. *Science*, 256(5054), pp.184–185. Available at: http://www.scopus.com/inward/record.url?eid=2-s2.0-0026597063&partnerID=tZOtx3y1.

Hegde, A.N. & Upadhya, S.C., 2011. Role of ubiquitin-proteasome-mediated proteolysis in nervous system disease. *Biochimica et Biophysica Acta - Gene Regulatory Mechanisms*, 1809(2), pp.128–140. Available at: http://linkinghub.elsevier.com/retrieve/pii/S187493991000091X [Accessed November 1, 2014].

Heintzmann, R. & Cremer, C.G., 1999. Laterally modulated excitation microscopy: improvement of resolution by using a diffraction grating. In *Proc.SPIE 3568, Optical Biopses and Microscopic Techniques III*. pp. 185–196. Available at: http://proceedings.spiedigitallibrary.org/proceeding.aspx?articleid=972650 [Accessed November 9, 2014].

Howes, S.C. et al., 2014. Effects of tubulin acetylation and tubulin acetyltransferase binding on microtubule structure. *Molecular biology of the cell*, 25(2), pp.257–66. Available at: http://www.pubmedcentral.nih.gov/articlerender.fcgi?artid=3890346&tool=pmcentrez&rendertype=abstract.

Hu, Y.-B. et al., 2015. The endosomal-lysosomal system: from acidification and cargo sorting to neurodegeneration. *Translational Neurodegeneration*, 4(1), p.18. Available at: http://translationalneurodegeneration.biomedcentral.com/articles/10.1186/s40035-015-0041-1.

Hunt, S.D. & Stephens, D.J., 2011. The role of motor proteins in endosomal sorting. *Biochemical Society Transactions*, 39, pp.1179–1184.

Huotari, J. & Helenius, A., 2011. Endosome maturation. *The EMBO journal*, 30(17), pp.3481–3500. Available at:

http://www.pubmedcentral.nih.gov/articlerender.fcgi?artid=3181477&tool=pmcentrez&rendertype=abstract\nhttp://dx.doi.org/10.1038/emboj.2011.286.

Ichimura, Y. et al., 2000. A ubiquitin-like system mediates protein lipidation. *Nature*, 408(6811), pp.488–492.

Itoh, K. et al., 2013. Mitochondrial dynamics in neurodegeneration. *Trends in Cell Biology*, 23(2), pp.64–71. Available at: http://dx.doi.org/10.1016/j.tcb.2012.10.006.

Ittner, L.M. & Götz, J., 2011. Amyloid-β and tau--a toxic pas de deux in Alzheimer's disease. *Nature reviews. Neuroscience*, 12(2), pp.65–72. Available at: http://www.scopus.com/inward/record.url?eid=2-s2.0-78751644048&partnerID=tZOtx3y1 [Accessed September 17, 2016].

de Jager, C.A. et al., 2015. Dementia in rural South Africa: A pressing need for epidemiological studies. *South African Medical Journal*, 105(3), pp.189–190. Available at: http://www.samj.org.za/index.php/samj/article/view/8904 [Accessed May 12, 2015].

Jahreiss, L., Menzies, F.M. & Rubinsztein, D.C., 2008. The itinerary of autophagosomes: From peripheral formation to kiss-and-run fusion with lysosomes. *Traffic*, 9(4), pp.574–587. Available at: http://doi.wiley.com/10.1111/j.1600-0854.2008.00701.x.

Jean, D.C. & Baas, P.W., 2013. It cuts two ways: microtubule loss during Alzheimer disease. *The EMBO journal*, 32(22), pp.2900–2. Available at: http://emboj.embopress.org/content/32/22/2900.abstract.

Johjima, A. et al., 2015. Microtubule severing by katanin p60 AAA+ATPase requires the C-terminal acidic tails of both ??-and ??-tubulins and basic amino acid residues in the AAA+ring pore. *Journal of Biological Chemistry*, 290(18), pp.11762–11770. Available at: http://www.jbc.org/lookup/doi/10.1074/jbc.M114.614768.

Kalula, S.Z. et al., 2010. O RIGINAL A RTICLES Profile and management of patients at a memory clinic. *South African Medical Journal*, 100(7), pp.449–451. Available at: http://www.scopus.com/inward/record.url?eid=2-s2.0-77954505295&partnerID=tZOtx3y1 [Accessed May 22, 2015].

Kamat, P.K. et al., 2016. Mechanism of Oxidative Stress and Synapse Dysfunction in the Pathogenesis of Alzheimer???s Disease: Understanding the Therapeutics Strategies. *Molecular Neurobiology*, 53(1), pp.648–661. Available at: http://link.springer.com/10.1007/s12035-014-9053-6.

Kasher, P.R. et al., 2009. Direct evidence for axonal transport defects in a novel mouse model of mutant spastin-induced hereditary spastic paraplegia (HSP) and human HSP patients. *Journal of Neurochemistry*, 110(1), pp.34–44.

Kermer, P. et al., 2004. Neuronal apoptosis in neurodegenerative diseases: From basic research to clinical application. *Neurodegenerative Diseases*, 1(1), pp.9–19.

Kimura, T., Ishiguro, K. & Hisanaga, S.-I., 2014. Physiological and pathological phosphorylation of tau by Cdk5. *Frontiers in molecular neuroscience*, 7(July), p.65. Available at: http://www.ncbi.nlm.nih.gov/pubmed/25076872.

Kleemann, B. et al., 2014. St John's Wort (Hypericum perforatum L.) photomedicine: Hypericin-photodynamic therapy induces metastatic melanoma cell death. *PLoS ONE*, 9(7), p.e103762. Available at: http://journals.plos.org/plosone/article?id=10.1371/journal.pone.0103762.

Klionsky, D.J. et al., 2008. Does bafilomycin A1 block the fusion of autophagosomes with lysosomes? *Autophagy*, 4(7), pp.849–850. Available at: http://www.scopus.com/inward/record.url?eid=2-s2.0-53549084325&partnerID=tZOtx3y1.

Klionsky, D.J. et al., 2012. Guidelines for the use and interpretation of assays for monitoring autophagy. *Autophagy*, 8(4), pp.445–544.

Klionsky, D.J., 2005. The molecular machinery of autophagy: unanswered questions. *Journal of Cell Science*, 118(Pt 1), pp.7–18.

Krüger, U. et al., 2012. Autophagic degradation of tau in primary neurons and its enhancement by trehalose. *Neurobiology of Aging*, 33(10), pp.2291–2305. Available at: http://dx.doi.org/10.1016/j.neurobiolaging.2011.11.009.

Lacroix, B. et al., 2010. Tubulin polyglutamylation stimulates spastin-mediated microtubule severing. *Journal of Cell Biology*, 189(6), pp.945–954.

Lee, M.J., Lee, J.H. & Rubinsztein, D.C., 2013. Tau degradation: The ubiquitin-proteasome system versus the autophagy-lysosome system. *Progress in Neurobiology*, 105, pp.49–59. Available at: http://dx.doi.org/10.1016/j.pneurobio.2013.03.001 [Accessed October 31, 2014].

Lee, S., Sato, Y. & Nixon, R.A., 2011. Primary lysosomal dysfunction causes cargo-specific deficits of axonal transport leading to Alzheimer-like neuritic dystrophy. *Autophagy*, 7(12), pp.1562–1563. Available at: http://www.ncbi.nlm.nih.gov/pubmed/22024748 [Accessed January 25, 2016].

Lekoubou, A., Echouffo-Tcheugui, J.B. & Kengne, A.P., 2014. Epidemiology of neurodegenerative diseases in sub-Saharan Africa: a systematic review. *BMC public health*, 14(1), p.653. Available at: http://www.pubmedcentral.nih.gov/articlerender.fcgi?artid=4094534&tool=pmcentrez&rendertype=abstract [Accessed November 2, 2014].

Li, H. et al., 2012. Sonic hedgehog promotes autophagy of vascular smooth muscle cells. *American journal of physiology. Heart and circulatory physiology*, 303(11), pp.H1319-31. Available at: http://www.pubmedcentral.nih.gov/articlerender.fcgi?artid=3532542&tool=pmcentrez&rendertype=abstract.

Li, S. et al., 2009. Soluble Oligomers of Amyloid ?? Protein Facilitate Hippocampal Long-Term Depression by Disrupting Neuronal Glutamate Uptake. *Neuron*, 62(6), pp.788–801. Available at: http://dx.doi.org/10.1016/j.neuron.2009.05.012.

Liu, C. & Gotz, J., 2013. Profiling murine tau with 0N, 1N and 2N isoform-specific antibodies in brain and peripheral organs reveals distinct subcellular localization, with the 1N isoform being enriched in the nucleus. *PLoS ONE*, 8(12), pp.1–18.

Liu, Y.H. et al., 2009. Proteasome inhibition increases tau accumulation independent of phosphorylation. *Neurobiology of Aging*, 30(12), pp.1949–1961. Available at: http://www.ncbi.nlm.nih.gov/pubmed/18403053.

Llewellyn, K.J., Nguyen, C. & Yazdi, P.G., 2015. Rapamycin and Chloroquine : The In Vitro and In Vivo Effects of Autophagy-Modifying Drugs Show Promising Results in Valosin Containing Protein Multisystem Proteinopathy. , pp.1–16.

Loos, B. et al., 2013. The variability of autophagy and cell death susceptibility: Unanswered questions. *Autophagy*, 9(9), pp.1270–1285. Available at: http://www.ncbi.nlm.nih.gov/entrez/query.fcgi?cmd=Retrieve&db=PubMed&dopt=Citation&list_uids=23846383.

Loos, B. et al., 2013. The variability of autophagy and cell death susceptibility: Unanswered questions. *Autophagy*, 9(9), pp.1270–1285. Available at: http://www.ncbi.nlm.nih.gov/entrez/query.fcgi?cmd=Retrieve&db=PubMed&dopt=Citation&list_uids=23846383.

Loos, B., du Toit, A. & Hofmeyr, J.-H.S., 2014. Defining and measuring autophagosome flux—

concept and reality. *Autophagy*, 10(11), pp.2087–96. Available at: http://www.pubmedcentral.nih.gov/articlerender.fcgi?artid=4502790&tool=pmcentrez&rendertype=abstract.

Lumb, J.H. et al., 2012. The AAA ATPase spastin links microtubule severing to membrane modelling. *Biochimica et Biophysica Acta - Molecular Cell Research*, 1823(1), pp.192–197. Available at: http://www.sciencedirect.com/science/article/pii/S0167488911002382 [Accessed February 11, 2016].

Maclean, K. et al., 2008. Targeting lysosomal degradation induces p53-dependent cell death and prevents cancer in mouse models of lymphomagenesis. *The Journal of Clinical Investigation*, 118(1), pp.9–11.

Mandelkow, E.M. et al., 2004. MARK/PAR1 kinase is a regulator of microtubule-dependent transport in axons. *Journal of Cell Biology*, 167(1), pp.99–110. Available at: http://www.jcb.org/cgi/doi/10.1083/jcb.200401085.

Matsuo, M. et al., 2013. Katanin p60 contributes to microtubule instability around the midbody and facilitates cytokinesis in rat cells. *PLoS ONE*, 8(11), p.e80392. Available at: http://dx.plos.org/10.1371/journal.pone.0080392.

Mclendon, P.M. et al., 2014. Tubulin hyperacetylation is adaptive in cardiac proteotoxicity by promoting autophagy.

McNally, K.P., Bazirgan, O. a & McNally, F.J., 2000. Two domains of p80 katanin regulate microtubule severing and spindle pole targeting by p60 katanin. *Journal of cell science*, 113 (Pt 9, pp.1623–1633.

McNally, K.P., Buster, D. & McNally, F.J., 2002. Katanin-mediated microtubule severing can be regulated by multiple mechanisms. *Cell Motility and the Cytoskeleton*, 53(4), pp.337–349.

Mellon, P.L. et al., 1990. Immortalization of hypothalamic GnRH by genetically targeted tumorigenesis. *Neuron*, 5(1), pp.1–10.

Mitchison, T. & Kirschner, M., 1984. Dynamic instability of microtubule growth. *Nature*, 312(5991), pp.237–42. Available at: http://www.ncbi.nlm.nih.gov/pubmed/6504138 [Accessed November 3, 2014].

Mizushima, N. et al., 2008. Autophagy fights disease through cellular self-digestion. *Nature*, 451(7182), pp.1069–1075.

Mizushima, N., 2003. In Vivo Analysis of Autophagy in Response to Nutrient Starvation Using Transgenic Mice Expressing a Fluorescent Autophagosome Marker. *Molecular Biology of the Cell*, 15(3), pp.1101–1111. Available at: http://www.molbiolcell.org/cgi/doi/10.1091/mbc.E03-09-0704 [Accessed November 3, 2014].

Mizushima, N. & Yoshimori, T., 2007. How to interpret LC3 immunoblotting. *Autophagy*, 3(6), pp.542–545.

Mokhtar, S.H. et al., 2013. The beta-amyloid protein of alzheimer's disease: Communication breakdown by modifying the neuronal cytoskeleton. *International Journal of Alzheimer's Disease*, 2013, p.910502. Available at: http://www.ncbi.nlm.nih.gov/pubmed/24416616.

Moscat, J. & Diaz-meco, M.T., 2009. Minireview p62 at the Crossroads of Autophagy , Apoptosis , and Cancer. *Cell*, 137(1), pp.1001–1004.

Murakami, N. et al., 1998. Accumulation of tau in autophagic vacuoles in chloroquine myopathy. *Journal of neuropathology and experimental neurology*, 57, pp.664–673.

Murakami, N., Ihara, Y. & Nonaka, I., 1995. Chloroquine treated rat: a possible model for Alzheimer's disease. *Muscle & nerve*, 18(1), pp.123–5. Available at:

http://www.scopus.com/inward/record.url?eid=2-s2.0-0028834209&partnerID=tZOtx3y1 [Accessed September 10, 2016].

Musiek, E.S. & Holtzman, D.M., 2015. Three dimensions of the amyloid hypothesis: time, space and "wingmen." *Nat Neurosci*, 18(6), pp.800–806. Available at: http://www.nature.com/doifinder/10.1038/nn.4018\nhttp://www.ncbi.nlm.nih.gov/pubmed/26007213\nhttp://www.nature.com/neuro/journal/v18/n6/pdf/nn.4018.pdf.

Myeku, N. & Figueiredo-Pereira, M.E., 2011. Dynamics of the degradation of ubiquitinated proteins by proteasomes and autophagy: Association with sequestosome 1/p62. *Journal of Biological Chemistry*, 286(25), pp.22426–22440. Available at: http://www.jbc.org/cgi/doi/10.1074/jbc.M110.149252.

Myers, K.A. et al., 2006. Antagonistic forces generated by cytoplasmic dynein and myosin-II during growth cone turning and axonal retraction. *Traffic*, 7(10), pp.1333–1351.

Ni, H.M. et al., 2011. Dissecting the dynamic turnover of GFP-LC3 in the autolysosome. *Autophagy*, 7(2), pp.188–204.

Nixon, R., 2007. Autophagy, amyloidogenesis and Alzheimer disease. *Journal of cell science*, 120, pp.4081–4091.

Nixon, R.A. et al., 2005. Extensive Involvement of Autophagy in Alzheimer Disease: An Immuno-Electron Microscopy Study. *Journal of Neuropathology & Experimental Neurology*, 64(2), pp.113–122. Available at: http://jnen.oxfordjournals.org/content/64/2/113.abstract [Accessed November 2, 2014].

Nixon, R.A., 2013. The role of autophagy in neurodegenerative disease. *Nature Medicine*, 19(8), pp.983–997. Available at: http://dx.doi.org/10.1038/nm.3232\npapers2://publication/doi/10.1038/nm.3232.

Nixon, R.A. & Yang, D.S., 2011. Autophagy failure in Alzheimer's disease-locating the primary defect. *Neurobiology of Disease*, 43(1), pp.38–45. Available at: http://www.pubmedcentral.nih.gov/articlerender.fcgi?artid=3096679&tool=pmcentrez&rendertype=abstract.

Nixon, R.A., Yang, D.S. & Lee, J.H., 2008. Neurodegenerative lysosomal disorders: A continuum from development to late age. *Autophagy*, 4(5), pp.590–599. Available at: http://www.scopus.com/inward/record.url?eid=2-s2.0-48249103491&partnerID=tZOtx3y1.

Olayinka, O.O. & Mbuyi, N.N., 2014. Epidemiology of Dementia among the Elderly in Sub-Saharan Africa. *International Journal of Alzheimer's Disease*, 2014, pp.1–15. Available at: http://downloads.hindawi.com/journals/ijad/2014/195750.pdf [Accessed May 22, 2015].

Ong, W.Y. et al., 2013. Slow excitotoxicity in alzheimer's disease. *Journal of Alzheimer's Disease*, 35(4), pp.643–668.

Oyama, F., Murakami, N. & Ihara, Y., 1998. Chloroquine myopathy suggests that tau is degraded in lysosomes: Implication for the formation of paired helical filaments in Alzheimer's disease. *Neuroscience Research*, 31(1), pp.1–8.

Papadopoulos, C. et al., 2015. Spastin binds to lipid droplets and affects lipid metabolism. *PLoS genetics*, 11(4), p.e1005149. Available at: http://www.pubmedcentral.nih.gov/articlerender.fcgi?artid=4395272&tool=pmcentrez&rendertype=abstract.

Perez, S.E. et al., 2015. Hippocampal Endosomal, Lysosomal, and Autophagic Dysregulation in Mild Cognitive Impairment. *Journal of Neuropathology & Experimental Neurology*, 74(4), pp.345–358. Available at: http://jnen.oxfordjournals.org/lookup/doi/10.1097/NEN.0000000000000179.

Petry, F.R. et al., 2014. Specificity of anti-Tau antibodies when analyzing mice models of Alzheimer's disease: Problems and solutions. *PLoS ONE*, 9(5), p.e94251. Available at: http://www.pubmedcentral.nih.gov/articlerender.fcgi?artid=4008431&tool=pmcentrez&rendertype=abstract.

Pivtoraiko, V.N. et al., 2010. Low-dose bafilomycin attenuates neuronal cell death associated with autophagy-lysosome pathway dysfunction. *Journal of Neurochemistry*, 114(4), pp.1193–1204. Available at: http://www.pubmedcentral.nih.gov/articlerender.fcgi?artid=2910188&tool=pmcentrez&rendertype=abstract.

Plattner, F., Angelo, M. & Giese, K.P., 2006. The roles of cyclin-dependent kinase 5 and glycogen synthase kinase 3 in tau hyperphosphorylation. *Journal of Biological Chemistry*, 281(35), pp.25457–25465. Available at: http://www.ncbi.nlm.nih.gov/pubmed/16803897.

Poruchynsky, M.S. et al., 2008. Proteasome inhibitors increase tubulin polymerization and stabilization in tissue culture cells: a possible mechanism contributing to peripheral neuropathy and cellular toxicity following proteasome inhibition. *Cell Cycle*, 7(7), pp.940–949. Available at: http://www.ncbi.nlm.nih.gov/pubmed/18414063 [Accessed May 12, 2015].

Prince, M. et al., 2015. World Alzheimer Report 2015: The Global Impact of Dementia - An analysis of prevalence, incidence, cost and trends. *Alzheimer's Disease International*, p.84.

Qiang, L. et al., 2006. Tau Protects Microtubules in the Axon from Severing by Katanin. *The Journal of Neuroscience* , 26(12), pp.3120–3129. Available at: http://www.jneurosci.org/content/26/12/3120.abstract [Accessed May 12, 2015].

Quinones, G.B. et al., 2011. The posttranslational modification of tubulin undergoes a switch from detyrosination to acetylation as epithelial cells become polarized. *Molecular biology of the cell*, 22(7), pp.1045–57. Available at: http://www.pubmedcentral.nih.gov/articlerender.fcgi?artid=3069008&tool=pmcentrez&rendertype=abstract.

Rajendran, L. & Annaert, W., 2012. Membrane Trafficking Pathways in Alzheimer's Disease. *Traffic*, 13(6), pp.759–770. Available at: http://doi.wiley.com/10.1111/j.1600-0854.2012.01332.x [Accessed May 12, 2015].

Reitz, C. & Mayeux, R., 2014. Alzheimer disease: Epidemiology, diagnostic criteria, risk factors and biomarkers. *Biochemical Pharmacology*, 88(4), pp.640–651. Available at: http://linkinghub.elsevier.com/retrieve/pii/S0006295213008083.

Rubinsztein, D.C. et al., 2009. In search of an "autophagomometer." *Autophagy*, 5(5), pp.585–589.

Rubinsztein, D.C. & Nixon, R. a, 2010. Rapamycin induces autophagic flux in neurons. *Proceedings of the National Academy of Sciences of the United States of America*, 107(49), p.E181; author reply E182.

Sahani, M.H., Itakura, E. & Mizushima, N., 2014. p62 is restored during prolonged starvation Expression of the autophagy substrate SQSTM1 / p62 is restored during prolonged starvation depending on transcriptional upregulation and autophagy-derived amino acids. , 8627(September 2016).

Schulman, B.A. & Wade Harper, J., 2009. Ubiquitin-like protein activation by E1 enzymes: the apex for downstream signalling pathways. *Nature Reviews Molecular Cell Biology*, 10(5), pp.319–331. Available at: http://www.pubmedcentral.nih.gov/articlerender.fcgi?artid=2712597&tool=pmcentrez&rendertype=abstract.

Schulze, E., 1987. Posttranslational modification and microtubule stability. *The Journal of Cell Biology*, 105(5), pp.2167–2177. Available at: http://jcb.rupress.org/cgi/content/long/105/5/2167 [Accessed April 22, 2016].

Shacka, J.J. et al., 2006. Bafilomycin A1 inhibits chloroquine-induced death of cerebellar granule neurons. *Molecular pharmacology*, 69(4), pp.1125–36. Available at: http://www.ncbi.nlm.nih.gov/pubmed/16391239.

Shankar, G.M. et al., 2008. Amyloid-beta protein dimers isolated directly from Alzheimer's brains impair synaptic plasticity and memory. *Nature medicine*, 14(8), pp.837–42. Available at: http://www.pubmedcentral.nih.gov/articlerender.fcgi?artid=2772133&tool=pmcentrez&rendertype=abstract [Accessed November 3, 2014].

Shankar, G.M. & Walsh, D.M., 2009. Alzheimer's disease: synaptic dysfunction and Abeta. *Molecular neurodegeneration*, 4(1), p.48. Available at: http://www.molecularneurodegeneration.com/content/4/1/48.

Sharifi, M.N. et al., 2015. Measuring autophagy in stressed cells. *Stress Responses: Methods and Protocols*, 1292, pp.129–150.

Shibutani, S.T. & Yoshimori, T., 2014. A current perspective of autophagosome biogenesis. *Cell research*, 24(1), pp.58–68. Available at: http://dx.doi.org/10.1038/cr.2013.159.

Singh, R. & Cuervo, A.M., 2011. Autophagy in the cellular energetic balance. *Cell Metabolism*, 13(5), pp.495–504. Available at: http://linkinghub.elsevier.com/retrieve/pii/S1550413111001471.

Sjöberg, M.K. et al., 2006. Tau protein binds to pericentromeric DNA: a putative role for nuclear tau in nucleolar organization. *Journal of cell science*, 119(Pt 10), pp.2025–34. Available at: http://www.ncbi.nlm.nih.gov/pubmed/16638814.

Solowska, J.M. et al., 2008. Quantitative and functional analyses of spastin in the nervous system: implications for hereditary spastic paraplegia. *The Journal of neuroscience : the official journal of the Society for Neuroscience*, 28(9), pp.2147–2157. Available at: http://www.scopus.com/inward/record.url?eid=2-s2.0-39849101639&partnerID=tZOtx3y1 [Accessed March 7, 2016].

Steinman, R.M. et al., 1983. Endocytosis and the recycling of plasma membrane. *Journal of Cell Biology*, 96(1), pp.1–27.

Stoothoff, W.H. & Johnson, G.V.W., 2005. Tau phosphorylation: Physiological and pathological consequences. *Biochimica et Biophysica Acta - Molecular Basis of Disease*, 1739(2), pp.280–297.

Sudo, H. & Baas, P.W., 2010. Acetylation of microtubules influences their sensitivity to severing by katanin in neurons and fibroblasts. *The Journal of neuroscience : the official journal of the Society for Neuroscience*, 30(21), pp.7215–26. Available at: http://www.pubmedcentral.nih.gov/articlerender.fcgi?artid=2891103&tool=pmcentrez&rendertype=abstract.

Sudo, H. & Baas, P.W., 2011. Strategies for diminishing katanin-based loss of microtubules in tauopathic neurodegenerative diseases. *Human Molecular Genetics*, 20(4), pp.763–778. Available at: http://www.pubmedcentral.nih.gov/articlerender.fcgi?artid=3024046&tool=pmcentrez&rendertype=abstract.

Sultan, A. et al., 2011. Nuclear Tau, a key player in neuronal DNA protection. *Journal of Biological Chemistry*, 286(6), pp.4566–4575.

Takeuchi, I.K.T.Y.K., 2001. S H O RT O R I G I N A L C O M M U N I C AT I O N Transient accumulation of Gallyas-Braak-positive and phosphorylated tau-immunopositive

substances in neuronal lipofuscin granules in the amygdala , hippocampus and entorhinal cortex of rats during long-ter. *Acta Neuropathologica*, pp.191–194.

Tarrade, A. et al., 2006. A mutation of spastin is responsible for swellings and impairment of transport in a region of axon characterized by changes in microtubule composition. *Human Molecular Genetics*, 15(24), pp.3544–3558.

Tiernan, C.T. et al., 2016. Protein homeostasis gene dysregulation in pretangle-bearing nucleus basalis neurons during the progression of Alzheimer's disease. *Neurobiology of Aging*, 42, pp.80–90. Available at: http://linkinghub.elsevier.com/retrieve/pii/S0197458016001974.

Torres, M. et al., 2012. Defective lysosomal proteolysis and axonal transport are early pathogenic events that worsen with age leading to increased APP metabolism and synaptic Abeta in transgenic APP/PS1 hippocampus. *Molecular Neurodegeneration*, 7(1), p.59. Available at: http://www.pubmedcentral.nih.gov/articlerender.fcgi?artid=3575255&tool=pmcentrez&rendertype=abstract [Accessed January 25, 2016].

Vale, R.D., 1991. Severing of stable microtubules by a mitotically activated protein in Xenopus egg extracts. *Cell*, 64(4), pp.827–839.

Vingtdeux, V. et al., 2011. AMPK is abnormally activated in tangle-and pre-tangle-bearing neurons in Alzheimer's disease and other tauopathies. *Acta Neuropathologica*, 121(3), pp.337–349.

Wang, J.Z. et al., 1995. Dephosphorylation of Alzheimer paired helical filaments by protein phosphatase-2A and -2B. *Journal of Biological Chemistry*, 270(9), pp.4854–4860.

Wang, J.Z., Grundke-Iqbal, I. & Iqbal, K., 2007. Kinases and phosphatases and tau sites involved in Alzheimer neurofibrillary degeneration. *European Journal of Neuroscience*, 25(1), pp.59–68.

Wang, J.Z., Grundke-Iqbal, I. & Iqbal, K., 1996. Restoration of biological activity of Alzheimer abnormally phosphorylated τ by dephosphorylation with protein phosphatase-2A, -2B and -1. *Molecular Brain Research*, 38(2), pp.200–208.

Wang, Y. et al., 2009. Tau fragmentation, aggregation and clearance: The dual role of lysosomal processing. *Human Molecular Genetics*, 18(21), pp.4153–4170.

Wang, Y. & Mandelkow, E., 2012. Degradation of tau protein by autophagy and proteasomal pathways. *Biochemical Society Transactions*, 40(4), pp.644–652. Available at: http://www.biochemsoctrans.org/bst/040/0644/bst0400644.htm.

Weissman, A.M., Shabek, N. & Ciechanover, A., 2011. The predator becomes the prey: regulating the ubiquitin system by ubiquitylation and degradation. *Nature reviews. Molecular cell biology*, 12(9), pp.605–20. Available at: http://www.pubmedcentral.nih.gov/articlerender.fcgi?artid=3545438&tool=pmcentrez&rendertype=abstract [Accessed October 13, 2015].

Wloga, D. & Gaertig, J., 2010. Post-translational modifications of microtubules. *Journal of cell science*, 123(Pt 20), pp.3447–55. Available at: http://jcs.biologists.org/cgi/doi/10.1242/jcs.083576\nhttp://www.pubmedcentral.nih.gov/articlerender.fcgi?artid=2951466&tool=pmcentrez&rendertype=abstract [Accessed November 3, 2014].

Xie, R. et al., 2010. Acetylated microtubules are required for fusion of autophagosomes with lysosomes. *BMC cell biology*, 11(1), p.89. Available at: http://www.pubmedcentral.nih.gov/articlerender.fcgi?artid=2995476&tool=pmcentrez&rendertype=abstract.

Yamamoto, M., Suzuki, S.O. & Himeno, M., 2010. The effects of dynein inhibition on the

autophagic pathway in glioma cells: Original Article. *Neuropathology*, 30(1), pp.1–6.

Yan, M.H., Wang, X. & Zhu, X., 2013. Mitochondrial defects and oxidative stress in Alzheimer disease and Parkinson disease. *Free Radical Biology and Medicine*, 62, pp.90–101. Available at: http://linkinghub.elsevier.com/retrieve/pii/S0891584912018230 [Accessed October 31, 2014].

Yang, S.W. et al., 2013. USP47 and C Terminus of Hsp70-Interacting Protein (CHIP) Antagonistically Regulate Katanin-p60-Mediated Axonal Growth. *Journal of Neuroscience*, 33(31), pp.12728–12738. Available at: http://www.jneurosci.org/cgi/doi/10.1523/JNEUROSCI.0698-13.2013 [Accessed May 12, 2015].

Yoon, Y.H. et al., 2010. Induction of lysosomal dilatation, arrested autophagy, and cell death by chloroquine in cultured ARPE-19 cells. *Investigative Ophthalmology and Visual Science*, 51(11), pp.6030–6037. Available at: http://iovs.arvojournals.org/article.aspx?doi=10.1167/iovs.10-5278.

Yu, L. et al., 2010. Termination of autophagy and reformation of lysosomes regulated by mTOR. *Nature*, 465(7300), pp.942–6. Available at: http://www.pubmedcentral.nih.gov/articlerender.fcgi?artid=2920749&tool=pmcentrez&rendertype=abstract.

Yu, W. et al., 2005. Regulation of Microtubule Severing by Katanin Subunits during Neuronal Development. *Journal Neuroscience*, 25(23), pp.5573–5583.

Yu, W. et al., 2008. The Microtubule-severing Proteins Spastin and Katanin Participate Differently in the Formation of Axonal Branch. *Molecular biology of the cell*, 19(1), pp.1485–1498.

Zempel, H. et al., 2013. Amyloid-b oligomers induce synaptic damage via Tau-dependent microtubule severing by TTLL6 and spastin. *The EMBO Journal*, 32(22), pp.2920–2937. Available at: http://dx.doi.org/10.1038/emboj.2013.207.

Zempel, H. & Mandelkow, E., 2014. Lost after translation: Missorting of Tau protein and consequences for Alzheimer disease. *Trends in Neurosciences*, 37(12), pp.721–732. Available at: http://www.sciencedirect.com/science/article/pii/S0166223614001313.

Zempel, H. & Mandelkow, E.-M., 2015. Tau missorting and spastin-induced microtubule disruption in neurodegeneration: Alzheimer Disease and Hereditary Spastic Paraplegia. *Molecular neurodegeneration*, 10(1), p.68. Available at: http://www.pubmedcentral.nih.gov/articlerender.fcgi?artid=4687341&tool=pmcentrez&rendertype=abstract [Accessed December 28, 2015].

Zhang, D. et al., 2007. Three microtubule severing enzymes contribute to the “Pacman- flux” machinery that moves chromosomes. *Journal of Cell Biology*, 177(2), pp.231–242.

Zhang, F. et al., 2015. Posttranslational modifications of α-tubulin in alzheimer disease. *Translational neurodegeneration*, 4, p.9. Available at: http://www.pubmedcentral.nih.gov/articlerender.fcgi?artid=4448339&tool=pmcentrez&rendertype=abstract.

Zhang, J.Y. et al., 2009. Inhibition of autophagy causes tau proteolysis by activating calpain in rat brain. *Journal of Alzheimer’s Disease*, 16(1), pp.39–47.